Spectral Analysis of Heat Flow in U-tube and Coaxial Shallow Geothermal Systems

by
Arsha Shiri

Student Number: 4402839

Committee Members: Prof. Dr. Ir. L.J. Sluys (Chair)
Dr. R. Al Khoury
Ir. L.J.M. Houben
Noori BniLam, MSc

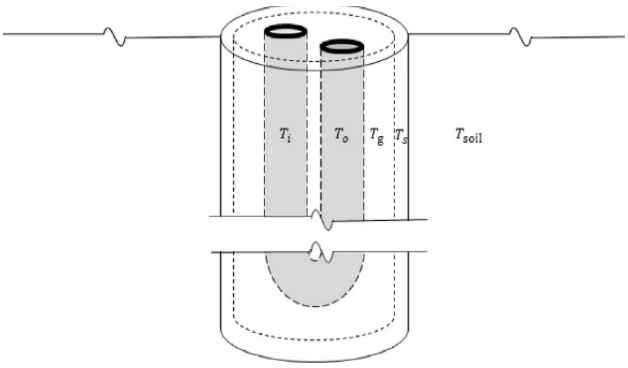

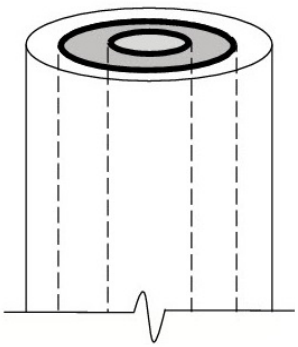

TU Delft

Spectral Analysis of Heat Flow in U-tube and Coaxial Shallow Geothermal Systems

by

Arsha Shiri

In partial fulfillment of the requirement for the degree of

Master of Science
in Structural Engineering Specialization: Structural Mechanics June 2017

at the Delft University of Technology.

Student number:	4402839	
Supervisors:	Prof. Dr. Ir. L.J. Sluys (Chair),	TU Delft
	Dr. R. Al Khoury,	TU Delft
	Ir. L.J.M. Houben,	TU Delft
	Noori BniLam, MSc	

TU Delft Delft University of Technology

ACKNOWLEDGEMENT

This research was conducted as a part of master program in Structural Engineering with a specialization in Structural Mechanics at TU Delft. My master program has been an exceptional experience in my life's journey. One of the main highlights of this experience was writing this thesis from September 2016 to June 2017. I would like to express my warmest appreciation to all who have assisted me in this path.

Initially, I would like to thank all of my committee members and specially my daily supervisor Dr. Rafid Al-Khoury. It was such a great pleasure to work on a challenging project alongside Rafid in a positive atmosphere. His enthusiasm in science coupled with a sense of humor have been great motivations for me. I have learned a lot from his thorough feedback on different parts of my work. I cannot thank him enough for all the time that he spent in order to guide me in this work. Next, I would like to thank Noori for providing me all the necessary tools and guidance in this project and for all the meetings in the weekends. Last but not least, I express my deepest gratitude to professor Bert Sluys and Lambert Houben for their time and advice.

Subsequently, I would like to thank my amazing parents who have supported me in every way. Thank you for all the emotional and financial support that you have provided me during my life and specially during my master program. I would like to thank my awesome friends both here in the Netherlands and outside. Thank you for being, thank you for all of the crazy things that we have done together and thank you for your support.

Finally, I would like to thank all of the things which helped me in my project. I would like to thank coffee star, wikipedia, google, all sorts of beers, De Lelie ice cream and of course the music band Tool.

ABSTRACT

This thesis investigates, modifies and verifies the accuracy of a new analytical model developed at TU Delft (Al-khoury et al ([1], [2], [3], [9])) describing fully transient conductive-convective heat transfer processes in a shallow geothermal system consisting of a U-tube borehole heat exchanger (BHE) embedded in a multilayer soil mass. The Spectral Element Method (SEM) is utilized for solving the involved coupled partial differential equations. The spectral element model combines the exactness of analytical methods with an important extent of generality in describing the geometry and boundary conditions of numerical methods. It calculates the temperature distribution in all involved borehole heat exchangers components and the surrounding soil mass using the discrete Fourier transform for the time domain and the modified Bessel functions for the spatial domain.

The conceptual model for shallow geothermal systems is simulated by thermal interactions between a U-tube borehole heat exchanger and a soil mass. The BHE is modeled by four thermal interactive components: pipe-in, pipe-out, grout and soil film. All these components have one-dimensional heat flow in the z direction whereas, the soil mass is modeled radially. In this model, pipe-in, pipe-out and grout have physical representations but, the soil film is not physically present in the system and can have different thicknesses. The soil film has been introduced in order to take into account the heat flow in the z direction for the soil mass. However, the temperature distribution at the interface between the BHE and the soil mass is affected by the soil film thickness. In this thesis, the effect of the soil film thickness on the results of the spectral element model is investigated thoroughly. Subsequently, the spectral element model is verified against detailed finite element analysis using COMSOL Multiphysics [4]. Several numerical examples comparing temperature distribution obtained from SEM and FEM models have been carried out. The results show that there is a rather good agreement between the two models. However, the differences between them are more pronounced in the grout and this might be due to neglecting the radial heat flow in it.

In order to study the radial heat flow in the grout and its effects on the whole system a new spectral element model for coaxial shallow geothermal system has been developed. The CPU time for calculating temperature distribution in all involved components; pipe-in, pipe-out, grout and soil is only a few seconds in a normal Intel PC. The main advantage of this model is that it can conveniently replace the detailed finite element analysis which normally requires hundreds of thousand of elements.

CONTENTS

1

INTRODUCTION

In this chapter an introduction to the geothermal energy and different types of geothermal systems is given.Various types of shallow geothermal systems are discussed. Subsequently, the focus is placed on a semi-analytical model for U-tube shallow geothermal systems. Finally the objectives of the thesis are defined.

1.1. GEOTHERMAL ENERGY SYSTEMS [1]

Geothermal energy is a form of thermal energy generated in the core of the earth, about 6000 km below the surface. It is renewable because temperatures hotter than the surface of the sun are continuously produced inside the earth. The temperature at the core of the earth reaches up to 5000°C. Far from the core and towards the surface of the earth, this temperature decreases gradually to reach around 10°C at the surface. This gradient of temperature drives a continuous flux of thermal energy from the core to the surface, forming a wide range of energy sources. Geothermal energy sources range from shallow depth, of the order of few tens to few hundreds meters; to intermediate depths, of order of few kilometers; to even deeper depths with extremely high temperatures of molten rocks. Energy systems relying on the first type of energy source are commonly known as shallow geothermal systems, whereas those based on the other two types of sources are commonly referred to as deep geothermal systems.

Geothermal energy offers a number of advantages over conventional fossil fuel resources. Primarily, the geothermal heat resources are renewable, economic, and their environmental impact in terms of CO_2 emission is significantly lower. However, there are mainly two limitations: availability and cost. Geothermal projects, especially deep, can only be established in regions with abundant geothermal resources; generally, areas with recent tectonic activity. The cost of establishing deep geothermal systems is quite high and there is high risk of failure. Slight difference in the temperature of the extracted water from the planned can mean a large loss of investment.

Geothermal energy can be produced by drilling deep holes into the earth crust. Two systems are in use: open and closed. In the open system, the energy is produced by pumping cold water through one side of the reservoir; circulating it through hot fractured rock; and then collecting it in the other side, to be brought back to the surface. In the closed system, the energy is produced using a single borehole where cold water is pumped in one path and returned in another, using the same pipe.

Many geothermal systems have been developed, making use of the many advantages of the geothermal energy. They are in general classified into two categories: deep geothermal energy systems, and shallow geothermal systems. Deep geothermal systems are mainly those which go as deep as few kilometers below the surface and reach hydrothermal aquifers, dry hot rocks or magma. Projects involving electricity production or direct heat production are classified in this category. Shallow geothermal systems, on the other hand, are those that do not go more than 250m below the surface. The ground heat pump (GHP) is classified in this category. In this thesis the focus is on shallow geothermal systems.

1.1.1. SHALLOW GEOTHERMAL SYSTEMS [1]

A shallow geothermal energy system is an important source of thermal energy suitable for heating and cooling of individual buildings and small compounds. It is a renewable source of energy as heat transfer due to temperature gradient between the bottom of the earth and the air is continuously taking place. The seasonal temperature variation at the ground surface is reduced to a nearly constant temperature of around 12°C at approximately 10m below the surface. Under this depth, the temperature is known to increase with an average gradient of 3°C per 100m depth. The continuous thermal interaction between the air and the earth makes the first 100m sustainable and hence, suitable for supply and storage of thermal energy, though at a relatively low temperature.

There are two commonly utilized energy systems that make use of this kind of energy: the ground source heat pumps, and the underground thermal energy storage. Here only the ground source heat pumps are introduced.

1.1.2. GEOTHERMAL HEAT PUMPS [1]

Geothermal heat pumps (GHP) constitutes one of the most easy to extract and locally available in all parts of the world. It does not share the requirements of the other geothermal energy types in terms of geology or equipment. Rather, it makes use of the relatively constant temperature at shallow depths. In shallow grounds, just 10m below the surface, the earth maintains nearly a constant temperature ranging between 10°C and 20°C, depending on the region. Usually, the ground temperature at this depth is warmer than the air in winter and cooler in summer. Geothermal heat pumps are commonly used to exploit this abundant source of energy for heating and cooling of individual buildings and small compounds.

Geothermal heat pump systems consist of basically two parts: the ground heat exchanger, and the heat pump unit. The ground heat exchanger is a system of pipes, known as a loop, which is buried in the ground either vertically or horizontally. In winter, heat from the earth is extracted via a fluid, usually water or a mixture of water and antifreeze, circulating through the pipes at a certain rate and collecting heat from the earth. The heat pump extracts heat from the fluid and pumps it into the building. In summer, the process is reversed, and the heat pump extracts heat from the indoor air and transfers it to the heat exchanger. Heat removed from the indoor air during summer can also be used for heating water, which can be used for cooking and bathing.

1.1.3. GROUND-SOURCE HEAT PUMPS [1]

The ground-source heat pump (GSHP), also known as the geothermal heat pump (mentioned above), or the downhole heat exchanger (DHE), is a shallow geothermal system. In practice, there are mainly two kinds of GSHP: open and closed. The open system, also known as doublet, extracts heat from the groundwater and carries it to the surface using at least two separate wells. One well is used for the extraction of the groundwater, and another is used for the reinjection of the groundwater. The basic advantage of this system, as compared to the closed system, is that it is around eight times more efficient. However, this can be realized if the aquifer formation is highly permeable and the groundwater is relatively low in metals, avoiding thus maintenance problems associated with scaling, clogging and corrosion.

The closed system, on the other hand, extracts heat from the earth using heat exchangers embedded in the soil mass. The heat is carried by a fluid circulating inside a heat exchanger pipe and passed to a heat pump at the surface, usually inside the building. At the heat pump the collected heat is increased and transported to the heating system. The main advantage of this system, as compared to the open, is that there is no need to an aquifer, and, in principle, only one borehole is necessary for the extraction of thermal energy. Furthermore, the circulating fluid is usually clean, and hence needs little maintenance.

Closed systems are installed in mainly two ways: horizontal and vertical. The horizontal systems, also known as ground heat collectors, and horizontal loops, are relatively easy to install as less complicated excavation equipment is needed. The main source of heat of this kind of systems is the surface temperature, which comes by direct exposure to the sun. Depending on the area available, the horizontal pipes are laid in different ways, including series, parallel or spiral.

The vertical system is widely used, especially in areas where the land is scarce. The heat in such a system is extracted by borehole heat exchangers (BHE), also known as vertical ground heat exchangers or downhole heat exchangers, which consist of plastic pipes, mainly polyethylene or polypropylene, installed in a borehole as U-tubes and fixed by filling the borehole with grout. The U-tube carries a circulating fluid, referred to in the literature as refrigerant or working fluid. The U-tube effectively forms two pipes. One pipe receives the circulating fluid from the heat pump and conveys it downward. This pipe is denoted as pipe-in throughout

this thesis. The other pipe collects the circulating fluid at the bottom of pipe-in and brings it out to the surface, to enter the heat pump. This pipe is denoted as pipe-out throughout this thesis. The heat pump, usually located inside the building, extracts designed amount of heat from the fluid and pumps it back to the BHE. The circulating fluid, usually water with 20%–25% anti-freezing coolant such as Mono Ethylene Glycol, gets into contact with the surrounding soil via the U-tube material and the grout. The grout, usually bentonite-cement mix, exchanges heat with the soil and the BHE inner pipes.

Borehole heat exchangers are slender heat pipes with dimensions of the order of 30mm in diameter for the inner pipes, 150mm in diameter for the borehole, and 100m in length for the borehole and the inner pipes. In practice there are different types of BHE. They mainly differ in their configurations. Here some examples of the most commonly used configurations are given, namely:

- U-tubes: This BHE configuration consists of one (or more) inner pipe, which is inserted in the borehole from its middle to form a U-shape. Two main configurations are in use: single U-tube BHE and double U-tube BHE. Figure 1.1a shows a sketch of these two types of BHEs. The single U-tube BHE consists of pipe-in, where the working fluid enters; pipe-out, where the working fluid leaves; and grout, where the contact with the surrounding soil mass takes place. The double U-tube consists of two pipes-in, two pipes-out and grout.
- Coaxial: This BHE configuration consists of concentric pipes. In practice, there are mainly two coaxial configurations: annular (CXA) and centered (CXC), figure 1.1b. In CXA, pipe-out is configured inside pipe-in, forming an annular inlet and a centered outlet. Heat exchange of the inner pipes with the grout occurs along the surface area of pipe-in. In CXC, pipe-in is configured inside pipe-out, forming a centered inlet and an annular outlet. Here, heat exchange with the grout occurs via pipe-out.

The captured temperature from the earth is elevated by a heat pump and conveyed to a heating system. A heat pump is an important part of the shallow geothermal system. It is a mechanical device that transfers thermal energy from a region of a lower temperature to a region of a higher temperature. In the heating mode, the circulating fluid absorbs thermal energy from the ground. The heat pump exerts work on it, to increase its temperature, and then conveys it to the heating system of the building. In the cooling mode, the system is reversed and heat from the building is extracted and injected into the ground.

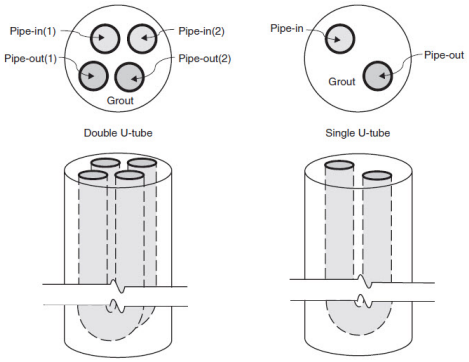

(a) U-tube shallow geothermal system

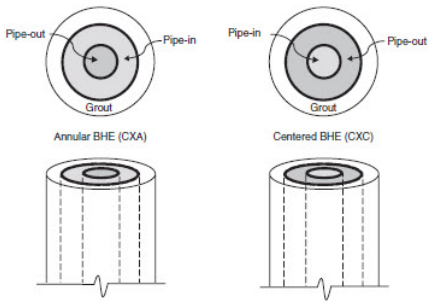

(b) Coaxial shallow geothermal system

Figure 1.1: Two main types of BHE [1]

1.1.4. PROBLEM DEFINITION

The U-tube shallow geothermal system consists of two main domains: the BHE and the soil mass surrounding it. The heat transfer in the system occurs by both conduction and convection mechanisms. While, from physical point of view the system is fairly simple to understand, the computational and modeling procedures can be extremely involved. The slenderness of the pipes due to their diameter/depth ratio along with the presence of both conduction and convection in the system, introduce computational challenges. Typical numerical tools to model such a system, namely finite element or finite difference, can be computationally demanding. In addition, inhomogeneities such as different soil layers with different physical properties will make the modeling procedures even more complicated.

In this thesis a semi-analytical model based on the spectral element method (SEM) for a U-tube shallow geothermal system, introduced by Al-khoury et al ([1], [2], [3], [9])), is modified and verified. In this model, the BHE is modeled using four main components: Pipe-in, where the refrigerant's inlet is located at its top; pipe-out, where the refrigerant's outlet is located at its top; grout, where the contact between the pipes and the soil mass is taken place; and soil film (figure (2.3b)).

The BHE is modeled as a pseudo 3D domain represented by one-dimensional heat flow in its components which are coupled to each other by means of thermal interaction coefficients. On the other hand, the soil mass surrounding the BHE is modeled radially. In order to connect the grout to the soil mass, the soil film has been introduced. The function of this film is to model heat flow in the soil mass in the z direction. The temperature of the soil film at a certain depth acts as an amplitude for the radial temperature of the soil mass. In this manner, the temperature of the soil mass can be obtained both in the z and the radial direction.

All components which are introduced here have physical representations; in contrast, the soil film is not physically present in the system and can have different thicknesses. Therefore, it is essential to investigate the effect of the soil film thickness on the heat flow in the system, which is one of the main goals of this thesis. Subsequently, the ability of the SEM model to predict the temperature of different domains in the U-tube shallow geothermal system is tested both in a single layer and multiple layers of soil.

The main advantage of the SEM model is that the computational time is significantly lower than conventional numerical techniques. In the SEM model, for each layer of soil only one element is required. Therefore, the need to deal with meshing techniques is limited. The only input to the model is the physical properties of the system which makes it extremely easy to work with.

As mentioned above, the heat flow in the grout is modeled in one dimension. In doing so, the grout is considered as a symmetrical annulus with inner radius of r_{eq} where r_{eq} is the equivalent radius for both pipe-in and pipe-out. The grout is subjected to the heat flow of both pipe-in and pipe-out (Figure 2.8b). Though, physically the positioning of pipe-in and pipe-out makes the grout act as a non-axially symmetric domain with nonuniform heat flow in radial direction. As a result, it would be a good practice to model the heat transfer of the grout using both radial and z directions. In order to make a step towards this goal and study the effect of the grout in radial direction, a model for coaxial shallow geothermal systems is developed using the same approach as the U-tube system. The symmetrical nature of coaxial shallow geothermal systems makes them a perfect candidate for modeling the grout and the soil mass in radial and z direction.

1.1.5. THESIS OBJECTIVES

The main objectives of this thesis are the following:

- **Modifying the U-tube SEM model:** as mentioned above, one of the main components of the BHE is the soil film. The soil film does not have any physical purpose and it was introduced in order to connect the grout which is modeled in the z direction to the soil mass which is modeled radially. With this approach, the temperature of the soil film acts as an amplitude for the temperature of the soil mass. As a results, the temperature of the soil mass can be obtained both in the radial and the z direction. It would be crucial to examine the effect of the soil film thickness on the model's behavior. The goal here is to observe how much the results are dependent on the soil film thickness. Ideally they should be independent. In this thesis this issue will be examined and after some minor modifications to the model, the computational results of the SEM model will become effectively independent of the soil film thickness.

- **Verification of U-tube SEM model:** upon implementing the modifications, the capabilities of the SEM model for modeling a U-tube shallow geothermal system embedded in a single-layer and a multi-layer soil mass will be verified. For this, two 3D detailed finite element models (For single and multiple layers of soil) will be simulated using COMSOL Multiphysics [4]. The computational results of the temperature distribution in pipe-in, pipe-out, grout and soil mass will be compared against results obtained from the SEM model. The geometrical dimensions of the models are made comparable to realistic dimensions of shallow geothermal systems.

- **Development of new coaxial model:** with a similar approach to the current SEM model for U-tube shallow geothermal systems and in order to study heat flow in the grout in the radial direction, a SEM model for coaxial shallow geothermal system will be developed.

2

SEM Model Modification and Verification

In this chapter the SEM model developed by Al-khoury et al ([2], [3]) is examined, modified and verified. Initially the theory behind the development of the model is introduced (This part is based on Noori BniLam and Rafid Al-Khoury [2]). Subsequently, a small example is solved using both detailed finite element in COMSOL Multiphysics [4] and the SEM model. This example is introduced in order to investigate the effect of the soil film on heat flow in the SEM model. Moreover, two modifications are done to the SEM model in order to reduce the effect of the soil film on the results. In the next step, an example with realistic geometrical dimensions is introduced and the temperature of different domains are investigated.

2.1. Original Spectral Element Model for U-tube Shallow Geothermal Systems

The original spectral model describing heat flow in shallow geothermal system has been introduced by Al-khoury [1]. In this model which consists of a borehole heat exchanger (BHE) and a soil mass, the heat flow in all of the components of the BHE, namely pipe-in, pipe-out and grout, are modeled in the z direction. The soil mass surrounding the BHE is modeled using cylindrical coordinates system (Figure 2.1). In order to link the BHE (modeled in the z direction) to the soil mass (modeled in the cylindrical coordinates system), an extra complex Fourier series is necessary in this model. To alleviate the need for this extra complex Fourier series, a soil film was introduced in the BHE model by Noori and Al-khoury [2] (Figure 2.2).

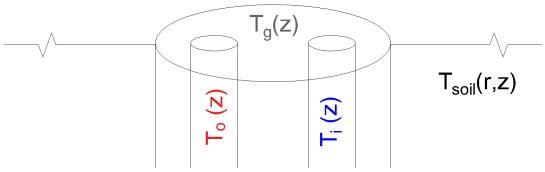

Figure 2.1: Original spectral element model

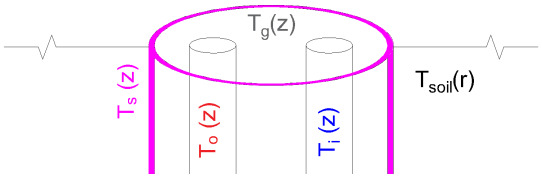

Figure 2.2: Current spectral element model

The soil film is a thin layer of soil surrounding the grout. The heat flow in this domain is also modeled in the z direction. The temperature of the soil film acts as an amplitude for the temperature of the soil mass. In this manner, the need for modeling the soil mass using cylindrical coordinates system is eliminated. Instead, heat flow in the soil mass is modeled only in the radial direction. This has improved the mathematical formulation and the computational implementation of the model. However, the soil film has no physical meaning and it is not obvious what thickness is optimal.

2.2. GOVERNING EQUATIONS FOR THE CURRENT SPECTRAL ELEMENT MODEL FOR U-TUBE SHALLOW GEOTHERMAL SYSTEMS

The conceptual model for U-tube shallow geothermal system along with its assumptions are shown in figure 2.3. The system consists of two main parts, the BHE and the soil mass. As it can be seen in figure 2.3a the refrigerant enters from one side of the system (Pipe-in) and after heat interaction with the grout, which is surrounded by the soil mass, leaves the system from the other side (Pipe-out).

The coupled heat transfer equations in all components of the BHE are modeled in one dimension, namely z axis. whereas, the heat transfer in the soil mass is modeled using an axially symmetric equation. The BHE components have the same coinciding z axis which is also the origin of the axially symmetric system for the soil mass domain (figure 2.3c). Moreover, the grout is surrounded by the soil film which is used to link the grout, which is modeled in the z direction, to the soil mass, which is modeled in the radial direction (figure 2.3b).

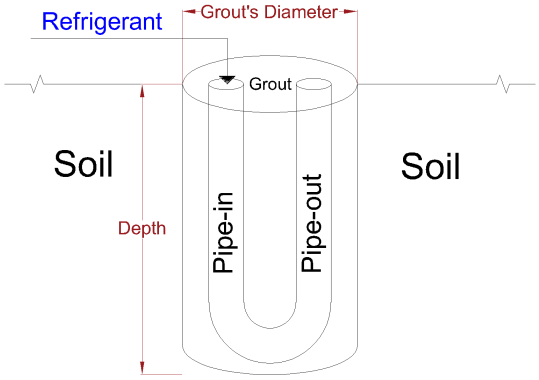

(a) Single U-tube shallow geothermal system

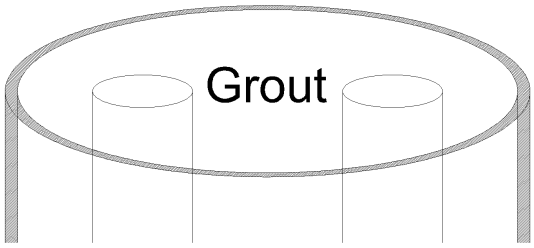

(b) Soil film surrounding the BHE

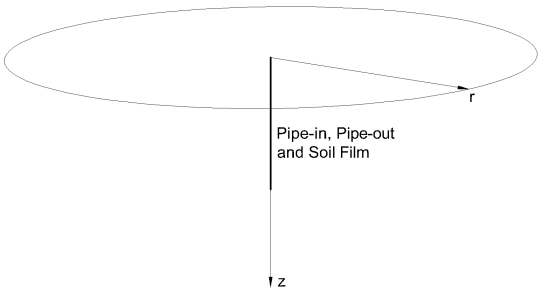

(c) The positive direction of coordinates system

Figure 2.3: Model's properties

The heat equations for the U-tube shallow geothermal system are:

Pipe-in

$$\rho c\frac{\partial T_i}{\partial t}dv_i-\lambda\frac{\partial^2 T_i}{\partial z^2}dv_i+\rho cu\frac{\partial T_i}{\partial z}dv_i+b_{ig}(T_i-T_g)ds_{ig}=0 \tag{2.2.1}$$

Pipe-out

$$\rho c\frac{\partial T_o}{\partial t}dv_o-\lambda\frac{\partial^2 T_o}{\partial z^2}dv_o-\rho cu\frac{\partial T_o}{\partial z}dv_o+b_{og}(T_o-T_g)ds_{og}=0 \tag{2.2.2}$$

Grout

$$\rho_g c_g\frac{\partial T_g}{\partial t}dv_g-\lambda_g\frac{\partial^2 T_g}{\partial z^2}dv_g+b_{og}(T_g-T_o)ds_{og}+b_{ig}(T_g-T_i)ds_{ig}+b_{gs}(T_g-T_s)ds_{gs}=0 \tag{2.2.3}$$

Soil Film

$$\rho_s c_s\frac{\partial T_s}{\partial t}dv_s-\lambda_s\frac{\partial^2 T_s}{\partial z^2}dv_s+b_{gs}(T_s-T_g)ds_{gs}+b_{ss}(T_s-T_{soil}|_{r=r_s})ds_{ss}=0 \tag{2.2.4}$$

where the subscript i, o, g and s represent pipe-in, pipe-out, grout and soil film respectively. T_i, T_o, T_g and T_s are the temperatures of pipe-in, pipe-out, grout and soil film which are a function of z; λ, λ_g and λ_s $(W/m.K)$ are the thermal conductivity of fluid, grout and soil film; u (m/s) is the velocity of the refrigerant in the pipes which has a positive sign in pipe-in (Towards positive z axis) and negative sign in pipe-out (Towards negative z axis); b_{ig}, b_{og}, b_{gs} and b_{ss} $(W/m^2.K)$ are the reciprocal of the thermal resistance between pipe-in-grout, pipe-out-gout, grout-soil film and soil film-soil mass respectively; c $(J/kg.K)$ stands for the specific heat of the domain and $\rho(kg/m^3)$ is the mass density; dv_i, dv_o, dv_g and dv_s (m^3) are partial volume of pipe-in, pipe-out, grout and soil film; ds_{ig}, ds_{og}, ds_{gs} and ds_{ss} (m^2) are partial surface area between pipe-in-grout, pipe-out-grout, grout-soil film and soil film-soil mass respectively.
The soil film is used in order to connect the BHE to the soil mass; moreover, the temperature of the soil film acts as an amplitude for the temperature of soil mass. In this manner, heat conduction in z direction in the soil mass is also taken into consideration.

The initial and boundary conditions for these domains are:

$$T_i(z,0)=T_o(z,0)=T_g(z,0)=T_s(z,0)=T_{soil}(r,z,0) \qquad \text{Initial temperature of all domains} \tag{2.2.5}$$

$$T_i(0,t)=T_{in}(t) \qquad \text{Input temperature} \tag{2.2.6}$$

$$T_i(h,t)=T_o(h,t) \qquad \text{Connecting the pipes at the bottom (z=h)} \tag{2.2.7}$$

The radial transient heat conduction equation for the soil domain can be described as:

$$\frac{1}{\alpha_{soil}}\frac{\partial T_{soil}}{\partial t}-\frac{\partial^2 T_{soil}}{\partial r^2}-\frac{1}{r}\frac{\partial T_{soil}}{\partial r}=0 \qquad \alpha_{soil}=\frac{\lambda_s}{\rho_s c_s} \tag{2.2.8}$$

There are 2 conditions that are needed to be applied to (2.2.8). A boundary condition at infinity and a boundary condition where the soil mass meets the soil film. At infinity, it is logical to neglect the effect of the BHE on soil mass temperature, leading to:

$$\Delta T|_{r=\infty}=T|_{r=\infty}-T_{st}=0 \tag{2.2.9}$$

T_{st} is the initial steady state temperature. At the interface where the soil mass meets the soil film, there are two choices, namely equalizing the temperatures or the fluxes. The former corresponds to a Dirichlet boundary condition while the latter to a Neumann boundary condition:

$$T_{soil}|_{r=r_s}=T_s \qquad \text{Dirichlet} \tag{2.2.10}$$

$$\lambda_{soil}\frac{\partial T_{soil}(r,t)}{\partial r}|_{r=r_s}ds_{ss}=b_{ss}(T_{soil}(r_s,t)-T_s(z,t))ds_{ss} \qquad \text{Neumann} \tag{2.2.11}$$

In which $r=r_s$ is where the soil domain and the soil film have contact. Moreover, the differential terms ds_{ss} on right side and left side of (2.2.11) will cancel out each other.

SOLUTION OF EQUATIONS

To eliminate the time derivative, Fourier transform is utilized. The transformed equations in the frequency domain are:

Pipe-in

$$-\lambda\frac{\partial^2\hat{T}_i}{\partial z^2}dv_i+\rho cu\frac{\partial\hat{T}_i}{\partial z}dv_i+(i\omega\rho cdv_i+b_{ig}ds_{ig})\hat{T}_i-b_{ig}ds_{ig}\hat{T}_g=0 \tag{2.2.12}$$

Pipe-out

$$-\lambda\frac{\partial^2\hat{T}_o}{\partial z^2}dv_o-\rho cu\frac{\partial\hat{T}_o}{\partial z}dv_o+(i\omega\rho cdv_o+b_{og}ds_{og})\hat{T}_o-b_{og}ds_{og}\hat{T}_g=0 \tag{2.2.13}$$

Grout

$$-\lambda_g\frac{\partial^2\hat{T}_g}{\partial z^2}dv_g+(i\omega\rho_g c_g dv_g+b_{ig}ds_{ig}+b_{og}ds_{og}+b_{gs}ds_{gs})\hat{T}_g$$
$$-b_{ig}ds_{ig}\hat{T}_i-b_{og}ds_{og}\hat{T}_o-b_{gs}ds_{gs}\hat{T}_s=0 \tag{2.2.14}$$

Soil film

$$-\lambda_s\frac{\partial^2\hat{T}_s}{\partial z^2}dv_s+(i\omega\rho_s c_s dv_s+b_{gs}ds_{gs}+b_{ss}ds_{ss})\hat{T}_s-b_{gs}ds_{gs}\hat{T}_g-b_{ss}ds_{ss}\hat{T}_{Soil}|_{r=r_s}=0 \tag{2.2.15}$$

Equations (2.2.12)-(2.2.15) form a system of non-homogeneous ordinary differential equations due to the presence of $\hat{T}_{Soil}$ in equation (2.2.15). As will be seen, after solving the radial transient heat conduction equation for the soil mass, the system will be changed to a homogeneous set of equations (see equation 2.2.26).
Using the Fourier transform, the transient heat conduction equation for the soil domain can be transformed into the frequency domain as well:

$$\frac{i\omega}{\alpha_{soil}}\hat{T}_{soil}-\frac{\partial^2\hat{T}_{soil}}{\partial r^2}-\frac{1}{r}\frac{\partial\hat{T}_{soil}}{\partial r}=0 \tag{2.2.16}$$

where $\hat{T}$ indicates the temperature of each domain in the frequency domain.
The boundary conditions can also be show in the frequency domain as:

$$\hat{\Delta}T|_{r=\infty}=\hat{T}|_{r=\infty}-\hat{T}_{st}=0 \tag{2.2.17}$$

$$\hat{T}_{soil}|_{r=r_s}=\hat{T}_s \qquad \text{Dirichlet} \tag{2.2.18}$$

$$\lambda_{soil}\frac{\partial\hat{T}_{soil}(r,\omega)}{\partial r}|_{r=r_s}=b_{ss}(\hat{T}_{soil}(r_s,\omega)-\hat{T}_s(z,\omega)) \qquad \text{Neumann} \tag{2.2.19}$$

Equation (2.2.16) is a complex ordinary differential equation, describing a modified Bessel equation. The solution of it can be expressed as:

$$\hat{T}_{soil}(r,\omega)=A_sK_0(k_{soil}r)+B_sI_0(k_{soil}r) \tag{2.2.20}$$

in which I_0 and K_0 are the modified Bessel functions of the first and second kind and $k_{soil}=\sqrt{\frac{i\omega}{\alpha_{soil}}}$.
Applying the boundary condition (2.2.17) to (2.2.20) gives:

$$\hat{T}_{soil}(r,\omega)=A_sK_0(k_{soil}r) \tag{2.2.21}$$

By imposing the boundary condition (2.2.18) or (2.2.19) on (2.2.21) $\hat{T}_{soil}(r,\omega)$ can be calculated as:

$$\hat{T}_{soil}(r,\omega)=\frac{T_s}{K_0(k_{soil}r_s)}K_0(k_{soil}r) \qquad \text{Dirichlet} \tag{2.2.22}$$

$$\hat{T}_{soil}(r,\omega)=-\frac{b_{ss}(\hat{T}_{soil}(r_s,\omega)-\hat{T}_s(z,\omega))}{\lambda k_{soil}}\frac{K_0(k_{soil}r)}{K_1(k_{soil}r_s)} \qquad \text{Neumann} \tag{2.2.23}$$

Calculating T_{soil} at r_s, the solution can be simplified in both cases:

$$\hat{T}_{soil}(r_s,\omega) = \hat{T}_s \qquad \text{Dirichlet} \tag{2.2.24}$$

$$\hat{T}_{soil}(r_s,\omega) = A_m \hat{T}_s \qquad \text{Neumann} \tag{2.2.25}$$

where $A_m = \dfrac{\Phi(r,\omega)}{\Phi(r,\omega)+1}$ by assuming $\Phi(r,\omega) = \dfrac{b_{ss}K_0(k_{soil}r)}{\lambda k K_1(k_{soil}r)}$. In order to eliminate the inhomogeneity in equation (2.2.15), $\hat{T}_{soil}(r_s,\omega)$ needs to be calculated which in case of Neumann boundary condition would be equal to:

$$\hat{T}_{soil}(r_s,\omega) = \frac{\Phi(r_s,\omega)}{\Phi(r_s,\omega)+1}\hat{T}_s(z,\omega) = A_m \hat{T}_s \tag{2.2.26}$$

Based on (2.2.26), (2.2.15) can be simplified to:

Soil Film

$$-\lambda_s \frac{d^2\hat{T}_s}{dz^2} dv_s + (i\omega\rho_s c_s dv_s + b_{gs}ds_{gs} + b_{ss}ds_{ss}(1-A_m)\hat{T}_s - b_{gs}ds_{gs}\hat{T}_g \tag{2.2.27}$$

It is worth mentioning that, in the equation 2.2.4 the heat interaction between the soil film and the soil mass is taken into consideration by the term $b_{ss}(T_s - T_{soil}|_{r=r_s})ds_{ss}$. This term is responsible for the exchange of heat flux between these two domains. As a result, it would be logical to choose the same type of boundary condition between these two domains while formulating the boundary conditions for the soil mass. This can be done by opting for the Neumann boundary condition which equalizes the fluxes between these two domains.

Using equation 2.2.27 instead of equation 2.2.15, the system of homogeneous differential equations for U-tube shallow geothermal system can be solved by eigenfunction expansion. As a result, the following solutions are proposed for each domain:

$$\hat{T}_i = A_i e^{-ikz}, \quad \hat{T}_o = A_o e^{-ikz}, \quad \hat{T}_g = A_g e^{-ikz}, \quad \hat{T}_s = A_s e^{-ikz} \tag{2.2.28}$$

After substitution of the above solution in each domain, (2.2.12)-(2.2.14) and (2.2.27) can be written as:

Pipe-in

$$k^2\lambda d v_i A_i e^{-ikz} - ik\rho c u d v_i A_i e^{-ikz} + (i\omega\rho c d v_i + b_{ig}ds_{ig})A_i e^{-ikz} - b_{ig}ds_{ig}A_g e^{-ikz} = 0 \tag{2.2.29}$$

Pipe-out

$$k^2\lambda d v_o A_o e^{-ikz} + ik\rho c u d v_o A_o e^{-ikz} + (i\omega\rho c d v_o + b_{og}ds_{og})A_o e^{-ikz} - b_{og}ds_{og}A_g e^{-ikz} = 0 \tag{2.2.30}$$

Grout

$$\begin{aligned} &k^2\lambda_g d v_g A_g e^{-ikz} + (i\omega\rho_g c_g d v_g + b_{ig}ds_{ig} + b_{og}ds_{og} + b_{gs}ds_{gs})A_g e^{-ikz} \\ &- b_{ig}ds_{ig}A_i e^{-ikz} - b_{og}ds_{og}A_o e^{-ikz} - b_{gs}ds_{gs}A_s e^{-ikz} = 0 \end{aligned} \tag{2.2.31}$$

Soil Film

$$k^2\lambda_s d v_s A_s e^{-ikz} + (i\omega\rho_s c_s d v_s + b_{gs}ds_{gs} + b_{ss}ds_s(1-A_m)A_s e^{-ikz} - b_{gs}ds_{gs}\hat{T}_g \tag{2.2.32}$$

In a matrix form:

$$\begin{pmatrix} a_{11} & 0 & a_{13} & 0 \\ 0 & a_{22} & a_{23} & 0 \\ a_{31} & a_{32} & a_{33} & 0 \\ 0 & 0 & a_{43} & a_{44} \end{pmatrix} \begin{pmatrix} A_i \\ A_o \\ A_g \\ A_s \end{pmatrix} = 0 \tag{2.2.33}$$

Where

$$a_{11} = k^2\lambda d v_i - ik\rho c u d v_i + i\omega\rho c d v_i + b_{ig} d s_{ig}$$
$$a_{13} = -b_{ig} d s_{ig}$$
$$a_{22} = k^2\lambda d v_o + ik\rho c u d v_o + i\omega\rho c d v_o + b_{og} d s_{og}$$
$$a_{23} = -b_{og} d s_{og}$$
$$a_{31} = -b_{ig} d s_{ig}$$
$$a_{32} = -b_{og} d s_{og}$$
$$a_{33} = k^2\lambda_g d v_g + i\omega\rho_g c_g d v_g + b_{ig} d s_{ig} + b_{og} d s_{og} + b_{gs} d s_{gs}$$
$$a_{34} = -b_{gs} d s_{gs}$$
$$a_{43} = -b_{gs} d s_{gs}$$
$$a_{44} = k^2\lambda_s d v_s + i\omega\rho_s c_s d v_s + b_{gs} d s_{gs} + b_{ss} d s_{ss}(1 - A_m)$$

Non-trivial solution of (2.2.33) can only be obtained by letting the determinant equal to zero. This will lead to the following complex eight degree polynomial:

$$a_8 k^8 + a_7 k^7 + a_6 k^6 + a_5 k^5 + a_4 k^4 + a_3 k^3 + a_2 k^2 + a_1 k + a_0 = 0 \tag{2.2.34}$$

The polynomial coefficients are given in [2]. By solving the above polynomial the eigenvalues of the system are calculated. Eight eigenvalues can be calculated which will be denoted by $k_i, i = 1\ldots8$. Because all the elements in the system are coupled, every constant in (2.2.33) can be related to the other constants:

$$A_i = -\frac{a_{13}}{a_{11}} A_g = Y^{ig} A_g$$
$$A_o = -\frac{a_{23}}{a_{22}} A_g = Y^{og} A_g$$
$$A_s = -\frac{a_{43}}{a_{44}} A_g = Y^{sg} A_g \tag{2.2.35}$$

SPECTRAL ELEMENT FORMULATION

Based on the derived equations above, a two-node spectral element can be formulated (The detailed formulation is given in Appendix A). The spectral element equations results to:

$$\hat{\mathbf{q}}_{node} = \mathbf{K}(k, \omega_n)\hat{\mathbf{T}}_{node} \tag{2.2.36}$$

Equation (2.2.36) describes a relationship between the fluxes and the temperatures in the element domain which is similar to finite element method. The main difference here with finite element method is the fact that all of the equations are solved analytically without any approximation in their solutions. This means that if the properties of the system do not change in the z direction, the system can be solved using only one element. On the other hand, if the properties change, for instance having multiple soil layers, only one element per soil layer is needed. Figure 2.4 shows a 2-node spectral element, the temperature of all the components of the BHE can be calculated within this element. Subsequently, the temperature of the soil mass can be calculated in the radial direction as well. Moreover, $\mathbf{K}(k, \omega_n)$ is the spectral element stiffness matrix which is frequency dependent. The assembly of the spectral element stiffness matrix can be done using the well-known finite element matrix assembling techniques. Dealing with small matrices results in the significant reduction of the computation time.

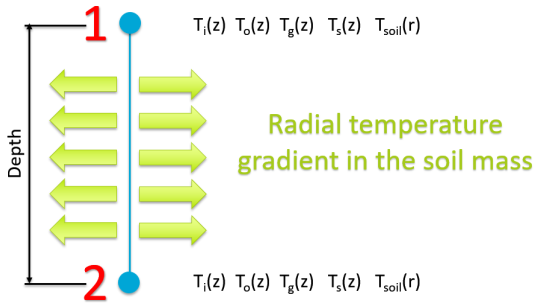

Figure 2.4: 2-node spectral element

2.3. EXAMINING THE EFFECT OF SOIL FILM THICKNESS VIA DETAILED FINITE ELEMENT MODEL

In this section, the effect of the soil film thickness on the results of the SEM model is examined. This is done by comparing the computational results of the SEM model to a detailed finite element model. This is necessary since all of the components in the SEM model have physical representations; whereas, the soil film is added in order to link the BHE to the soil mass. This means that the soil film is not physical and can have different thicknesses. The main goal of this part is to examine the influence of the soil film thickness on the heat flow in the system. Ideally, the results should have little dependency, if any, on the soil film thickness.

The geometry of the system in COMOSOL Multiphysics [4] consists of a U-tube pipe, a grout and a soil mass. In order to decrease the computation time, symmetry is used for modeling. Figure (2.5) shows the geometry of the system and its meshing. The depth of the BHE is 1.1 meter while the depth of the soil mass is 1.2 meters. The soil block surrounding the BHE is 3×3 meters. As will be mentioned, at the boundaries of the soil mass zero temperature has been applied, this is because of the fact that at infinity the effect of the BHE on the soil mass vanishes. Ideally it would be beneficial to choose the dimensions of the soil mass relatively large in order to prevent any impact from its boundary conditions on the BHE temperature. In this small model however, since the focus is mostly on the effect of the soil film thickness on the SEM results, the soil mass in the FEM model is chosen to be only 3×3 meters to reduce the computation time. More details are given in table 2.1 and 2.2

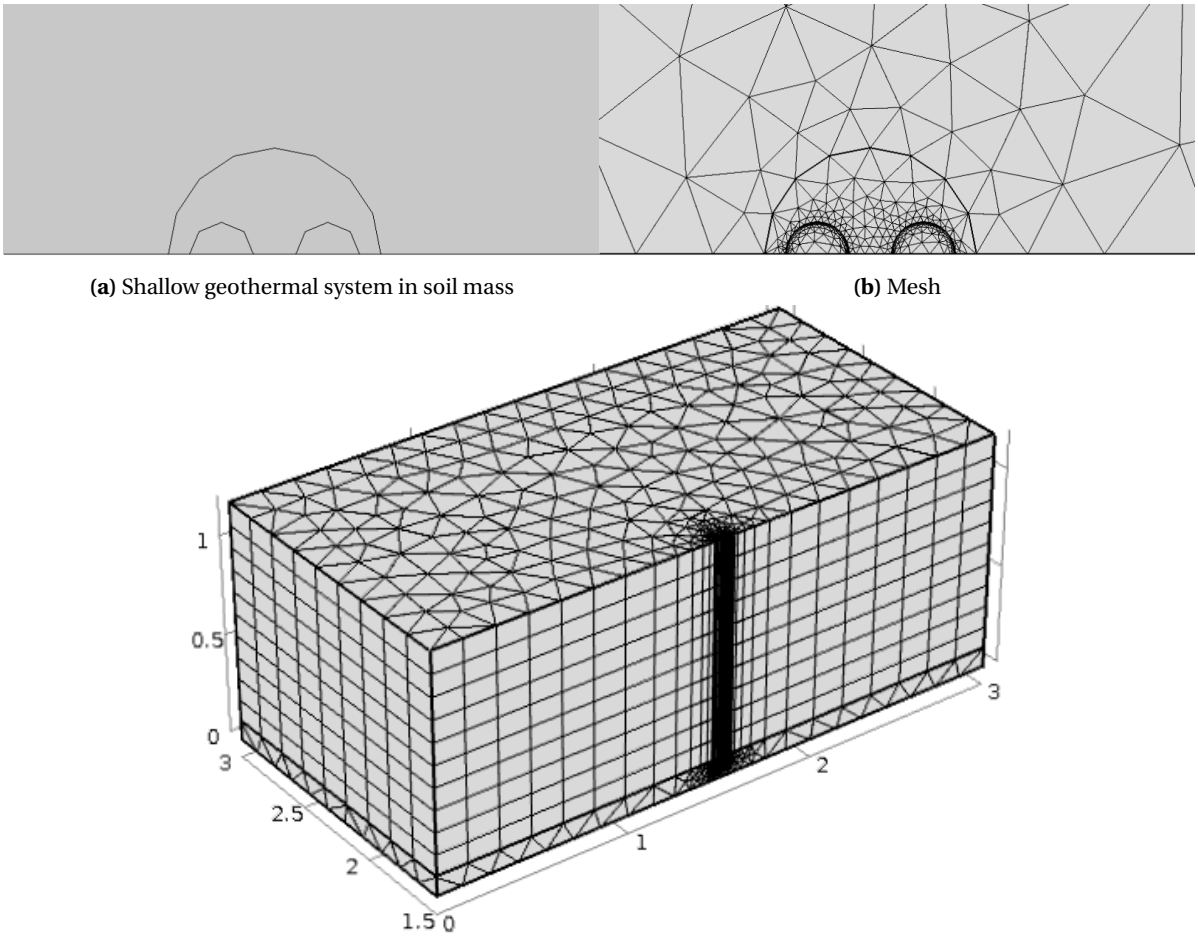

(a) Shallow geothermal system in soil mass

(b) Mesh

(c) Top view

Figure 2.5: COMSOL multiphysics model

SEM Model	
Number of Elements	1
Computational Time	Under 20 seconds
FEM Model	
Number of Elements	15779
Computational Time [min]	3

Table 2.1: Computational information

Borehole's Properties	
Borehole Length (L) [m]	1.1
Borehole Radius (r_g) [m]	0.05
Pipe Inner Radius (r_i) [m]	0.015
Pipe wall thickness (ds) [m]	0.002
Fluid Flow Situation	Laminar
Pipe wall Thermal Conductivity) (λ_{pipe}) [W/(m.K)]	0.42
Fluid's Properties	
Density (ρ) [$kg/(m^3)$]	1000
Specific Thermal Capacity (c) [J/(kg.K)]	4186
Thermal Conductivity (λ) [W/(m.K)]	0.56
Dynamic Viscosity (μ) [Pa.s]	0.001
Velocity (u) [m/s]	0.1
Input temperature (T_{in}) [°C]	20
Grout's Properties	
Density (ρ_g) [$kg/(m^3)$]	1420
Specific Thermal Capacity (c_g) [J/(kg.K)]	1197
Thermal Conductivity (λ) [W/(m.K)]	0.65
Soil Film Thickness (dg) [m]	Varying
Soil's Properties	
Depth (h) [m]	1.2
Density (ρ_g) [$kg/(m^3)$]	1680
Specific Thermal Capacity (c_g) [J/(kg.K)]	400
Thermal Conductivity (λ) [W/(m.K)]	2.5

Table 2.2: Properties of the model

The following boundary conditions are applied in COMSOL:

- **Inlet of pipe-in:** Input temperature $\big(T(0,t) = T_{in}\big)$, Input Velocity $\big(u(0,t) = u\big)$.
- **Outlet of pipe-out:** Outlet (Zero pressure at pipe's outlet) , Outflow (This node provides a suitable boundary condition for convection-dominated heat transfer at outlet boundaries. In a model with convective heat transfer, this condition states that the only heat transfer occurring across the boundary is by convection. The temperature gradient in the normal direction is zero, and there is no radiation. This is usually a good approximation of the conditions at an outlet boundary in a heat transfer model with fluid flow. [4]).
- **Top and bottom of the soil mass and grout**: Fully insulated which implies that the interaction with air and also the soil beneath the model is neglected. This is an accurate assumption due to the fact that in the SEM model these factors are not considered as well.
- **Soil mass's boundary:** $T_{soil} = 0$

Due to the small scale of the model and the goal of this analysis, only the temperature of the grout domain is examined. Subsequently, the temperature of the other domains will be verified with a model which its dimensions are closer to realistic cases (See section 2.4).

GROUT'S TEMPERATURE (DIRICHLET BOUNDARY CONDITION AT THE SURFACE BETWEEN SOIL MASS AND SOIL FILM)

The temperature of the grout domain from the detailed FEM model is compared to the SEM model. In order to investigate the impact of the soil film on the results, different thicknesses for the soil film are considered. Figure (2.6) shows the temperature of the grout in different times during the analysis (after 0.5 hour, 5 hours, 24 hours and 48 hours). The results from COMSOL are given using a solid line, whereas the SEM model results are given in dashed lines.

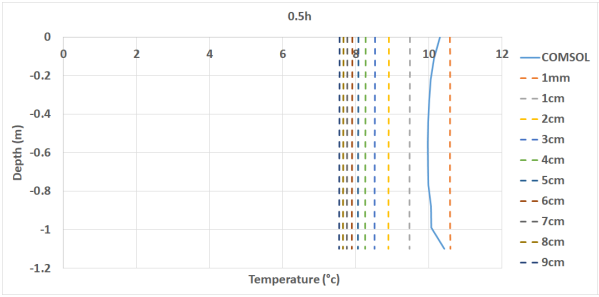

(a) t=0.5 hour

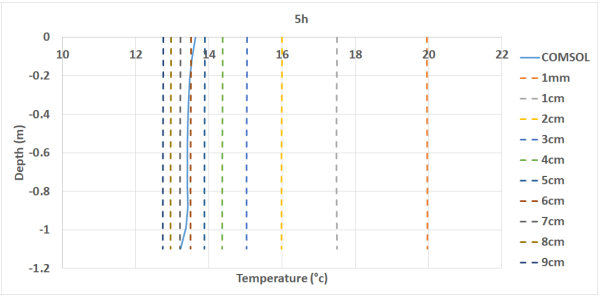

(b) t=5 hours

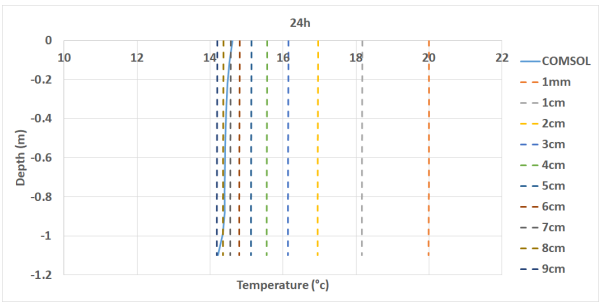

(c) t=24 hours

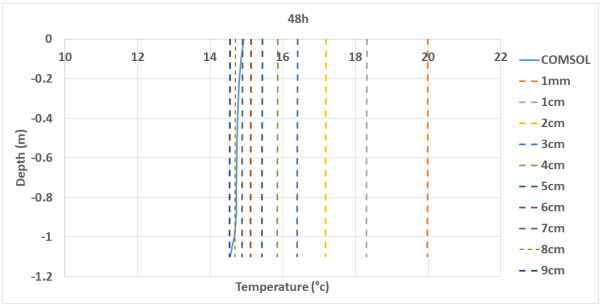

(d) t=48 hours

Figure 2.6: Temperature of grout at different times with respect to depth

As it can be seen, the results of the SEM model are significantly dependent on the soil film thickness. If the soil film thickness is 1mm, the grout temperature based on the SEM results reach 20°C after 5 hours (Figure 2.6b, 2.6c and 2.6d). This is is far from what COMSOL predicts which is between 13°C to 15°C depending on the output time. More importantly, since the fluid input temperature is 20°C, the grout temperature should indeed be lower than that. Moreover, additional observations on figure 2.6b reveals that by changing the soil film thickness from 1mm to 9cm the temperature prediction for the grout domain changes around 7°C. If this model is intended to be used in engineering practices, the soil film thickness must have little to no influence on the results. In this thesis, this issue has been solved.

In the upcoming sections, two main modifications are proposed in order to improve the results and reduce the dependency on the soil film thickness. These modifications focus on the boundary condition between the soil film and the soil mass and subsequently on the thermal interaction coefficients which are responsible for the heat transfer between different components of the system.

GROUT'S TEMPERATURE (NEUMANN BOUNDARY CONDITION AT THE SURFACE BETWEEN SOIL MASS AND SOIL FILM)

The same results as the previous section are shown here with the difference that instead of using Dirichlet boundary condition for connecting the soil film and the soil mass, the Neumann boundary condition is used (equation 2.2.11). As it was mentioned in section 2.2, in equation 2.2.4 the heat interaction between the soil film and the soil mass is modeled by equalizing the fluxes. The same type of boundary condition should be chosen while formulating the boundary condition for the soil mass. This can be done by opting for the Neumann boundary condition which equalizes the fluxes between these two domains.

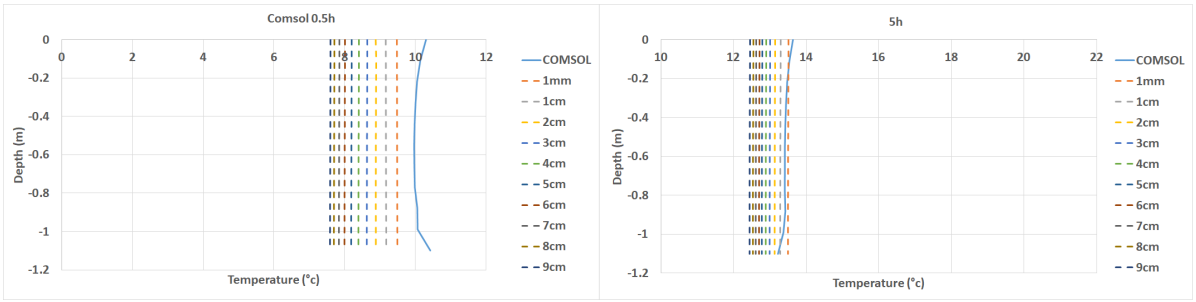

(a) t=0.5 hour

(b) t=5 hours

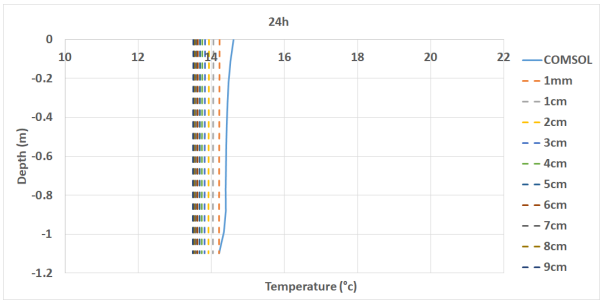

(c) t=24 hours

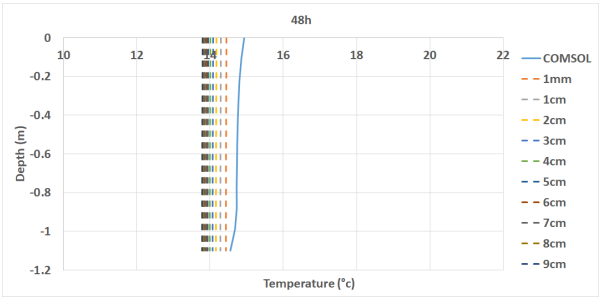

(d) t=48 hours

Figure 2.7: Temperature of grout at different times with respect to depth

The graphs show that the dependency on the soil film thickness is indeed reduced compared to the previous chapter. This, as mentioned above, is due to the use of the Neumann boundary condition. The term $b_{ss}(T_s - T_{soil}|_{r=r_s})ds_{ss}$ in equation 2.2.4 is responsible for the heat interaction between the soil mass and the soil film by means of flux exchange. The Neumann boundary condition, equation 2.2.19, uses the same term and equalizes it to the flux in the soil mass. Therefore, the Nuemann boundary condition is more accurate to use in the context of the SEM formulation. In the next section, another modification is done to the model. All the results presented hereafter from the SEM model are given based on the Neumann boundary condition between the soil film and the soil mass.

THERMAL INTERACTION COEFFICIENTS EXAMINATION

One of the key elements in the SEM model is the thermal interaction coefficients. These terms are responsible for the coupling between different parts of the system. As a result, it is beneficial to examine them with more details. In the initial model, which all the results so far are based upon, the thermal interaction coefficients are defined as the following [2]:

$$b_{ig} = b_{og} = \frac{1}{R_{pipe} + R_{conv}} \quad \left(R_{conv} = \frac{1}{r_i / r_o \bar{h}} \; (\bar{h} = \frac{Nu \cdot \lambda}{2r_i}), \quad R_{pipe} = r_o \frac{\mathrm{Ln}(r_o/r_i)}{\lambda_{pipe}}\right) \tag{2.3.1}$$

$$R_g = r_g \frac{\mathrm{Ln}(r_g/r_{eq})}{\lambda_g} (r_{eq} = \sqrt{2r_o^2}) \tag{2.3.2}$$

$$R_s = r_s \frac{\mathrm{Ln}(r_s/r_g)}{\lambda_s} \tag{2.3.3}$$

In which r_i and r_o are inner and outer radius of pipes; r_g is the grout radius while r_s is the soil film radius from the center of the system. r_{eq} is the equivalent radius corresponding to both pipe-in and pipe-out where the two pipes are approximated with a bigger pipe with the radius of r_{eq} (figure 2.8b). λ_{pipe}, λ_g and λ_{soil} are the thermal conductivity of pipes' material, grout and soil respectively. $\bar{h}$ is the convective heat transfer coefficient where Nu is the Nusselt number. The thermal resistivity which is based on Y-configuration analogy to Ohm's law [1] are given as below (figure 2.8a):

$$R_{gs} = \frac{1}{R_{ig}||R_{og} + R_g} = \frac{1}{\frac{R_{ig}R_{og}}{R_{ig}+R_{og}} + R_g} \quad \text{Grout-Soil Film} \tag{2.3.4}$$

$$R_{ss} = \frac{1}{R_{gs} + R_s} \quad \text{Soil Film-Soil Mass} \tag{2.3.5}$$

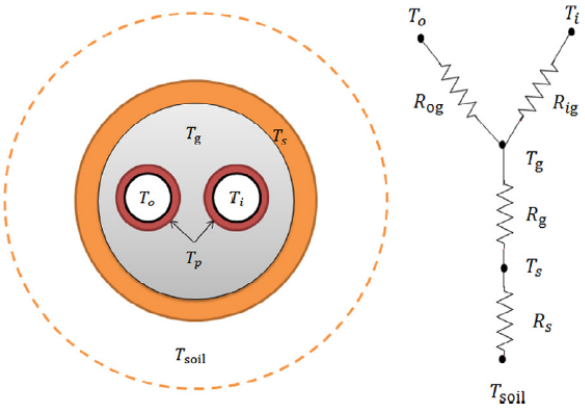

(a) Analogy of BHE and Y-configuration [2]

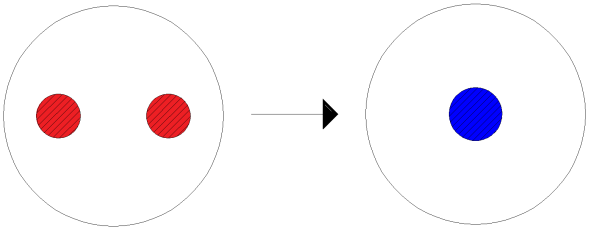

(b) Pipes area approximation

Figure 2.8: Resistance of BHE components

It can be noted from (2.3.4) and (2.3.5) that the thermal resistance between each domain and the one adjacent to it is dependent on the other domains as well. For example, the resistance between the grout and the soil Film is also a function of the resistance of the pipes. Looking at the set of equations which define the BHE ((2.2.1)-(2.2.4)) it can be observed that each equation is written independently and then connected using the thermal coefficients. Therefore, the coefficients should be defined only based on each domain and they should not be dependent on other domains, in other words changing the material of the pipes should not affect the resistance of the grout. As a result, the dependency of the domains to each other should be eliminated. This also can be observed in figure 2.8, the resistance between T_g and T_s is only R_g and it's not a function of other domains. The new proposed thermal coefficients terms are as following:

$$R_{gs} = R_g = r_g \frac{\mathrm{Ln}(r_g/r_{eq})}{\lambda_g} (r_{eq} = \sqrt{2r_{out}^2}) \qquad \text{Grout-Soil Film} \qquad (2.3.6)$$

$$R_{ss} = R_s = r_s \frac{\mathrm{Ln}(r_s/r_g)}{\lambda_s} \qquad \text{Soil Film-Soil Mass} \qquad (2.3.7)$$

With the above modification, the results of the same region is shown one more time:

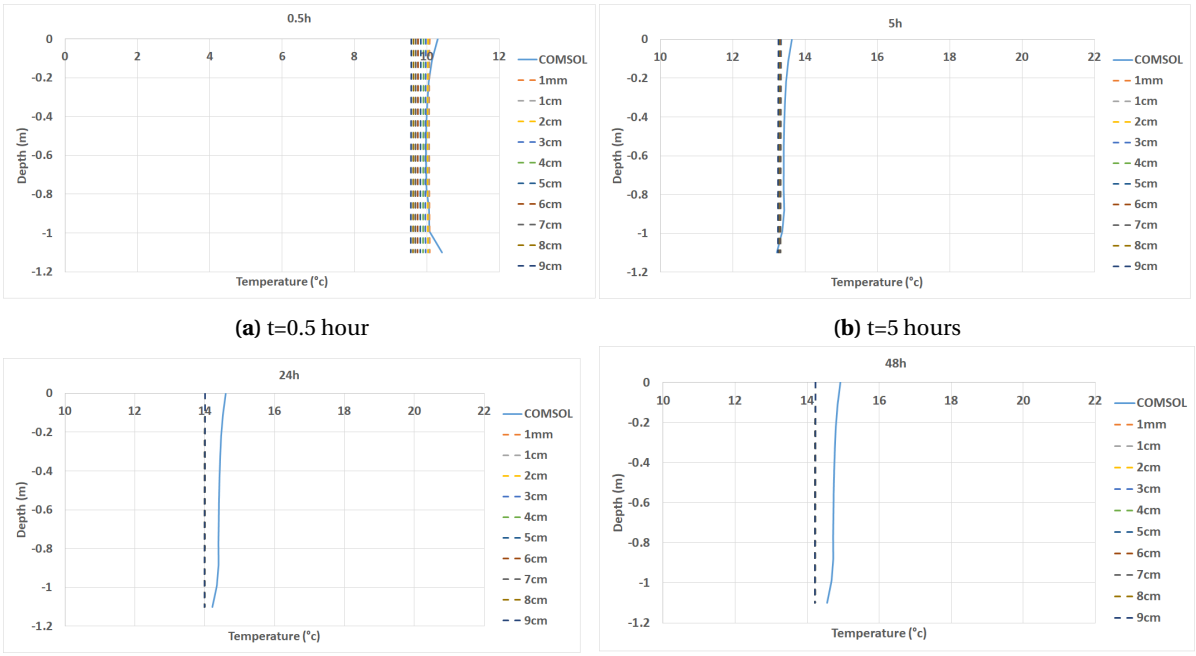

(a) t=0.5 hour

(b) t=5 hours

(c) t=24 hours

(d) t=48 hours

Figure 2.9: Temperature of grout at different times with respect to depth

As it can be seen, the dependency of the SEM model on the thickness of the soil film has been reduced significantly. Though, it is apparent that the SEM results does not match COMSOL results and there is around 1°C difference between the two models (Figure 2.9d). This temperature difference can be related to the fact that the FEM model is 3D and detailed, whereas the SEM model assumes a one-dimensional heat flow in the grout. The grout in the FEM model contains both of the pipe-in and the pipe-out and it is under the influence of non-uniform heat flow coming from both of the pipes. Whereas, in the SEM model the two pipes are represented as one equivalent heat source to the grout as shown in figure 2.8b. In addition, the velocity of the refrigerant in the SEM model is constant while in the FEM model the fluid has a velocity profile in pipes' cross section (Figure 2.12). It is essential to highlight the fact that the goal of this section was to eliminate the effect of the soil film thickness in the temperature distribution. Therefore, no further attempts were made to obtain a better match between the SEM and the FEM models.

2.4. VERIFICATION OF SEM MODEL VERSUS DETAILED FEM MODEL

After reducing the effect of the soil film on the results, it would be beneficial to observe the capability of the model for predicting the temperature in a simulation with realistic geometrical dimensions.

Similar to section 2.3 the geometry of the system in COMOSOL Multiphysics [4] consists of a U-tube pipe, grout and soil mass. The difference lies in the fact the the dimensions of the system are now close to a realistic case. Symmetry is utilized to reduce the computation time. Figure 2.10a shows the BHE embedded in the soil mass. The BHE is 100 meters deep and the soil block is 100×100 to prevent the effect of the temperature at soil boundaries. The slenderness of BHE components compared to the soil mass can be clearly seen. Figures 2.10b to 2.10c show the meshing of the system from different views. The finer mesh in the pipes compared to the other parts of the system can be observed in 2.10c and 2.10d. Two different examples are examined with different refrigerant velocities, in the first case the velocity of the refrigerant is 0.5m/s and in the second case the velocity is 1m/s. More details of the model are given in table 2.3 and 2.4.

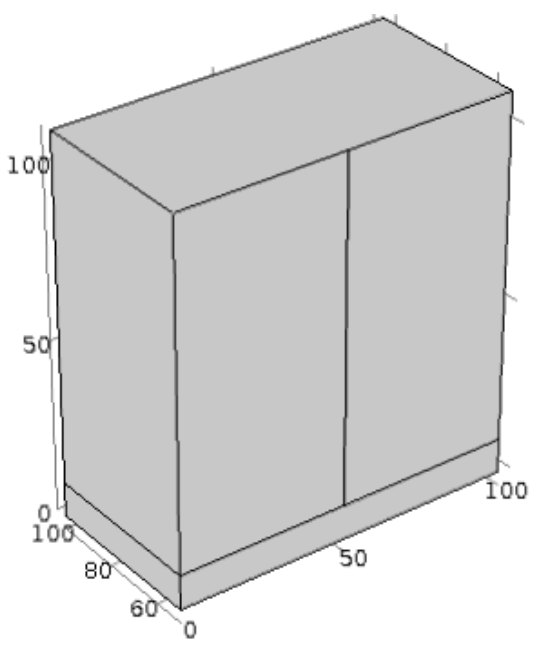

(a) The model's block

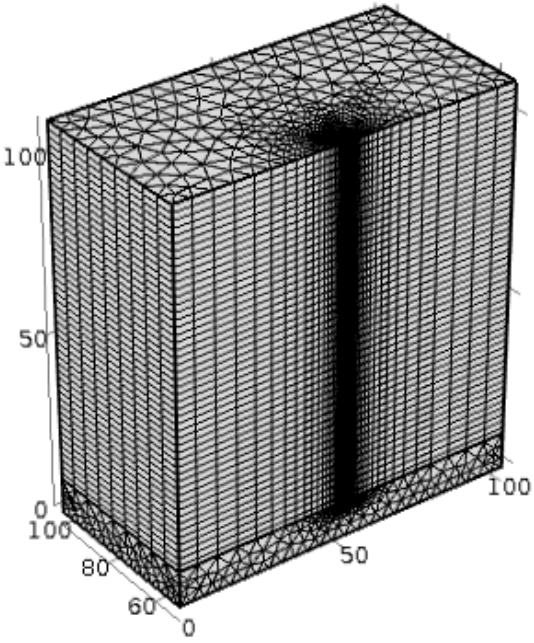

(b) Mesh

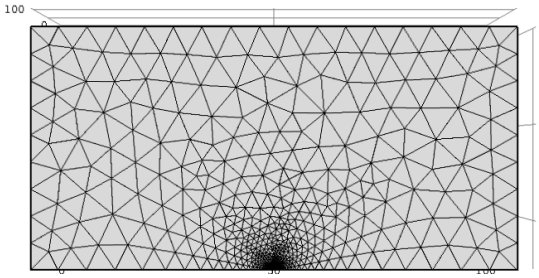

(c) Top view

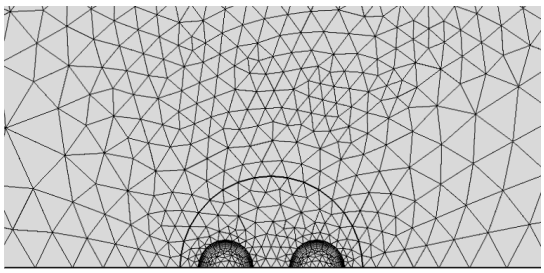

(d) Meshing details near the pipes

Figure 2.10: FEM model

SEM Model	
Number of Elements	1
Computational Time	Under 1 minute
FEM Model	
Number of Elements	230732
Computational Time [min]	35 (v=0.5m/s) 55 (v=1m/s)

Table 2.3: Computational information

Borehole's Properties	
Borehole Length (L) [m]	100
Borehole Radius (r_g) [m]	0.05
Pipe Inner Radius (r_i) [m]	0.015
Pipe wall thickness (ds) [m]	0.002
Fluid Flow Situation	Turbulent
Pipe wall Thermal Conductivity) (λ_{pipe}) [W/(m.K)]	0.42
Fluid's Properties	
Density (ρ) [$kg/(m^3)$]	1000
Specific Thermal Capacity (c) [J/(kg.K)]	4186
Thermal Conductivity (λ) [W/(m.K)]	0.56
Dynamic Viscosity (μ) [Pa.s]	0.001
Velocity (u) [m/s]	0.5 and 1
Input temperature (T_{in}) [°C]	20
Grout's Properties	
Density (ρ_g) [$kg/(m^3)$]	1420
Specific Thermal Capacity (c_g) [J/(kg.K)]	1197
Thermal Conductivity (λ) [W/(m.K)]	0.65
Soil Film Thickness (dg) [m]	Varying
Soil's Properties	
Depth (h) [m]	110
Density (ρ_g) [$kg/(m^3)$]	1680
Specific Thermal Capacity (c_g) [J/(kg.K)]	400
Thermal Conductivity (λ) [W/(m.K)]	2.5

Table 2.4: Properties of the Model

The boundary conditions of the model are similar to section (2.3) with the difference only in the velocity of the refrigerant and the dimensions of the model.

2.5. RESULTS FOR THE MODEL WITH U=0.5M/S

PIPE-IN AND PIPE-OUT TEMPERATURE FOR U=0.5M/S

Although it was proven in the previous section that the dependency of the results on the soil film thickness is eliminated, it is interesting to observe whether if other domains of the system are also independent of it as well. Initially, the temperature of both pipes are shown after 0.5 hour, 5 hours, 24 hours and 48 hours.

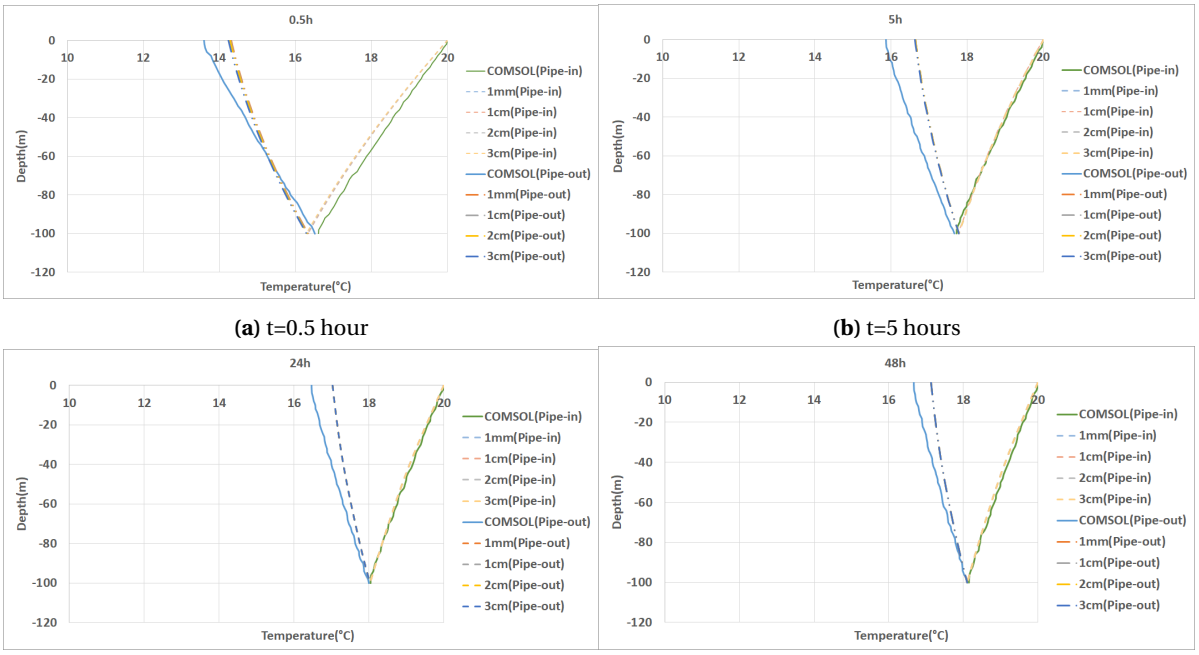

(a) t=0.5 hour **(b)** t=5 hours

(c) t=24 hours **(d)** t=48 hours

Figure 2.11: Temperature of pipes at different times with respect to depth

The results of the SEM and the FEM models are in a good match; moreover, the results from the SEM show no dependency on the soil film thickness. However, some deviation can be observed in the computational results from the two models. These deviations are more apparent in the pipe-out. It is worth mentioning that, the SEM model assumes one-dimensional heat flow in the pipes whereas in COMSOL the pipes are modeled in 3D. All of the components of the BHE, namely pipe-in, pipe-out, grout and soil film, have the same coinciding axis in the SEM model. On the other hand, in the FEM model the geometry of the shallow geothermal system is taken into account without any simplifications. The grout in the FEM model contains both of pipe-in and pipe-out and it is under the influence of non-uniform heat flow coming from both of the pipes. In the SEM model however, the two pipes are approximated as one equivalent heat source to the grout as shown in figure 2.8b.

Another possible reason for this deviation can be the fact that the velocity of the refrigerant in the SEM model is assumed to be constant, but in COMSOL a separate turbulent/laminar analysis is performed in order to compute the velocity profile of the fluid which gives a variable velocity in pipe's cross section. The difference between the velocity profile of SEM and COMSOL can be seen schematically in figure 2.12. It is extremely important to notice the fact that all of the above-mentioned differences between the SEM and the FEM models do not lead to a temperature deviation bigger than 1°C.

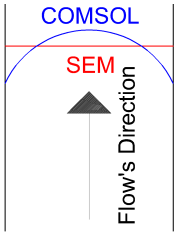

Figure 2.12: Velocity profile in the pipe's cross section in COMSOL and SEM model

GROUT'S TEMPERATURE FOR U=0.5M/S

In this section the temperature of the grout after 0.5 hour, 5 hours, 24 hours and 48 hours are shown and again the results are independent of the soil film thickness. Since the grout is modeled in 3D in COMOSL, the results of COMSOL depends on the location of the output. The temperature output location can be seen in figure 2.13e

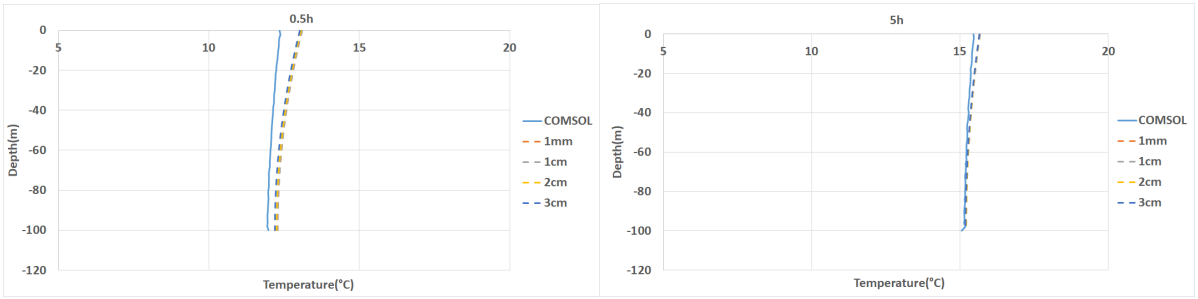

(a) t=0.5 hour

(b) t=5 hours

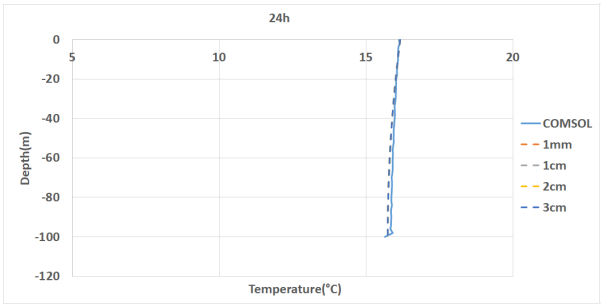

(c) t=24 hours

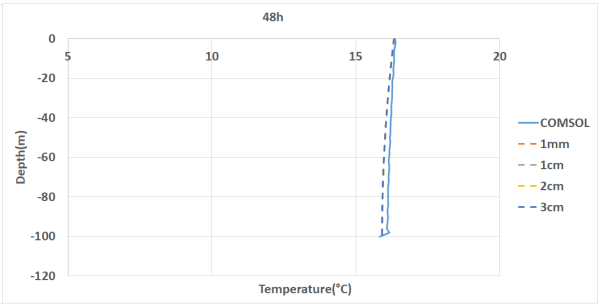

(d) t=48 hours

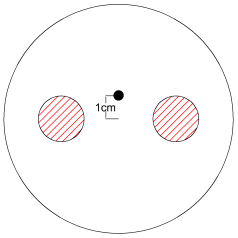

(e) Grout's output location

Figure 2.13: Temperature of grout at different times with respect to depth

RADIAL SOIL'S TEMPERATURE FOR U=0.5M/S

Finally, the temperature in the soil domain surrounding the BHE is examined. Figure 2.14 shows the radial temperature of the soil mass after 0.5 hour, 5 hours, 24 hours and 48 hours. As it can be seen there is a good match between two models.

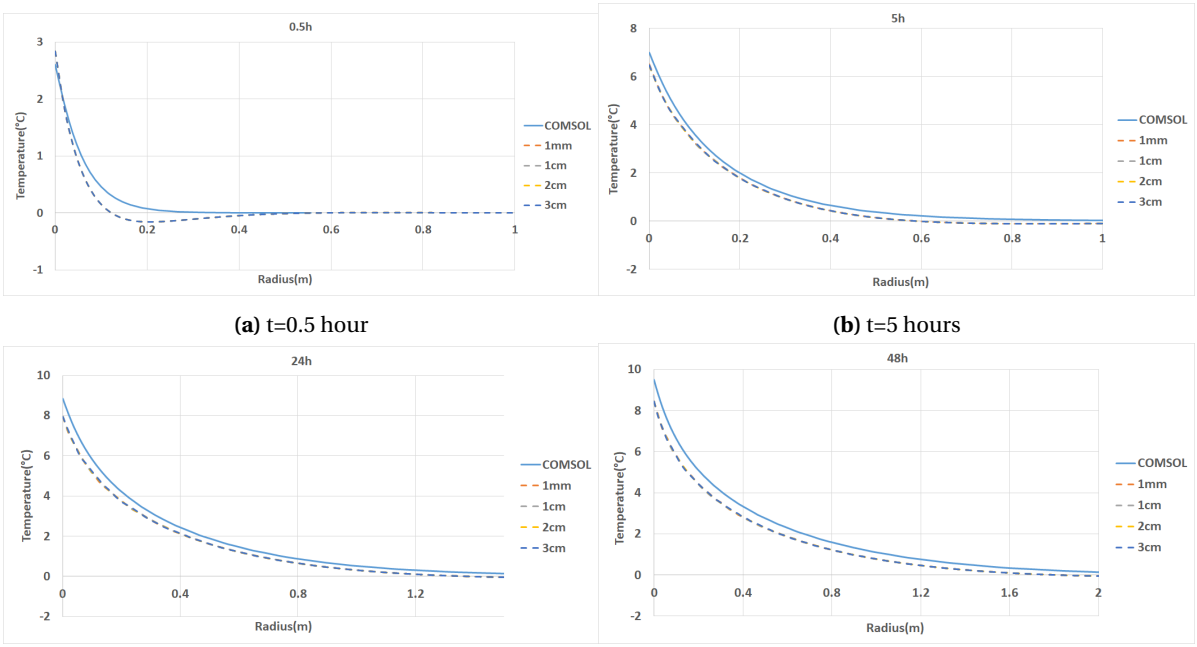

(a) t=0.5 hour

(b) t=5 hours

(c) t=24 hours

(d) t=48 hours

Figure 2.14: Temperature of soil mass at different times with respect to depth

It is worth mentioning that in the first case ($t = 0.5$ hour) it can be observed that some of the results from the SEM model are negative. However, the results at other time steps are not suffering from this issue and therefor no more investigations were performed. This oscillation can be attributed to the fast Fourier transform sampling time and windowing in the SEM model which would be explained more in the recommendation chapter of this thesis (Chapter 6).

2.6. RESULTS FOR THE MODEL WITH U=1M/S

The same results are shown here for the case where the velocity of the refrigerant is 1m/s.

PIPE-IN AND PIPE-OUT TEMPERATURE FOR U=1M/S

The same deviations between the results of the SEM and the FEM model which were mentioned in section 2.5 can be observed here as well.

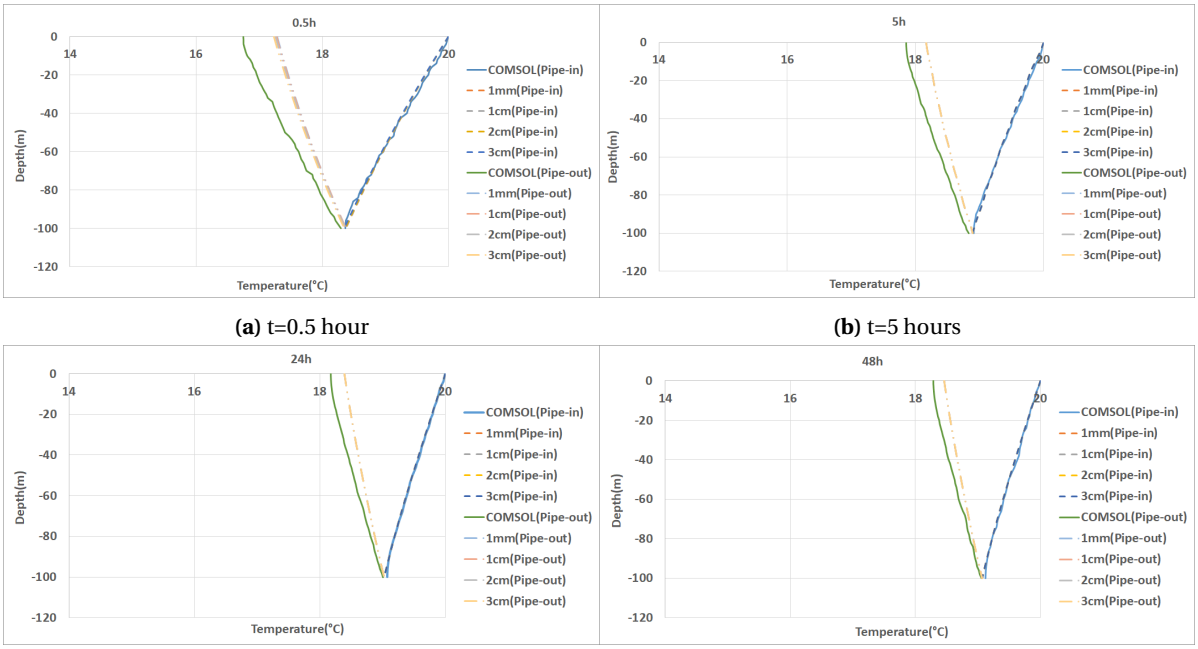

(a) t=0.5 hour **(b)** t=5 hours

(c) t=24 hours **(d)** t=48 hours

Figure 2.15: Temperature of pipes at different times with respect to depth

GROUT'S TEMPERATURE FOR U=1M/S

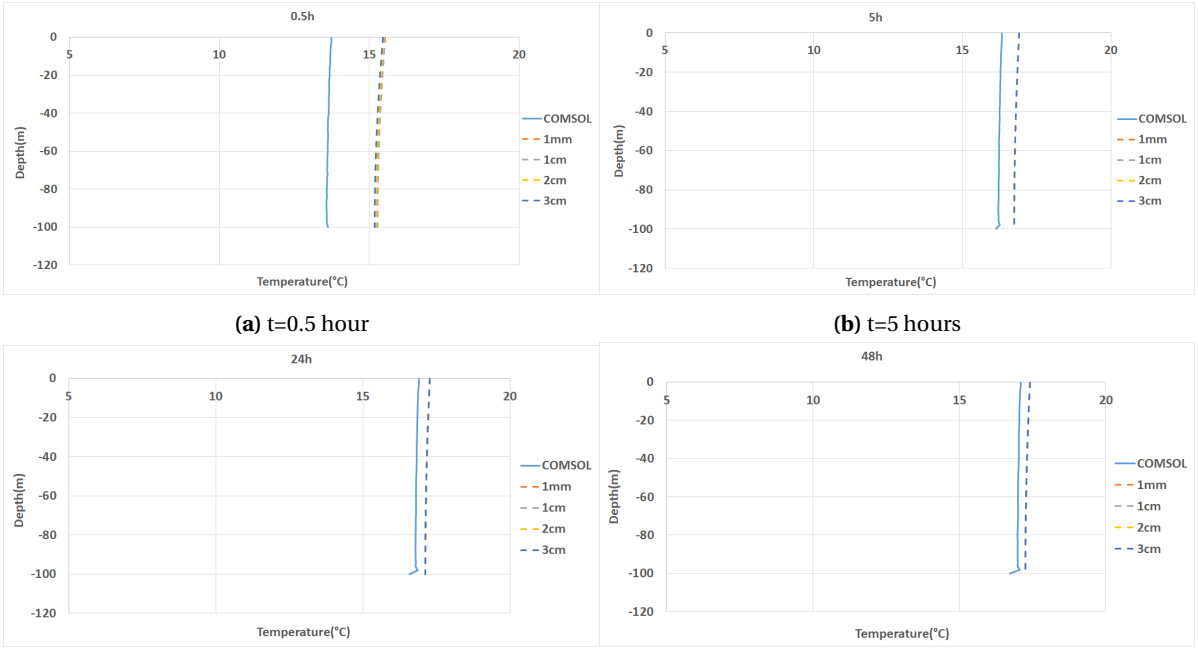

(a) t=0.5 hour **(b)** t=5 hours

(c) t=24 hours **(d)** t=48 hours

Figure 2.16: Temperature of grout at different times with respect to depth

The difference between the two models in the grout domain is more apparent than section 2.5. Specially the results after 0.5 hour show a temperature difference around 1°C between the prediction of the SEM and the FEM model (figure 2.13e)). It is important to highlight the fact that the only difference between this model and the previous one is the refrigerant's velocity. As a result, more research should be conducted in order to investigate the reason of this extra deviation between the results.

RADIAL SOIL'S TEMPERATURE FOR U=1M/S

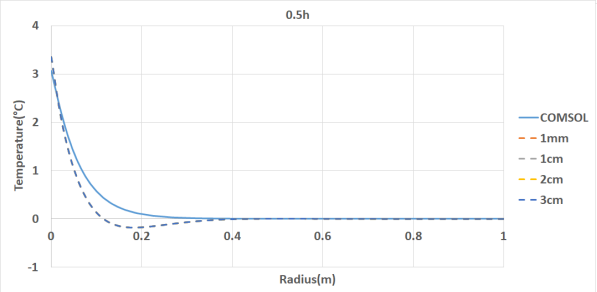

(a) t=0.5 hour

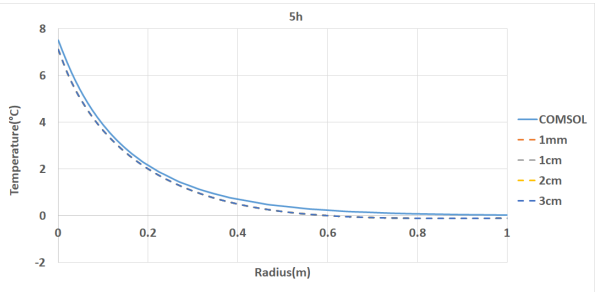

(b) t=5 hours

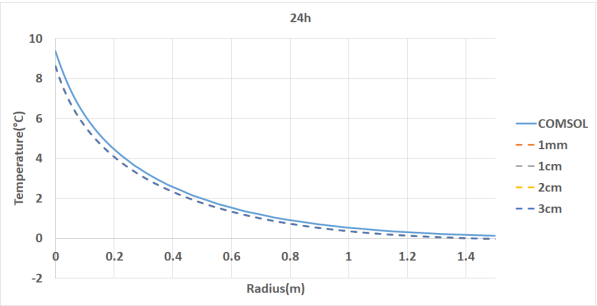

(c) t=24 hours

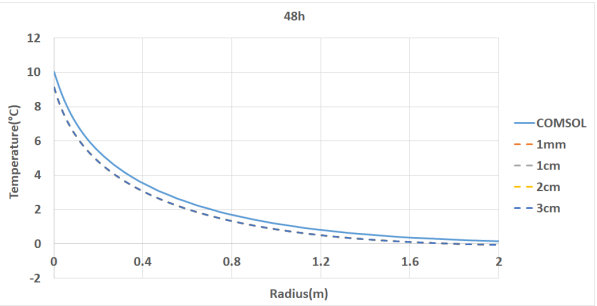

(d) t=48 hours

Figure 2.17: Temperature of soil mass at different times with respect to depth

2.7. CONCLUSION

Examining all the results in section 2.3 and 2.4 the following points can be deduced:

- In section 2.3, by redefining the the thermal coupling between different domains, the dependency of the results on the soil film thickness has been eliminated. Theoretically speaking, since the temperature gradient of the soil film in the radial direction is neglected, it is logical to assume a small thickness for it and as can be seen from the results, assuming a thickness equal to 1mm yields reasonable results.

- The calculations show that it is reasonable to simulate pipe-in and pipe-out in one dimension because the radius of the pipes are relatively small and due to the dominance of convective heat transfer, the temperature has less gradient in the radial direction. This is also applicable to the grout, though since the grout domain is larger and heat transfer in it is due to conduction, there is a possible temperature gradient in the radial direction of this domain. In the SEM model, the grout is modeled as a one-dimensional domain having a heat flow only in the z direction while neglecting its heat flow in the radial direction. In COMSOL the three-dimensional geometry of the grout is taken into account. As a consequence, the results extracted from COMSOL are dependent on the output location. Figure 2.13e shows the location that was chosen to match the results of the FEM model to the SEM model. In order to check the consistency of the results in the grout domain, the same location is used for the other analyses throughout this thesis. To have a better match between the FEM and the SEM models, the grout domain needs to be modeled using a cylindrical coordinates system and the improvements should be verified. This will be discussed more in the recommendation section (Chapter 6).

- As it can be seen by comparing the results of section 2.5 and 2.6, the FEM and the SEM have closer results to each other when the velocity of the refrigerant is smaller. Moreover, the values of the two models become closer at later stages of the analysis versus the earlier stages. It can be argued that in

the SEM model, all the equations are solved analytically and without any approximation in their solutions. On the other hand, the FEM analysis uses approximated shape functions to predict the results, this makes the FEM results dependent on the physical properties of the system. As a result, two systems with different velocities would need different meshing in order to yield acceptable results. This can be an additional topic of research which is out of scope of this thesis. In addition, the coupling between convection and conduction in FEM programs makes the simulating procedures even more cumbersome.

The main advantage of the SEM model is its computational efficiency. While for the FEM model it takes hours to calculate results, the SEM model can deliver the results within few seconds. This make the SEM model very much suitable for engineering practices. However, the SEM model cannot handle the heat flow analysis for complex geometries and boundary conditions. Moreover, it cannot deal with complicated physical properties (Material nonlinearities etc). It is important to highlight the fact that even though two different mathematical approaches in the formulation of the SEM and the FEM theories are used, both models predict the temperature of different domains in the system with close match.

3

MULTI-LAYER MODEL

As it was stated before, the SEM model for U-tube shallow geothermal systems is capable of modeling a BHE in multiple layers of soil. This can be done by assembling the spectral stiffness matrix using the well-known finite element matrix assembly algorithms. In this chapter, a multilayer example is introduced in order to examine this feature. The example has geometrical dimensions comparable to a realistic case. The theory behind the SEM model is exactly the same as in previous chapter and it is not presented here. The computational results in different domains are compared to each other in the FEM and the SEM model.

3.1. COMSOL MULTIPHYSICS MODELING ASSUMPTIONS

In order to test the SEM model, a system with 5 soil layers is modeled in COMSOL Multiphysics[4]. The BHE is 100 meters deep, resulting in each layer to be 20 meters. The soil mass is made 100 × 100 meters in order to prevent the boundary conditions at the soil mass boundary from affecting the results. Symmetry is used to increase the computation speed. For modeling in COMSOL, both fluid flow and heat transfer in solids and fluids are utilized. The flow is turbulent with $Re > 3600$. Figures 3.1 and 3.2 show the model in COMSOL. The components of the model are the same as the model presented in section 2.4, the only difference is that the soil mass has multiple layers with different heat conductivity. More details are given in table 3.1 and 3.2.

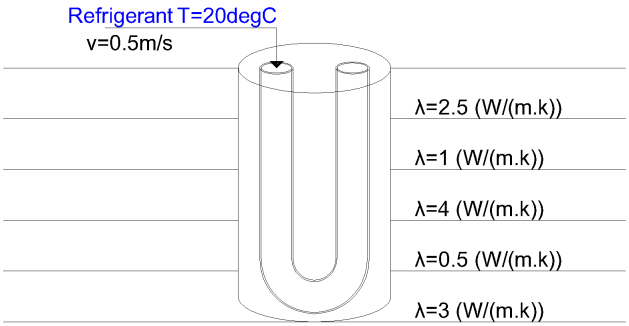

Figure 3.1: Schematic of the system

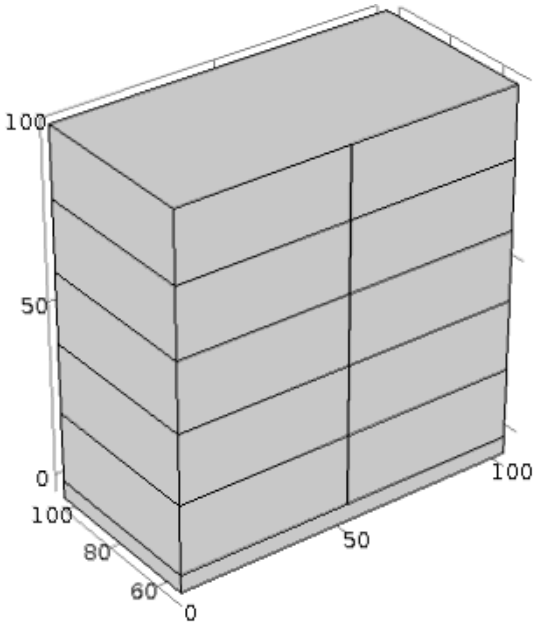

(a) Shallow geothermal system with 5 soil layers

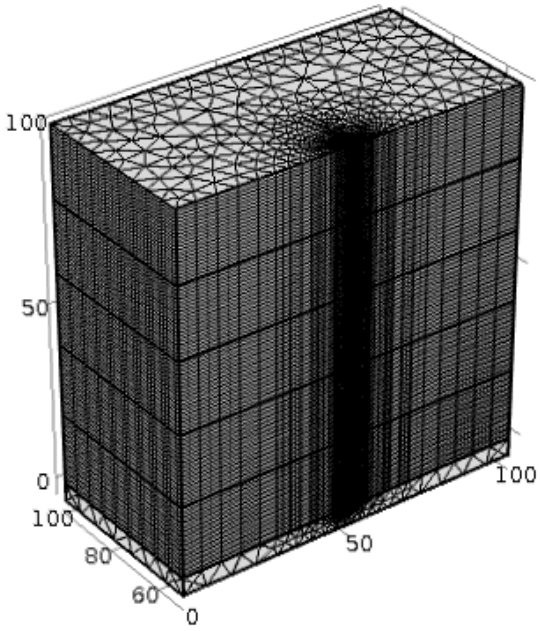

(b) Mesh

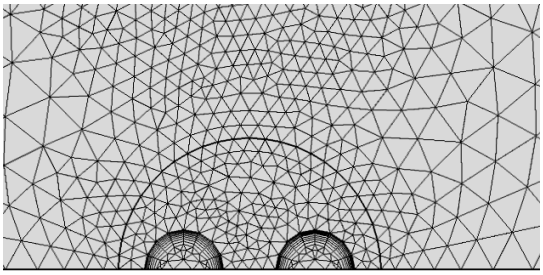

(c) Top view

Figure 3.2: COMSOL Multiphysics model

The following boundary conditions are applied in COMSOL:

- **Inlet of pipe-in:** Input temperature $\big(T(0,t) = T_{in}\big)$, Input Velocity $\big(u(0,t) = u\big)$.
- **Outlet of pipe-out:** Outlet (Zero pressure at pipe's outlet) , Outflow (This node provides a suitable boundary condition for convection-dominated heat transfer at outlet boundaries. In a model with convective heat transfer, this condition states that the only heat transfer occurring across the boundary is by convection. The temperature gradient in the normal direction is zero, and there is no radiation. This is usually a good approximation of the conditions at an outlet boundary in a heat transfer model with fluid flow. [4]).
- **Top and bottom of the soil mass and grout**: Fully insulated which implies that the interaction with air and also the soil beneath the model is neglected. This is an accurate assumption due to the fact that in the SEM model these factors are not considered as well.
- **Soil mass's boundary:** $T_{soil} = 0$

Borehole's Properties	
Borehole Length (L) [m]	100
Borehole Radius (r_g) [m]	0.05
Pipe Inner Radius (r_i) [m]	0.015
Pipe wall thickness (ds) [m]	0.002
Fluid Flow Situation	Laminar
Pipe wall Thermal Conductivity) (λ_{pipe}) [W/(m.K)]	0.42
Fluid's Properties	
Density (ρ) [$kg/(m^3)$]	1000
Specific Thermal Capacity (c) [J/(kg.K)]	4186
Thermal Conductivity (λ) [W/(m.K)]	0.56
Dynamic Viscosity (μ) [Pa.s]	0.001
Velocity (u) [m/s]	0.5
Input temperature (T_{in}) [°C]	20
Grout's Properties	
Density (ρ_g) [$kg/(m^3)$]	1420
Specific Thermal Capacity (c_g) [J/(kg.K)]	1197
Thermal Conductivity (λ) [W/(m.K)]	0.65
Soil Film Thickness (dg) [m]	Varying
Soil's Properties	
Depth (h) [m]	105
Density (ρ_g) [$kg/(m^3)$]	1680
Specific Thermal Capacity (c_g) [J/(kg.K)]	400
Thermal Conductivity for 1st Layer (λ) [W/ (m.K)]	2.5
Thermal Conductivity for 2nd Layer (λ) [W/ (m.K)]	1
Thermal Conductivity for 3rd Layer (λ) [W/ (m.K)]	4
Thermal Conductivity for 4th Layer (λ) [W/ (m.K)]	0.5
Thermal Conductivity for 5th Layer (λ) [W/ (m.K)]	3

Table 3.1: Properties of the model

SEM Model	
Number of Elements	5
Computational Time	Under 1 minute
FEM Model	
Number of Elements	514708
Computational Time [min]	132

Table 3.2: Computational information

In the upcoming sections, the temperature of the U-tube shallow geothermal system in different domains in both of the SEM and the FEM models are compared. In the BHE components, namely pipe-in, pipe-out and grout, the temperature is given versus depth. For the soil mass, the temperature is presented radially in the middle of each layer.

PIPE-IN AND PIPE-OUT TEMPERATURE

Figure 3.3 shows the temperature of pipe-in and pipe-out with respect to depth. The results are shown after 0.5 hour, 2 hours, 24 hours, 10 days and 1 month. The temperature profile of the pipes show different slopes in different layers. This is indeed because of different heat conductivity of each soil layer. As can be expected, the soil layer with the highest heat conduction, $\lambda = 4$ [W/(m.K)], results in the most temperature drop in the fluid (Layer 3 between 40-60 meters). There are some differences in the temperature prediction from COMSOL Multiphysics and the SEM model. These differences can be explained as below:

- In the SEM model the velocity of the refrigerant is constant; however, in COMSOL Multiphysics the velocity profile is extracted from a fluid analysis and depending on the fluid state (laminar or turbulent) the velocity profile would be different (Figure 2.12). The results could potentially be closer if the velocity of the pipes were modeled as a constant in COMSOL Multiphysics. However, the goal here is to compare the SEM model with a realistic simulation. To minimize this, the results of COMSOL Multiphysics are extracted at the center of each pipe.
- In COMSOL Multiphysics the system is modeled in details and it is in three dimensions. The grout contains both of the pipes and it is under the influence of heat flow from both of them. In the SEM model however, all the BHE components have one-dimensional heat flow in the z direction and pipe-in and pipe-out are approximated with a larger pipe in the middle of the grout.
- The difference in the temperature prediction accumulates from pipe-in resulting in the most difference in the outlet of pipe-out. This temperature difference does not exceed 1°C (Figure 3.3c).

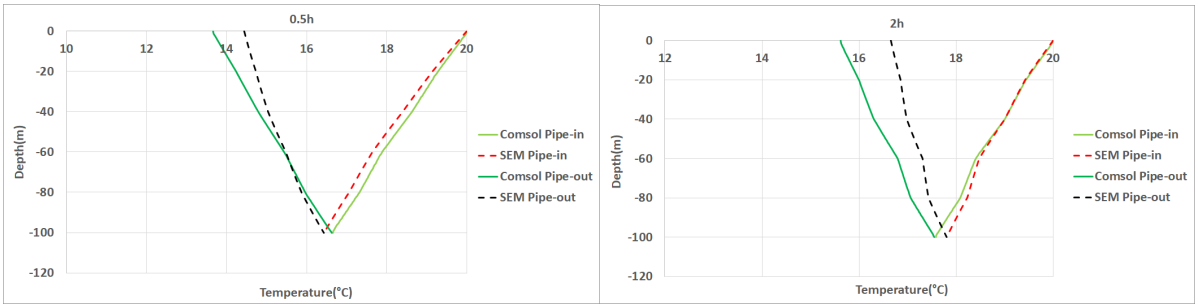

(a) t=0.5 hour

(b) t=2 hours

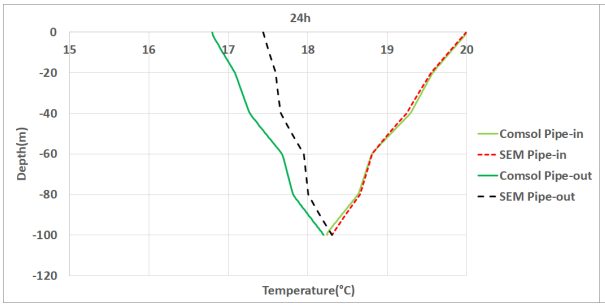

(c) t=24 hours

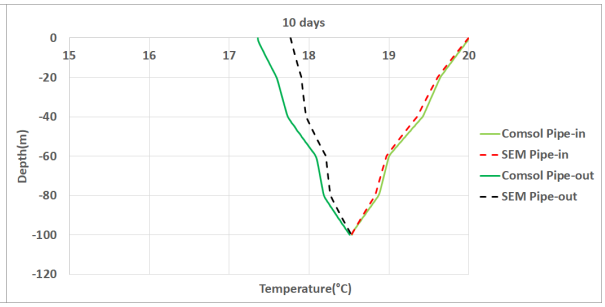

(d) t=10 days

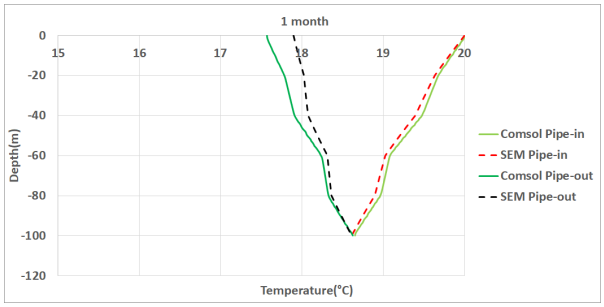

(e) t=1 month

Figure 3.3: Temperature of pipe-in and pipe-out at different times with respect to depth

GROUT TEMPERATURE

In this section the temperature of the grout is shown (Figure 3.4). The grout temperature profile in both of the SEM and the FEM model is given with respect to depth after 0.5 hour, 2 hours, 24 hours, 10 days and 1 month. The difference between the SEM and the FEM model is more noticeable in this case. Although, as the time passes, the difference becomes smaller. The difference is due to the fact that the grout is not axially symmetric in reality and it is subjected to two different heat sources, namely pipe-in and pipe-out. As a result, the temperature is extremely dependent on the location of the output. It would be beneficial to model the grout domain in the SEM model in the cylindrical coordinate systems and check the probable improvement. As can be seen from the results, all the mentioned assumptions in the SEM model does not lead to an incorrect prediction. In fact, the temperature difference between the two models does not exceed 1°C.

Another aspect of the results which can be observed is the oscillation of results from COMSOL. This oscillation occurs at the boundaries between soil layers. It is worth mentioning that the largest oscillation can be seen between 60 and 80 meters below the surface. This is where the fourth soil layer exists. The fourth layer's thermal conductivity is 4 [W/(m.K)] while the thermal conductivity of the layer above it is 1 [W/(m.K)] and the layer below it is 0.5 [W/(m.K)]. This results in the biggest difference in the thermal conductivity of two adjacent layers and leads to the biggest oscillation. The SEM results do not suffer from the same problem which is one of the advantages of analytical solution and a proof that the consistency of the results do not depend on the physical properties of the system. (The output location of the grout is similar to figure 2.13e)

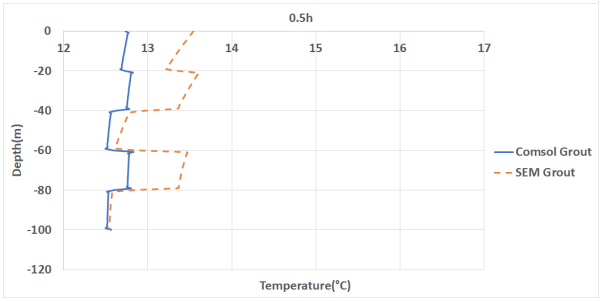

(a) t=0.5 hour

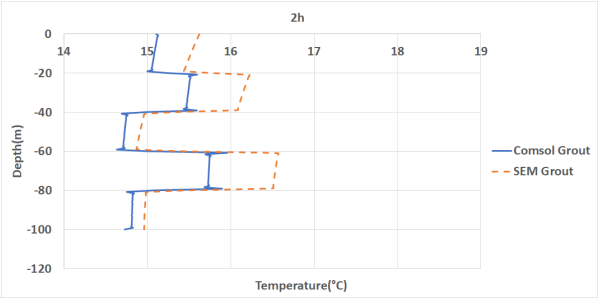

(b) t=2 hours

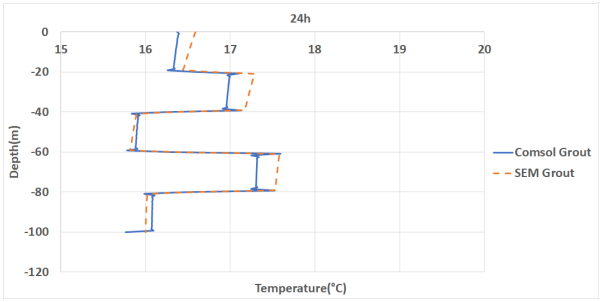

(c) t=24 hours

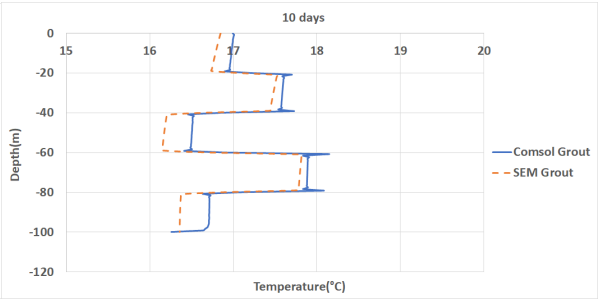

(d) t=10 days

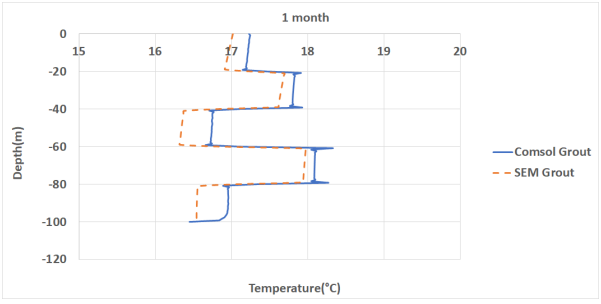

(e) t=1 month

Figure 3.4: Temperature of grout at different times with respect to depth

3.1.1. SOIL TEMPERATURE IN THE THE MIDDLE OF EACH LAYER

In this subsection, the temperature of the soil in the radial direction in the middle of each layer in different times (After 2 hours, 24 hours, 10 days, 1 month and 1 year) is given.

SOIL TEMPERATURE AFTER 2 HOURS

The temperature profile of the soil in each layer in the radial direction can be seen in figure 3.5. The temperature is extracted in the middle of each layer (10, 30, 50, 70, 90 meters deep) starting next to the grout and continuing radially. In all of the cases, a decaying temperature profile with respect to radial direction can be seen. As it is expected, the decaying rate is dependent on the soil thermal conductivity.

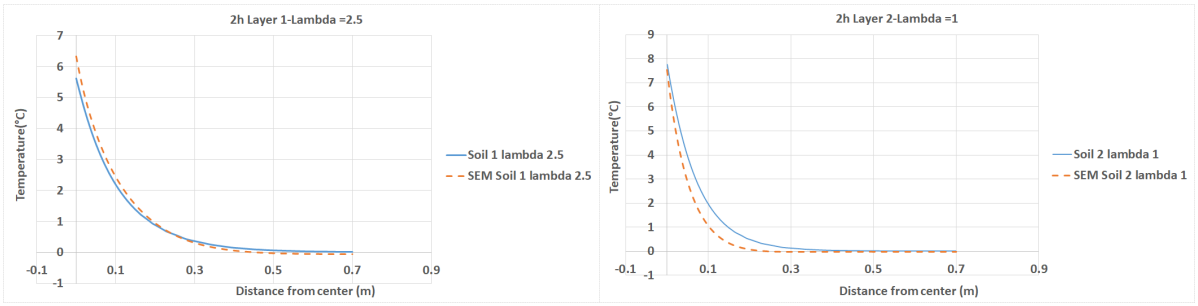

(a) Layer 1($\lambda = 2.5$)

(b) Layer 2($\lambda = 1$)

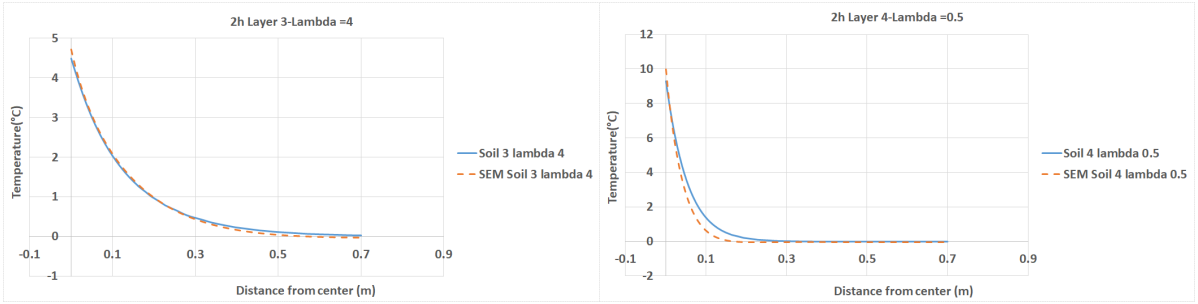

(c) Layer 3($\lambda = 4$)

(d) Layer 4($\lambda = 0.5$)

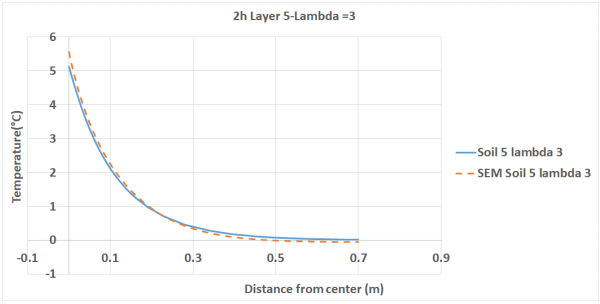

(e) Layer 5($\lambda = 3$)

Figure 3.5: Radial temperature of each layer after 2 hours

SOIL TEMPERATURE AFTER 24 HOURS

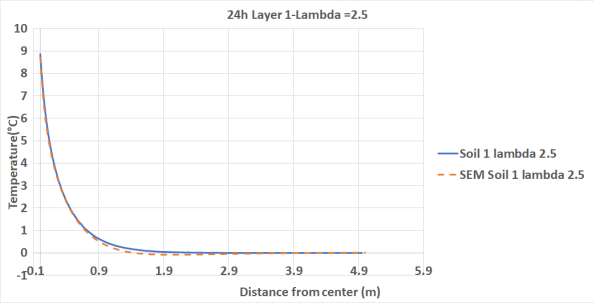

(a) Layer 1($\lambda = 2.5$)

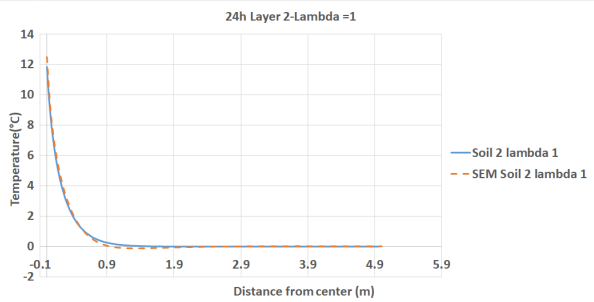

(b) Layer 2($\lambda = 1$)

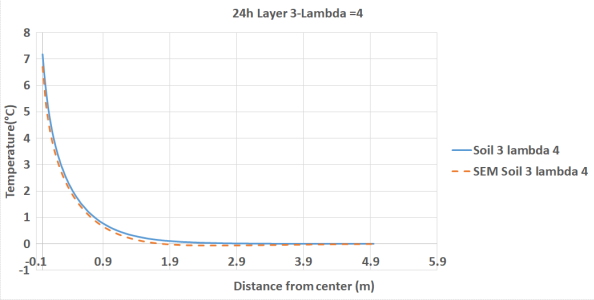

(c) Layer 3($\lambda = 4$)

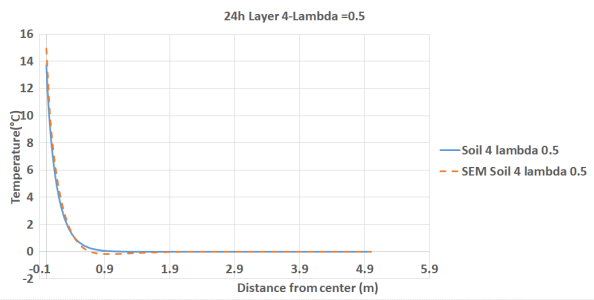

(d) Layer 4($\lambda = 0.5$)

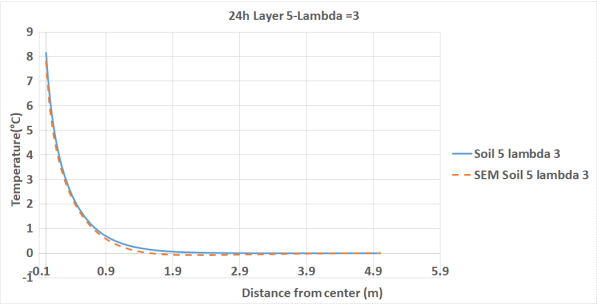

(e) Layer 5($\lambda = 3$)

Figure 3.6: Radial temperature of each layer after 24 hours

SOIL TEMPERATURE AFTER 10 DAYS

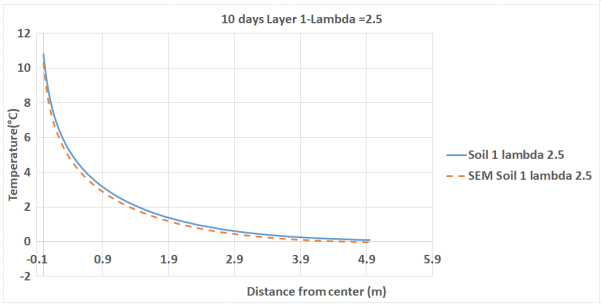

(a) Layer 1($\lambda = 2.5$)

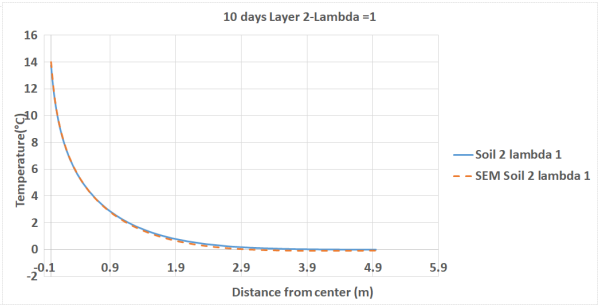

(b) Layer 2($\lambda = 1$)

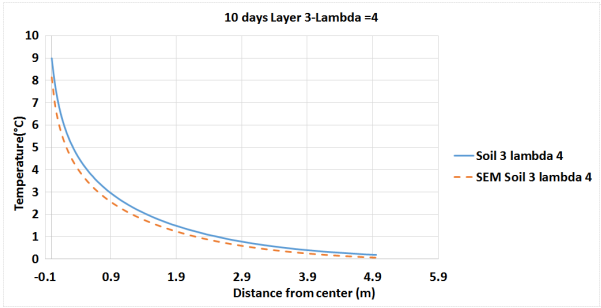

(c) Layer 3($\lambda = 4$)

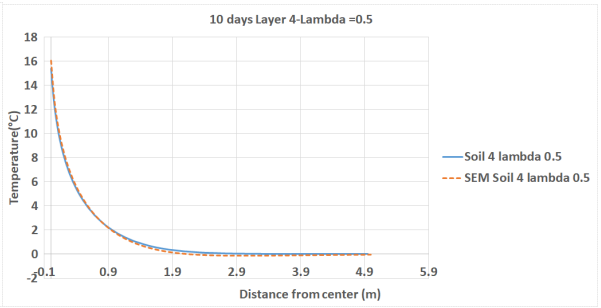

(d) Layer 4($\lambda = 0.5$)

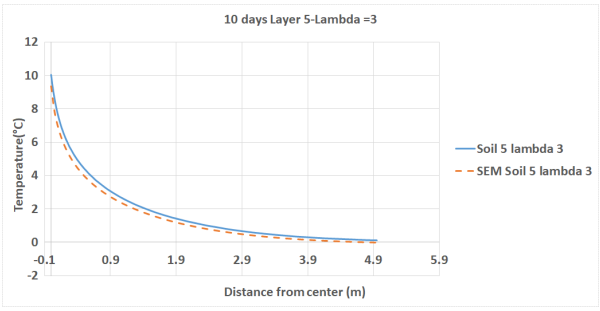

(e) Layer 5($\lambda = 3$)

Figure 3.7: Radial temperature of each layer after 10 days

SOIL TEMPERATURE AFTER 1 MONTH

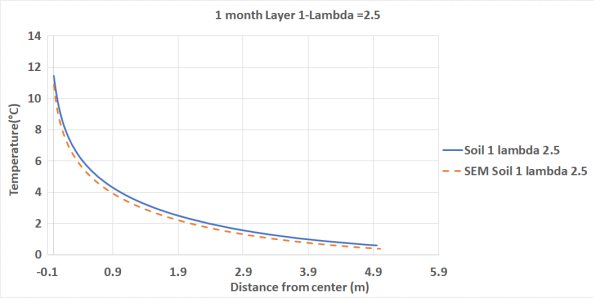

(a) Layer 1($\lambda = 2.5$)

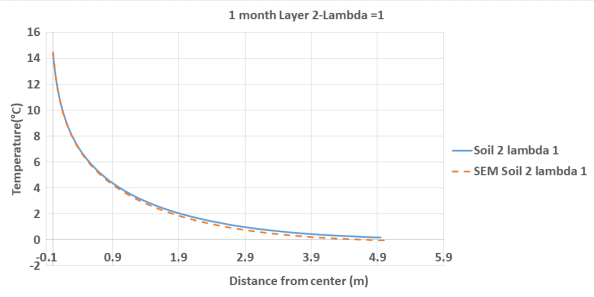

(b) Layer 2($\lambda = 1$)

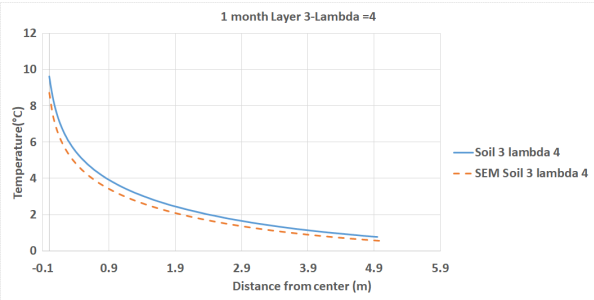

(c) Layer 3($\lambda = 4$)

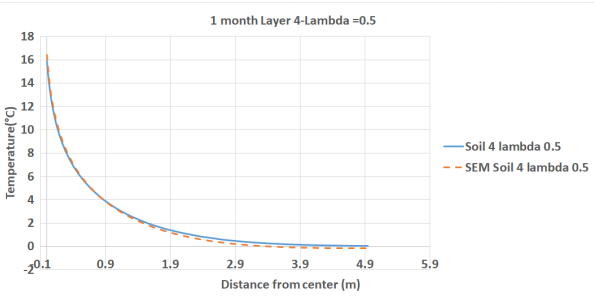

(d) Layer 4($\lambda = 0.5$)

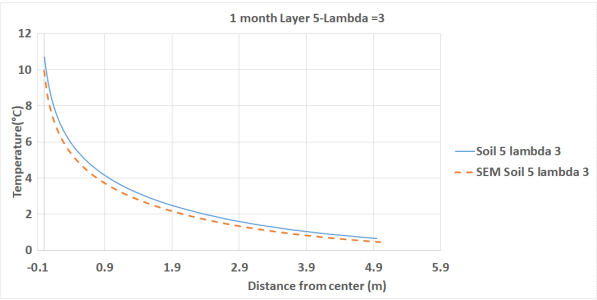

(e) Layer 5($\lambda = 3$)

Figure 3.8: Radial temperature of each layer after 1 month

SOIL TEMPERATURE AFTER 1 YEAR

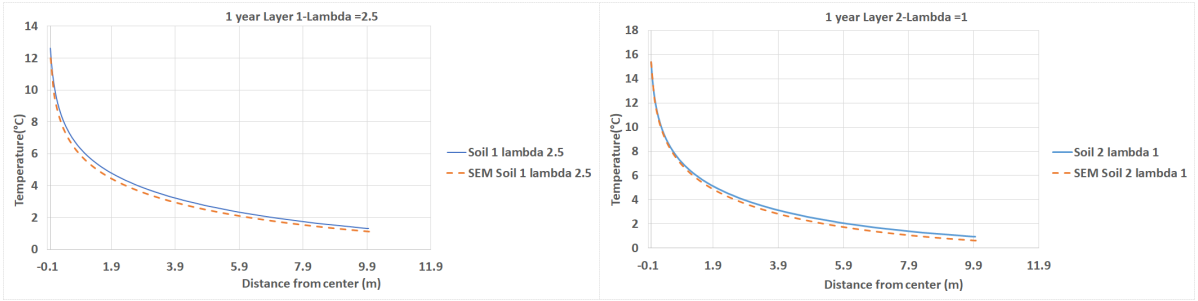

(a) Layer 1($\lambda = 2.5$)

(b) Layer 2($\lambda = 1$)

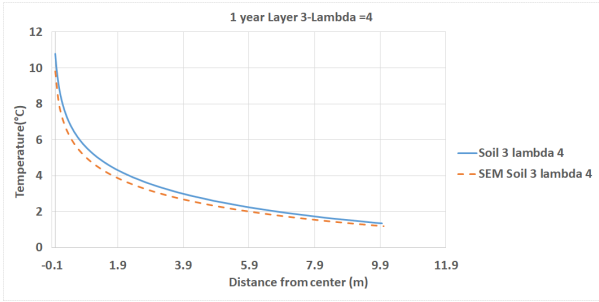

(c) Layer 3($\lambda = 4$)

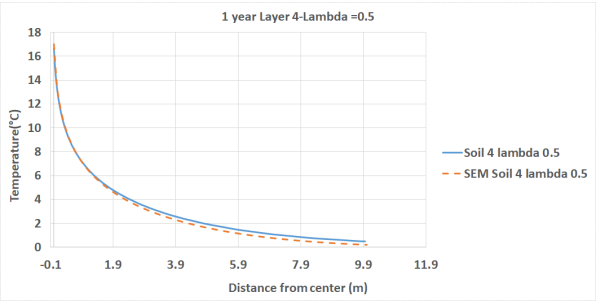

(d) Layer 4($\lambda = 0.5$)

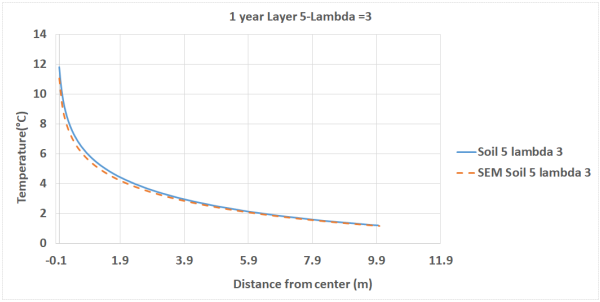

(e) Layer 5($\lambda = 3$)

Figure 3.9: Radial temperature of each layer after 1 year

3.2. CONCLUSION

There are few points worth mentioning by examining the results

- As it can be seen, the SEM model is capable of modeling a BHE embedded in multiple layers of soil and the results are comparable to a detailed FEM model.
- The temperature profile of pipe-in and pipe-out in both models are very similar. As it was mentioned in the previous chapter, the biggest temperature difference is seen in pipe-out which can reach up to 1°C in its outlet. Moreover, the results of two models are closer to each other in later stages of analysis.
- The temperature profile of the grout in the FEM model is dependent on the location of output. In the SEM model the grout is modeled as an axially symmetric domain with one-dimensional heat flow which is not the case in reality. Although the temperature difference between two models is less than 1°C, it would be beneficial to model the grout domain in the SEM model using cylindrical coordinates system.
- The radial soil temperature shows a good match between the SEM model and the FEM model. It is interesting to state the fact that the results from the FEM and the SEM analyses have some differences which is also dependent on the soil layer and the time of the output. As mentioned in the conclusion part of the previous chapter, this can be linked to the dependency of the FEM model to physical properties of the system which indeed require further research.

The computational efficiency of the SEM model in modeling a shallow geothermal system embedded in multiple layers of soil is apparent compared to the FEM model. The SEM model can deliver results in less than a minute while the FEM model takes up to two hours to compute the results. Additional meshing techniques for coupling convection and conduction in the system adds to the complexity of the FEM model. With all the results presented in this chapter, the SEM model proves to be extremely suitable for real engineering practices. If there are no geometrical complexity or material nonlinearities, the SEM model would be a better choice over the FEM model. The SEM model does not depend on the physical properties of the system and if there is a sudden change of soil properties, the SEM model can handle it much better. This is because of the fact that all the equations in the SEM model are solved analytically. In the FEM model, since the computational results are given using approximations, the results depend on the physical properties of the system. Consequently, changing the physical properties of the system might require a change in meshing. Moreover, sudden change of material properties can result into unwanted oscillations.

4

COAXIAL SHALLOW GEOTHERMAL SYSTEMS

In the previous chapters it was observed that the temperature profile of pipe-in, pipe-out and soil mass extracted from the SEM model have a good match with the results from COMSOL Multiphysics. However, it was discussed that the temperature of the grout can be affected by the radial heat flow in it. In order to study this issue, a model for coaxial shallow geothermal systems is developed in this chapter. In this type of shallow geothermal systems, the BHE consists of a set of concentric pipes. There are two main configurations: annular (CXA) and centered (CXC) (Figure 4.1). In the first type pipe-out is embed inside pipe-in making an annular inlet and centered outlet and only pipe-in exchange heat with the grout while pipe-out is in contact with pipe-in. The second type is opposite of the first type in which pipe-in is embed in pipe-out.

In order to increase the feasibility of the modeling process, this model has been developed in 3 steps: in section 4.1 the ability of Bessel functions in order to predict the temperature in a small annulus in 2D is tested. Subsequently in section 4.2, a single pipe embedded in a grout and soil mass is modeled using spectral element method (SEM)[1]. Finally, the SEM model for coaxial shallow geothermal systems is developed with the same approach as the preceding steps (Section 4.3).

4.1. TRANSIENT TEMPERATURE IN AN AXIALLY SYMMETRIC DOMAIN

GOVERNING EQUATIONS

Consider an annulus, with an inner radius r_1, an outer radius r_2 and a constant thermal conductivity λ (Figure 4.2a). The domain is exposed to a time-dependent temperature $\theta(t)$ at its inner perimeter and zero flux at its outer perimeter.

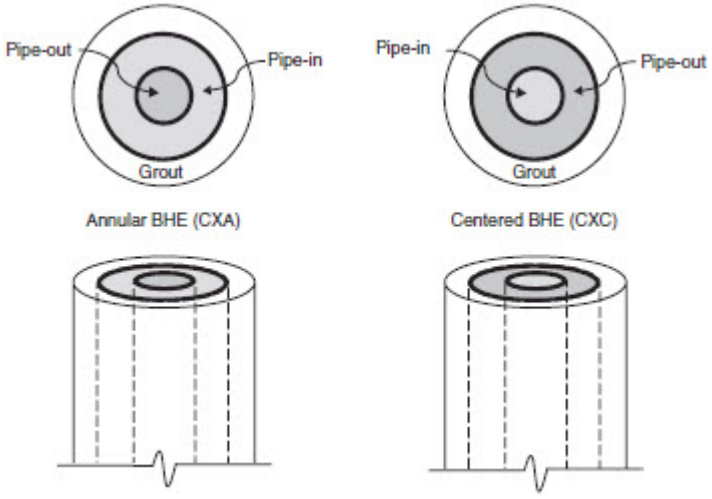

Figure 4.1: Two types of coaxial geothermal systems [1]

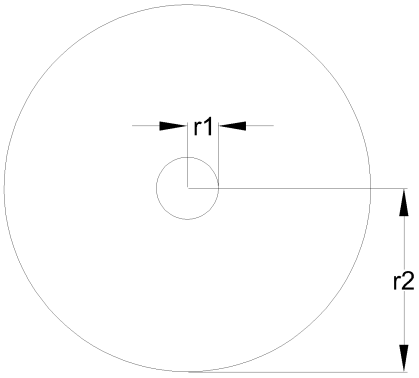

(a) Dimensions

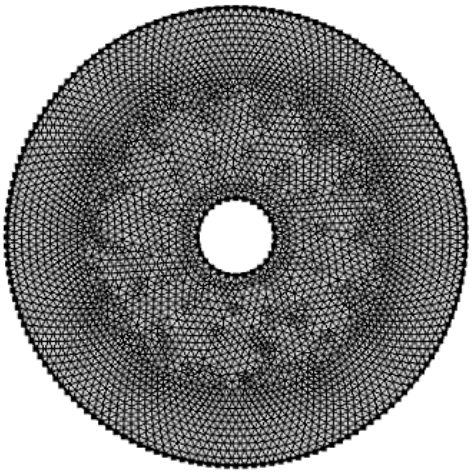

(b) Mesh in COMSOL Multiphysics[4]

Figure 4.2: Domain properties

The transient heat conduction equation for this domain is:

$$\frac{1}{\alpha}\frac{\partial T}{\partial t} - \frac{\partial^2 T}{\partial r^2} - \frac{1}{r}\frac{\partial T}{\partial r} = 0 \qquad \alpha = \frac{\lambda}{\rho c} \tag{4.1.1}$$

where T is the temperature of the domain which is a function of time (t) and radial distance (r). The boundary conditions for the domain are:

$$T(r_1, t) = \theta(t) \tag{4.1.2}$$

$$-\lambda \frac{\partial T(r_2, t)}{\partial r} ds = 0 \tag{4.1.3}$$

Using the Fourier transform in order to eliminate the time derivative, equation (4.1.1) is transformed to the frequency domain:

$$\frac{i\omega}{\alpha}\hat{T} - \frac{\partial^2 \hat{T}}{\partial r^2} - \frac{1}{r}\frac{\partial \hat{T}}{\partial r} = 0 \tag{4.1.4}$$

The boundary conditions in the frequency domain are:

$$\hat{T}(r_1, t) = \hat{\theta}(\omega) \tag{4.1.5}$$

$$-\lambda \frac{\partial \hat{T}_g(r_2, \omega)}{\partial r} = 0 \tag{4.1.6}$$

The solution of (4.1.4) can be given using the modified Bessel functions:

$$\hat{T}(r, \omega) = AK_0(kr) + BI_0(kr) \qquad k = \sqrt{\frac{i\omega}{\alpha}} \tag{4.1.7}$$

By applying the boundary conditions and solving the resulting equation using Maple[5] software, A and B can be calculated:

$$A = \frac{\hat{\theta}(\omega) I_1(kr_2)}{K_0(kr_1) I_1(kr_2) + I_0(kr_1) K_1(k_g r_2)} \tag{4.1.8}$$

$$B = \frac{\hat{\theta}(\omega) K_1(kr_2)}{K_0(kr_1) I_1(kr_2) + I_0(kr_1) K_1(kr_2)} \tag{4.1.9}$$

By calculating A and B the temperature of the domain at any location as a function of time can be calculated.

VERIFICATION

To verify the model, the computed results from the above analytical model is compared to a FEM model using COMSOL Multiphysics [4] (Figure (4.2a)). The parameters of the model are presented in table 4.1. The temperature of the domain versus time is given in two locations (0.05 meter and 0.1 meter from the center of the opening). The results are presented in figure (4.3).

Inner Radius(r_1) [m]	0.017
Outer Radius(r_2) [m]	0.1
Thermal Conductivity(λ) [W/(m.K)]	0.65
Density(ρ_g) [$kg/(m^3)$]	1420
Specific Thermal Capacity(c_g) [J/(kg.K)]	1197
Temperature(θ) [°C]	20

Table 4.1: Values for the Case Study

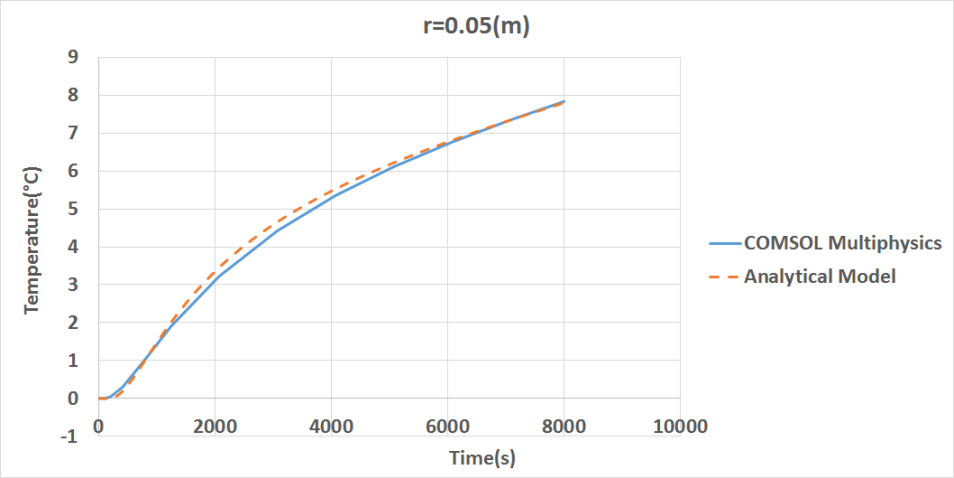

(a) r=0.05(m)

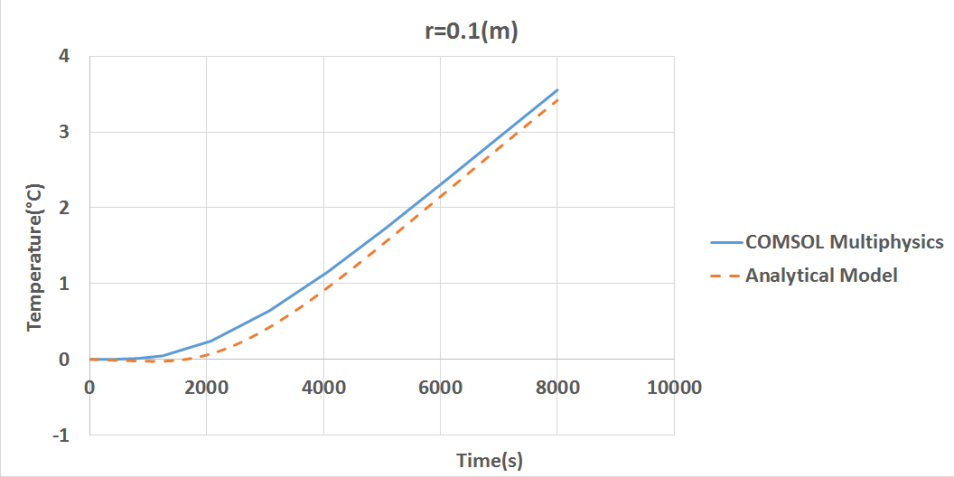

(b) r=0.1(m)

Figure 4.3: Temperature VS time at two locations in the domain

The results show a good agreement between the FEM and the analytical model. In the next section, it is attempted to model a single pipe embedded in a grout and a soil mass domain.

4.2. PRELIMINARY MODEL

GOVERNING EQUATIONS

Prior to modeling the coaxial BHE, a model is presented with only one pipe embedded in a grout domain and a soil mass. For connecting the pipe which is modeled in the z direction to the grout which is modeled radially, a grout film is introduced. This will also take into account the temperature of the grout in the z direction due to the fact that the temperature of the grout film will act as an amplitude for the grout domain. The grout domain and soil domain are both modeled radially.

The refrigerant enters from top of the pipe with a certain temperature which is a function of time and it exits from bottom of the pipe. Heat flow in the pipe and the grout film is modeled in one dimension, while the grout and the soil mass have a heat flow in the z and the radial direction. The pipe and the grout film axis are coinciding which are also the origin for radial coordinates system (Figure 4.4c).

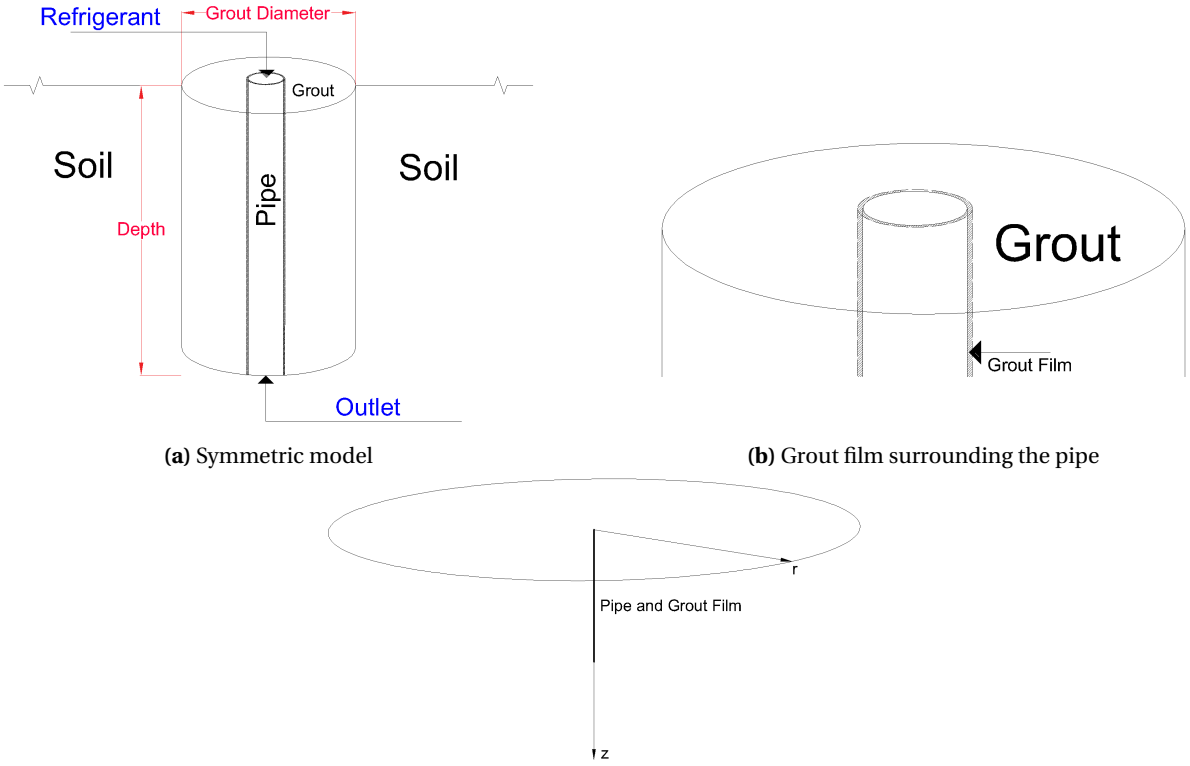

(a) Symmetric model

(b) Grout film surrounding the pipe

(c) The positive direction of coordinate system

Figure 4.4: Preliminary Model

The heat equations for the system are

Pipe-in

$$\rho c \frac{\partial T_i}{\partial t} dv_i - \lambda \frac{\partial^2 T_i}{\partial z^2} dv_i + \rho c u \frac{\partial T_i}{\partial z} dv_i + b_{ig}(T_i - T_g) ds_{ig} = 0 \tag{4.2.1}$$

grout film

$$\rho_g c_g \frac{\partial T_g}{\partial t} dv_g - \lambda_g \frac{\partial^2 T_g}{\partial z^2} dv_g + b_{ig}(T_g - T_i) ds_{ig} + b_{gg}(T_g - T_{grout}|_{r=r_g}) ds_{gg} = 0 \tag{4.2.2}$$

where the subscript i and g represent pipe (pipe-in) and grout film respectively. T_i and T_g are the temperature of pipe and grout film which are both a function of z; λ and λ_g $(W/m.K)$ are thermal conductivity of fluid and grout film; u (m/s) is the velocity of the refrigerant in the pipe; b_{ig} and b_{gg} $(W/m^2.K)$ are the reciprocal of the thermal resistance between pipe-grout film and grout film-grout domain respectively; c $(J/kg.K)$ stands for the specific heat of the domain and $\rho(kg/m^3)$ is the mass density; dv_i and dv_g (m^3) are partial volumes of pipe and grout film; ds_{ig} and ds_{gg} (m^2) are partial surface area between pipe-grout and grout-film-grout respectively.

The initial and boundary conditions for these domains are:

$$T_i(z,0) = T_g(z,0) = T_{grout}(r,z,0) = T_{soil}(r,z,0) \qquad \text{Initial temperature of all domains} \qquad (4.2.3)$$

$$T_i(0,t) = T_{in}(t) \qquad \text{Input temperature} \qquad (4.2.4)$$

In an axial-symmetric system, the transient heat conduction equation for the grout and the soil mass can be described as:

$$\frac{1}{\alpha_{grout}}\frac{\partial T_{grout}}{\partial t} - \frac{\partial^2 T_{grout}}{\partial r^2} - \frac{1}{r}\frac{\partial T_{grout}}{\partial r} = 0 \qquad \text{Grout Domain} \qquad \alpha_{grout} = \frac{\lambda_g}{\rho_g c_g} \qquad (4.2.5)$$

$$\frac{1}{\alpha_{soil}}\frac{\partial T_{soil}}{\partial t} - \frac{\partial^2 T_{soil}}{\partial r^2} - \frac{1}{r}\frac{\partial T_{soil}}{\partial r} = 0 \qquad \text{Soil Domain} \qquad \alpha_{soil} = \frac{\lambda_{soil}}{\rho_{soil} c_{soil}} \qquad (4.2.6)$$

The corresponding boundary conditions are:

$$\lambda_{grout}\frac{\partial T_{grout}(r,t)}{\partial r}|_{r=r_g} ds_{gg} = b_{gg}(T_{grout}(r_g,t) - T_g(z,t))ds_{gg} \qquad (4.2.7)$$

$$\lambda_{grout}\frac{\partial T_{grout}(r,t)}{\partial r}|_{r=r_s} ds_{gs} = \lambda_{soil}\frac{\partial T_{soil}(r,t)}{\partial r}|_{r=r_s} ds_{gs} \qquad (4.2.8)$$

$$T_{grout}|_{r=r_s} = T_{soil}|_{r=r_s} \qquad (4.2.9)$$

$$\Delta T|_{r=\infty} = T|_{r=\infty} - T_{st} = 0 \qquad (4.2.10)$$

in which r_g is where the grout domain and the grout film are in contact. Similarly r_s is where the grout domain and the soil domain are in contact. T_{st} is the initial steady state temperature. (4.2.7) is a Neumann boundary condition equalizing the fluxes between the grout film and the grout domain and (4.2.10) is a Dirichlet boundary condition which states that at infinity the effect of the pipe system disappears. Moreover, the differential terms ds_{gg} and ds_{gs} on right and left hand side of (4.2.7) and (4.2.8) will cancel out each other.

SOLUTION OF EQUATIONS

In order to eliminate the time derivative in the presented equations, Fourier transform is used which gives:

Pipe-in

$$-\lambda\frac{d^2\hat{T}_i}{dz^2}dv_i + \rho c u\frac{d\hat{T}_i}{dz}dv_i + (i\omega\rho c dv_i + b_{ig}ds_{ig})\hat{T}_i - b_{ig}ds_{ig}\hat{T}_g = 0 \qquad (4.2.11)$$

Grout film

$$-\lambda_g\frac{\partial^2\hat{T}_g}{\partial z^2}dv_g + (i\omega\rho_g c_g dv_g + b_{ig}ds_{ig} + b_{gg}ds_{gg})\hat{T}_g - b_{ig}ds_{ig}\hat{T}_i - b_{gg}ds_{gg}\hat{T}_{Grout}|_{r=r_g} = 0 \qquad (4.2.12)$$

Equations (4.2.11) and (4.2.12) form a system of non-homogeneous ordinary differential equations. The non-homogeneity is due to the presence of $\hat{T}_{Grout}$ in equation (4.2.12). As will be seen, after solving the radial transient heat conduction equations for the grout and the soil mass, the system will be changed to a homogeneous set of equations (see equation 4.2.29).
Using Fourier transform, the transient heat conduction equation for the grout and the soil mass can be transformed to the frequency domain as well:

$$\frac{i\omega}{\alpha_{grout}}\hat{T}_{grout} - \frac{\partial^2\hat{T}_{grout}}{\partial r^2} - \frac{1}{r}\frac{\partial\hat{T}_{grout}}{\partial r} = 0 \qquad \text{Grout Domain} \qquad (4.2.13)$$

$$\frac{i\omega}{\alpha_{soil}}\hat{T}_{soil} - \frac{\partial^2\hat{T}_{soil}}{\partial r^2} - \frac{1}{r}\frac{\partial\hat{T}_{soil}}{\partial r} = 0 \qquad \text{Soil Domain} \qquad (4.2.14)$$

The boundary conditions can also be shown in the frequency domain as:

$$\lambda_{grout}\frac{\partial \hat{T}_{grout}(r,\omega)}{\partial r}|_{r=r_g} = b_{gg}(\hat{T}_{grout}(r_g,\omega) - \hat{T}_g(z,\omega)) \tag{4.2.15}$$

$$\lambda_{grout}\frac{\partial \hat{T}_{grout}(r,\omega)}{\partial r}|_{r=r_s} = \lambda_{soil}\frac{\partial \hat{T}_{soil}(r,\omega)}{\partial r}|_{r=r_s} \tag{4.2.16}$$

$$\hat{T}_{grout}|_{r=r_s} = \hat{T}_{soil}|_{r=r_s} \tag{4.2.17}$$

$$\Delta\hat{T}|_{r=\infty} = \hat{T}|_{r=\infty} - \hat{T}_{st} = 0 \tag{4.2.18}$$

Equation (4.2.13) and (4.2.14) are complex ordinary differential equation, describing a modified Bessel equation. The solution of these equations can be expressed as:

$$\hat{T}_{grout}(r,\omega) = A_g K_0(k_{grout}r) + B_g I_0(k_{grout}r) \tag{4.2.19}$$

$$\hat{T}_{soil}(r,\omega) = A_s K_0(k_{soil}r) + B_s I_0(k_{soil}r) \tag{4.2.20}$$

in which I_0 and K_0 are the modified Bessel functions of the first and second kind and $k_{grout} = \sqrt{\frac{i\omega}{\alpha_{grout}}}$ and $k_{soil} = \sqrt{\frac{i\omega}{\alpha_{soil}}}$.

Applying boundary condition (4.2.18) to (4.2.20), the 2nd term in (4.2.20) can be eliminated:

$$\hat{T}_{soil}(r,\omega) = A_s K_0(k_{soil}r) \tag{4.2.21}$$

By imposing the remaining boundary conditions, namely (4.2.15)-(4.2.17), on (4.2.19) and (4.2.20), $\hat{T}_{grout}(r,\omega)$ and $\hat{T}_{soil}(r,\omega)$ can be calculated using Maple [5] software as:

$$\hat{T}_{grout}(r,\omega) = (\frac{Q_1}{\xi}K_0(k_{grout}r) + \frac{Q_2}{\xi}I_0(k_{grout}r))\hat{T}_g \tag{4.2.22}$$

$$\hat{T}_{soil}(r,\omega) = \frac{Q_3}{\xi}K_0(k_{soil}r)\hat{T}_g \tag{4.2.23}$$

where Q_1, Q_2, Q_3 and ξ are:

$$Q_1 = b_{gg}\left(I_1\left(k_{grout}r_s\right)K_0\left(k_{soil}r_s\right)k_{grout}\lambda_{grout} + K_1\left(k_{soil}r_s\right)I_0\left(k_{grout}r_s\right)k_{soil}\lambda_s\right) \tag{4.2.24}$$

$$Q_2 = b_{gg}\left(K_1\left(k_{grout}r_s\right)K_0\left(k_{soil}r_s\right)k_{grout}\lambda_{grout} - K_1\left(k_{soil}r_s\right)k_{soil}\lambda_s K_0\left(k_{grout}r_s\right)\right) \tag{4.2.25}$$

$$Q_3 = k_{grout}\lambda_{grout}\left(K_1\left(k_{grout}r_s\right)I_0\left(b_{gg}k_{grout}r_s\right) + I_1\left(k_{grout}r_s\right)K_0\left(k_{grout}r_s\right)\right) \tag{4.2.26}$$

$$\begin{aligned}\xi = {} & K_0\left(k_{grout}r_s\right)I_1\left(k_{grout}r_g\right)K_1\left(k_{soil}r_s\right)k_{grout}k_{soil}\lambda_g\lambda_s + I_0\left(k_{grout}r_s\right)K_1\left(k_{grout}r_g\right)K_1\left(k_{soil}r_s\right)k_{grout}k_{soil}\lambda_g\lambda_s + \\ & K_0\left(k_{soil}r_s\right)K_1\left(k_{grout}r_g\right)I_1\left(k_{grout}r_s\right){k_{grout}}^2{\lambda_g}^2 - K_0\left(k_{soil}r_s\right)I_1\left(k_{grout}r_g\right)K_1\left(k_{grout}r_s\right){k_{grout}}^2{\lambda_g}^2 - \\ & K_0\left(k_{grout}r_s\right)I_0\left(k_{grout}r_g\right)K_1\left(k_{soil}r_s\right)b_{gg}k_{soil}\lambda_s + I_0\left(k_{grout}r_s\right)K_0\left(k_{grout}r_g\right)K_1\left(k_{soil}r_s\right)b_{gg}k_{soil}\lambda_s + \\ & K_0\left(k_{soil}r_s\right)K_0\left(k_{grout}r_g\right)I_1\left(k_{grout}r_s\right)b_{gg}k_{grout}\lambda_g + K_0\left(k_{soil}r_s\right)I_0\left(k_{grout}r_g\right)K_1\left(k_{grout}r_s\right)b_{gg}k_{grout}\lambda_g\end{aligned} \tag{4.2.27}$$

Subsequently $\hat{T}_{grout}(r_g,\omega)$ can be calculated as:

$$\hat{T}_{grout}(r_g,\omega) = \bar{A}_m\hat{T}_g(z,\omega) \tag{4.2.28}$$

Substituting (4.2.28) into (4.2.12), the grout film equations can be re-written as:

Grout film

$$-\lambda_g \frac{\partial^2 \hat{T}_g}{\partial z^2} d v_g + (i\omega\rho_g c_g d v_g + b_{ig} d s_{ig} + b_{gg} d s_{gg})\hat{T}_g - b_{ig} d s_{ig} \hat{T}_i - b_{gg} d s_{gg} \bar{A}_m \hat{T}_g = 0$$

after re-arrangement, the above equations is simplified to:

$$-\lambda_g \frac{\partial^2 \hat{T}_g}{\partial z^2} d v_g + (i\omega\rho_g c_g d v_g + b_{ig} d s_{ig} + b_{gg} d s_{gg}(1-\bar{A}_m))\hat{T}_g - b_{ig} d s_{ig} \hat{T}_i = 0 \tag{4.2.29}$$

Using equation 4.2.29 instead of equation 4.2.12, the system of homogeneous differential equations for the problem can be solved by eigenfunction expansion. As a result, the following solutions are proposed for each domain:

$$\hat{T}_i = A_i e^{-ikz} \quad \hat{T}_g = A_g e^{-ikz} \tag{4.2.30}$$

Substitution of proposed solutions in 4.2.30 into each component of the system gives:

Pipe-in

$$k^2 \lambda d v_i A_i e^{-ikz} - ik\rho c u d v_i A_i e^{-ikz} + (i\omega\rho c d v_i + b_{ig} d s_{ig}) A_i e^{-ikz} - b_{ig} d s_{ig} A_g e^{-ikz} = 0 \tag{4.2.31}$$

Grout film

$$k^2 \lambda_g d v_g A_g e^{-ikz} + (i\omega\rho_g c_g d v_g + b_{ig} d s_{ig} + b_{gg} d s_{gg}(1-\bar{A}_m)) A_g e^{-ikz} - b_{ig} d s_{ig} A_i e^{-ikz} = 0 \tag{4.2.32}$$

The above system of equations can be further simplified by writing it in the following matrix form:

$$\mathrm{H} = \begin{pmatrix} a_{11} & a_{12} \\ a_{21} & a_{22} \end{pmatrix} \begin{pmatrix} A_i \\ A_g \end{pmatrix} = 0 \tag{4.2.33}$$

where

$$\begin{aligned} a_{11} &= k^2 \lambda d v_i - ik\rho c u d v_i + i\omega\rho c d v_i + b_{ig} d s_{ig} \\ a_{12} &= -b_{ig} d_{ig} \\ a_{21} &= -b_{ig} d s_{ig} \\ a_{22} &= k^2 \lambda_g d v_g + i\omega\rho_g c_g d v_g + b_{ig} d s_{ig} + b_{gg} d s_{gg}(1-\bar{A}_m) \end{aligned} \tag{4.2.34}$$

Non-trivial solution of (4.2.33) can only be obtained by letting the determinant equal to zero. This will lead to the following complex four degree polynomial:

$$a_4 k^4 + a_3 k^3 + a_2 k^2 + a_1 k + a_0 = 0 \tag{4.2.35}$$

By solving the above polynomial the eigenvalues of the system are calculated. Four eigenvalues can be calculated which will be denoted by $k_i, i = 1 \ldots 4$. Because all the elements in the system are coupled, the constants in (4.2.33) can be related to each other:

$$A_i = Y^{ig} A_g \ (Y^{ig} = -\frac{a_{12}}{a_{11}}) \tag{4.2.36}$$

SPECTRAL ELEMENT FORMULATION

The system is described by a one-dimensional spectral element which has two nodes. Following the eigenvalues from equation (4.2.35) the temperature of each component of the system can be described as:

$$\hat{T}_i = A_{i1} e^{-ik_1 z} + B_{i1} e^{-ik_2 z} + A_{i2} e^{-ik_3 (h-z)} + B_{i2} e^{-ik_4 (h-z)} \tag{4.2.37}$$

$$\hat{T}_g = A_{g1} e^{-ik_1 z} + B_{g1} e^{-ik_2 z} + A_{g2} e^{-ik_3 (h-z)} + B_{g2} e^{-ik_4 (h-z)} \tag{4.2.38}$$

At z=0:

$$\hat{T}_{i1} = A_{g1}Y_1^{ig} + B_{g1}Y_2^{ig} + A_{g2}Y_3^{ig}e^{-ik_3h} + B_{g2}Y_4^{ig}e^{-ik_4h} \tag{4.2.39}$$

$$\hat{T}_{g1} = A_{g1} + B_{g1} + A_{g2}e^{-ik_3h} + B_{g2}e^{-ik_4h} \tag{4.2.40}$$

At z=h:

$$\hat{T}_{i2} = A_{g1}Y_1^{ig}e^{-ik_1h} + B_{g1}Y_2^{ig}e^{-ik_2h} + A_{g2}Y_3^{ig} + B_{g2}Y_4^{ig} \tag{4.2.41}$$

$$\hat{T}_{g2} = A_{g1}e^{-ik_1h} + B_{g1}e^{-ik_2h} + A_{g2} + B_{g2} \tag{4.2.42}$$

In a matrix form:

$$\hat{\mathbf{T}}_{node} = \mathbf{H}(k,\omega_n)\mathbf{A}$$
$$\rightarrow \mathbf{A} = \mathbf{H}^{-1}(k,\omega_n)\hat{\mathbf{T}}_{node} \tag{4.2.43}$$

$$\mathrm{H} = \begin{pmatrix} Y_1^{ig} & Y_2^{ig} & Y_3^{ig}e^{-ik_3h} & Y_4^{ig}e^{-ik_4h} \\ 1 & 1 & e^{-ik_3h} & e^{-ik_4h} \\ Y_1^{ig}e^{-ik_1h} & Y_2^{ig}e^{-ik_2h} & Y_3^{ig} & Y_4^{ig} \\ e^{-ik_1h} & e^{-ik_2h} & 1 & 1 \end{pmatrix}, \quad \mathrm{A} = \begin{pmatrix} A_{g1} \\ B_{g1} \\ A_{g2} \\ B_{g2} \end{pmatrix} \tag{4.2.44}$$

Relating the heat flux of each domain to its temperature gives:

$$\hat{q}_i = \mp\lambda\frac{\partial\hat{T}_i}{\partial z}dA_i \tag{4.2.45}$$

$$\hat{q}_g = \mp\lambda_g\frac{\partial\hat{T}_g}{\partial z}dA_g \tag{4.2.46}$$

Substituting (4.2.37) and (4.2.38) into (4.2.45) and (4.2.46) gives:

$$\hat{q}_i = \mp\lambda dA_i(-ik_1A_{g1}Y_1^{ig}e^{-ik_1z} - ik_2B_{g1}Y_2^{ig}e^{-ik_2z} + ik_3A_{g2}Y_3^{ig}e^{-ik_3(h-z)} + ik_4B_{g2}Y_4^{ig}e^{-ik_4(h-z)}) \tag{4.2.47}$$

$$\hat{q}_g = \mp\lambda_g dA_g(-ik_1A_{g1}e^{-ik_1z} - ik_2B_{g1}e^{-ik_2z} + ik_3A_{g2}e^{-ik_3(h-z)} + ik_4B_{g2}e^{-ik_4(h-z)}) \tag{4.2.48}$$

where dA_i and dA_g are the cross section of the pipe and the grout film respectively. The $\mp$ depends on the direction of heat flux at each node. The heat flux at the top node is in the minus direction; whereas, at the bottom node it is in the positive direction.
At z=0:

$$\hat{q}_{i1} = -\lambda dA_i(-ik_1A_{g1}Y_1^{ig} - ik_2B_{g1}Y_2^{ig} + ik_3A_{g2}Y_3^{ig}e^{-ik_3h} + ik_4B_{g2}Y_4^{ig}e^{-ik_4h}) \tag{4.2.49}$$

$$\hat{q}_{g1} = -\lambda_g dA_g(-ik_1A_{g1} - ik_2B_{g1} + ik_3A_{g2}e^{-ik_3h} + ik_4B_{g2}e^{-ik_4h}) \tag{4.2.50}$$

At z=h:

$$\hat{q}_{i2} = \lambda dA_i(-ik_1A_{g1}Y_1^{ig}e^{-ik_1h} - ik_2B_{g1}Y_2^{ig}e^{-ik_2h} + ik_3A_{g2}Y_3^{ig} + ik_4B_{g2}Y_4^{ig}) \tag{4.2.51}$$

$$\hat{q}_{g2} = \lambda_g dA_g(-ik_1A_{g1}e^{-ik_1h} - ik_2B_{g1}e^{-ik_2h} + ik_3A_{g2} + ik_4B_{g2}) \tag{4.2.52}$$

In a matrix form the above relations can be written as:

$$\hat{\mathbf{q}}_{node} = \mathbf{M}(k,\omega_n)\mathbf{A} \tag{4.2.53}$$

$$\mathrm{M} = \begin{pmatrix} b_{11} & b_{12} & b_{13} & b_{14} \\ b_{21} & b_{22} & b_{23} & b_{24} \\ b_{31} & b_{32} & b_{33} & b_{34} \\ b_{41} & b_{42} & b_{43} & b_{44} \end{pmatrix}, \quad \mathrm{A} = \begin{pmatrix} A_{g1} \\ B_{g1} \\ A_{g2} \\ B_{g2} \end{pmatrix} \tag{4.2.54}$$

The components of (4.2.54) are given by:

$$
\begin{aligned}
b_{11} &= ik_1 Y_1^{ig} \lambda dA_i \\
b_{12} &= ik_2 Y_2^{ig} \lambda dA_i \\
b_{13} &= -ik_3 Y_3^{ig} \lambda dA_i e^{-ik_3 h} \\
b_{14} &= -ik_4 Y_4^{ig} \lambda dA_i e^{-ik_4 h} \\
b_{21} &= ik_1 \lambda_g dA_g \\
b_{22} &= ik_2 \lambda_g dA_g \\
b_{23} &= -ik_3 \lambda_g dA_g e^{-ik_3 h} \\
b_{24} &= -ik_4 \lambda_g dA_g e^{-ik_4 h} \\
b_{31} &= -ik_1 Y_1^{ig} \lambda dA_i e^{-ik_1 h} \\
b_{32} &= -ik_2 Y_2^{ig} \lambda dA_i e^{-ik_2 h} \\
b_{33} &= ik_3 Y_3^{ig} \lambda dA_i \\
b_{34} &= ik_4 Y_4^{ig} \lambda dA_i \\
b_{41} &= -ik_1 \lambda_g dA_g e^{-ik_1 h} \\
b_{42} &= -ik_2 \lambda_g dA_g e^{-ik_2 h} \\
b_{43} &= ik_3 \lambda_g dA_g \\
b_{44} &= ik_4 \lambda_g dA_g
\end{aligned}
\tag{4.2.55}
$$

Based on (4.2.43), (4.2.53) can be re-written as:

$$
\begin{aligned}
\hat{\mathbf{q}}_{node} &= \mathbf{K}(k,\omega_n)\hat{\mathbf{T}}_{node} \\
\mathbf{K}(k,\omega_n) &= \mathbf{M}(k,\omega_n)\mathbf{H}^{-1}(k,\omega_n)
\end{aligned}
\tag{4.2.56}
$$

Similar to section 2.2 equation (4.2.56) describes a relationship between the fluxes and the temperatures in the element domain which is similar to finite element method. Since all the equations are solved analytically, if the properties of the system do not change in the z direction, the system can be solved using only one element. Figure 4.5 shows a 2-node spectral element, the temperature of the pipe and the grout film can be calculated within this element. Subsequently, the temperature of the grout and the soil mass can be calculated in the radial direction as well. Moreover, $\mathbf{K}(k,\omega_n)$ is the spectral element stiffness matrix which is frequency dependent. The assembly of the spectral element stiffness matrix can be done using the well-known finite element matrix assembling techniques. Dealing with small matrices results in the significant reduction of the computation time.

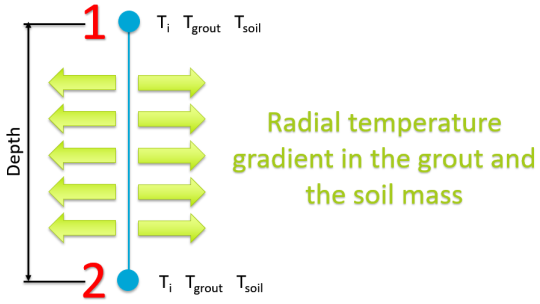

Figure 4.5: 2-node spectral element

THERMAL INTERACTION COEFFICIENTS

The thermal interaction coefficients of the above model are as following:

$$b_{ig} = \frac{1}{R_{pipe} + R_{conv}} \quad \left(R_{conv} = \frac{1}{r_i / r_o \bar{h}} \; (\bar{h} = \frac{Nu \cdot \lambda}{2r_i}), \quad R_{pipe} = r_o \frac{\mathrm{Ln}(r_o / r_i)}{\lambda_{pipe}}\right) \tag{4.2.57}$$

$$b_{gg} = \frac{1}{R_g} \quad \left(R_{gg} = r_g \frac{\mathrm{Ln}(r_g / r_o)}{\lambda_g}\right) \tag{4.2.58}$$

in which r_i and r_o are the inner and the outer radius of the pipe; r_g is the grout film radius from the origin of the system. $\bar{h}$ is the convective heat transfer coefficient where Nu is the Nusselt number.

VERIFICATION

To verify the proposed solution, a two-meter model using COMSOL Multiphysics [4] is developed and compared with the theoretical model. The COMSOL model is shown in figure 4.6 and it is 2 meters deep. The pipe, the grout and the soil mass can be seen in figure 4.6a and the meshing is shown in figure 4.6b and 4.6d. The soil block surrounding the model is considered to be 100 × 100 meters, this is in order to avoid the boundary conditions in the soil mass's boundary to impact the results of the region of interest. Moreover, symmetry is used in order to reduce the computation cost. Two cases with different velocities for the refrigerant is considered. For modeling in COMSOL both fluid flow and heat transfer in solids and fluids are utilized. In both cases, the flow is laminar ($Re < 3600$) due to the low speed of refrigerant. More details are given in table 4.2 and 4.3.

Borehole's Properties	
Borehole Length (L) [m]	2
Borehole Radius (r_g) [m]	0.05
Pipe Inner Radius (r_i) [m]	0.015
Pipe wall thickness (ds) [m]	0.002
Fluid Flow Situation	Laminar
Pipe wall Thermal Conductivity) (λ_{pipe}) [W/(m.K)]	0.42
Fluid's Properties	
Density (ρ) [$kg/(m^3)$]	1000
Specific Thermal Capacity (c) [J/(kg.K)]	4186
Thermal Conductivity (λ) [W/(m.K)]	0.56
Dynamic Viscosity (μ) [Pa.s]	0.001
Velocity (u) [m/s]	0.01 and 0.1
Input temperature (T_{in}) [°C]	3
Grout's Properties	
Density (ρ_g) [$kg/(m^3)$]	1420
Specific Thermal Capacity (c_g) [J/(kg.K)]	1197
Thermal Conductivity (λ) [W/(m.K)]	0.65
Grout Film Thickness (dg) [m]	Varying
Soil's Properties	
Depth (h) [m]	2
Density (ρ_g) [$kg/(m^3)$]	1680
Specific Thermal Capacity (c_g) [J/(kg.K)]	400
Thermal Conductivity (λ) [W/(m.K)]	2.5

Table 4.2: Properties of the Model

SEM Model	
Number of Elements	1
Computational Time	Approximately 5 minutes
FEM Model	
Number of Elements	519200
Computational Time [min]	40

Table 4.3: Computational information

The following boundary conditions are applied in COMSOL:

- **Inlet of pipe-in:** Input temperature $\big(T(0,t) = T_{in}\big)$, Input Velocity $\big(u(0,t) = u\big)$.
- **Outlet of pipe-out:** Outlet (Zero pressure at pipe's outlet) , Outflow (This node provides a suitable boundary condition for convection-dominated heat transfer at outlet boundaries. In a model with convective heat transfer, this condition states that the only heat transfer occurring across the boundary is by convection. The temperature gradient in the normal direction is zero, and there is no radiation. This is usually a good approximation of the conditions at an outlet boundary in a heat transfer model with fluid flow. [4]).
- **Top and bottom of the soil mass and grout**: Fully insulated which implies that the interaction with air and also the soil beneath the model is neglected. This is an accurate assumption due to the fact that in the SEM model these factors are not considered as well.
- **Soil mass's boundary:** $T_{soil} = 0$

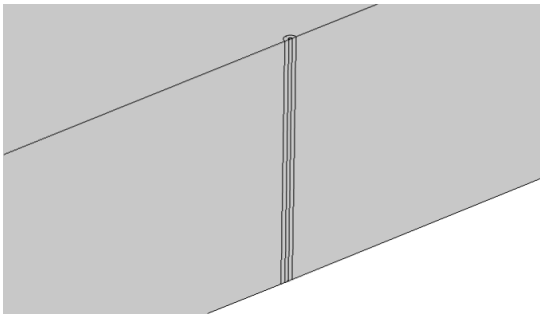

(a) Details of Symmetric Model

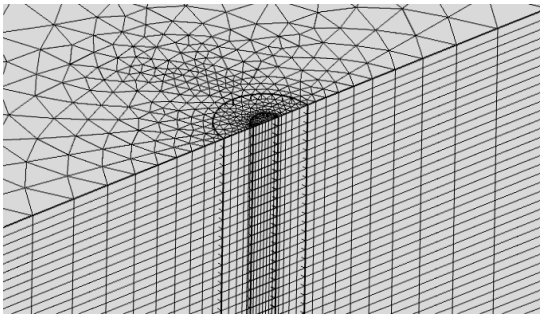

(b) Details of symmetric model mesh

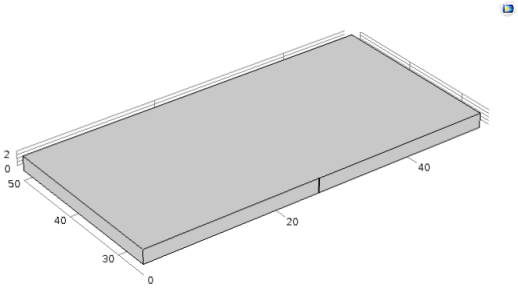

(c) Symmetric model

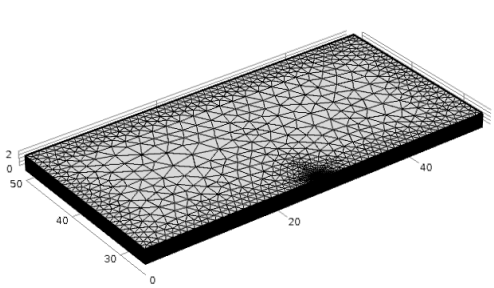

(d) Symmetric model mesh

Figure 4.6: COMSOL model

In order to compare the analytical model with the COMSOL model, the radial temperature of both the grout and the soil mass in the middle of the system (1 meter from the surface) are shown in figure (4.7) and (4.8). The temperature of aforementioned domains are given after 900 seconds, 0.5 hour, 5 hours, 24 hours and 48 hours. As can be observed the results are matching with a small difference. At the earlier stages of analysis, namely after 900 seconds and 0.5 hour, only the temperature of the grout region is shown since the soil mass would not be affected by the heat flow considerably.

4.2.1. VELOCITY OF REFRIGERANT=0.01M/S

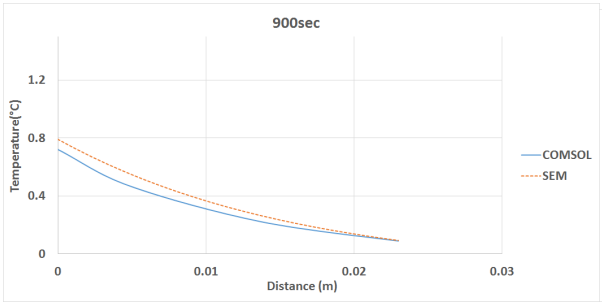

(a) Grout temperature after 900 seconds

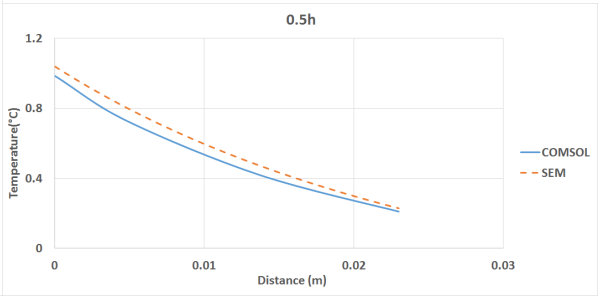

(b) Grout temperature after 0.5 hour

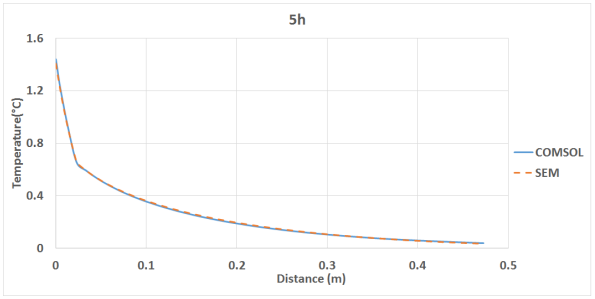

(c) Grout and soil temperature after 5 hours

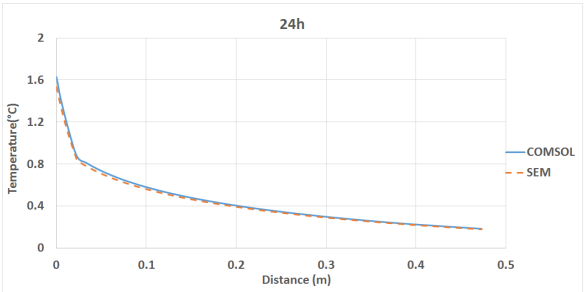

(d) Grout and soil temperature after 24 hours

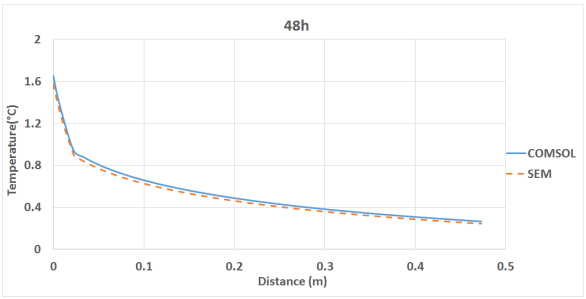

(e) Grout and soil temperature after 48 hours

Figure 4.7: Radial temperature in grout and soil domain for v=0.01 m/s

As it can be seen from the figures above, the temperature of the grout and the soil mass in both models have the same behavior. A different decaying rate of the temperature can be seen in the grout and the soil mass which is because of different heat conduction of the two domains.

4.2.2. VELOCITY OF REFRIGERANT=0.1M/S

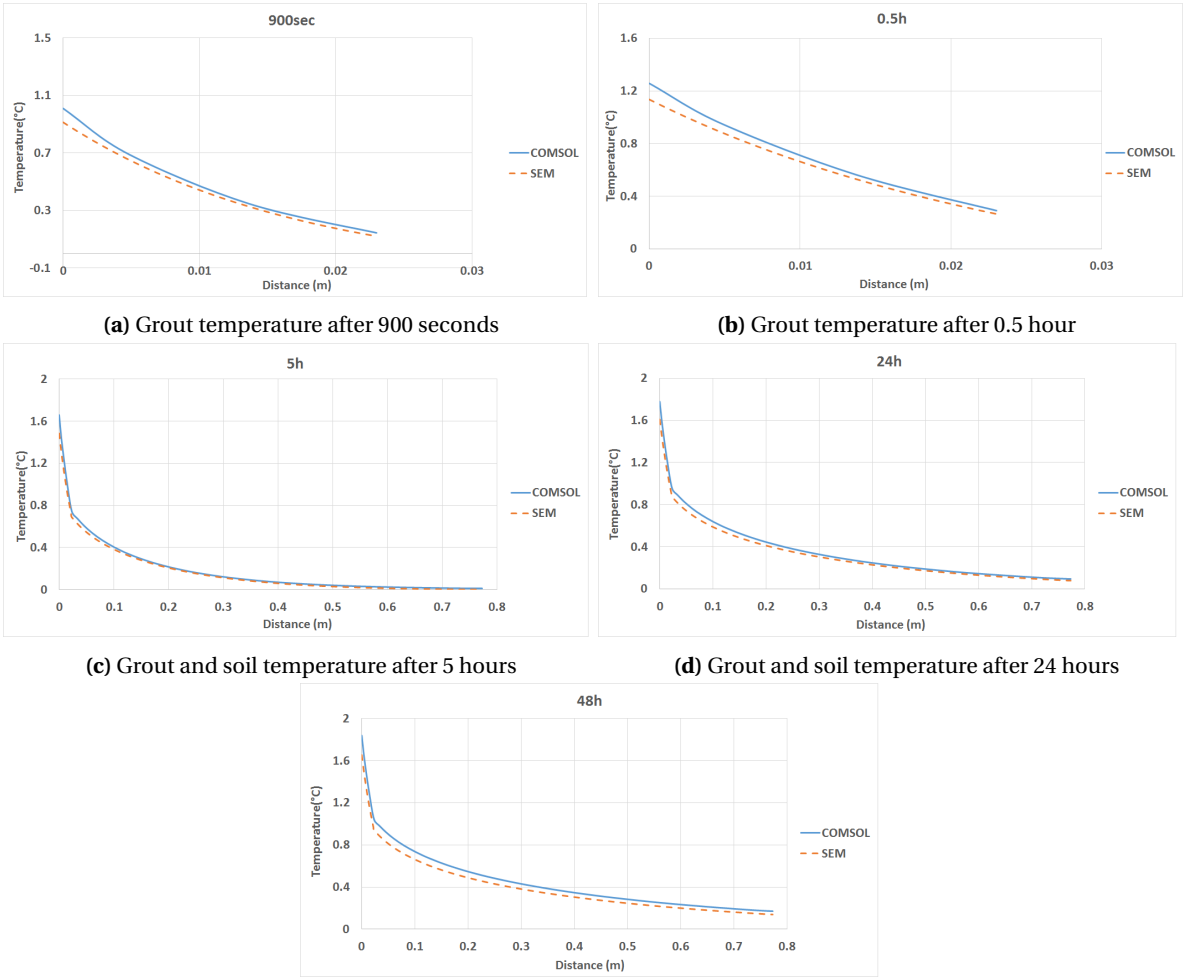

(a) Grout temperature after 900 seconds

(b) Grout temperature after 0.5 hour

(c) Grout and soil temperature after 5 hours

(d) Grout and soil temperature after 24 hours

(e) Grout and soil temperature after 48 hours

Figure 4.8: Radial temperature in grout and soil domain for v=0.1 m/s

The difference between the two models in this case is more apparent. This can be linked to the higher velocity of the refrigerant. In the FEM model any change to the velocity of the refrigerant will affect the meshing for the pipe. As it was mentioned before, the FEM model is dependent on the physical properties of the system and as the physical properties change, the meshing approach and density should also change.

4.3. COAXIAL MODEL

Based on the previous sections, here a formulation for coaxial shallow geothermal system is presented. It is assumed that the pipe-in is embedded inside the pipe-out (CXC) and the pipe-out exchanges heat with the grout. With the same reasoning as previous section a grout film is introduced between the pipe-out and the grout.

The refrigerant enters inside pipe-in from its inlet and after traveling downwards it comes back throughout pipe-out. (figure 4.9). The same approach can be utilized for modeling the other type of coaxial shallow geothermal system (CXA).

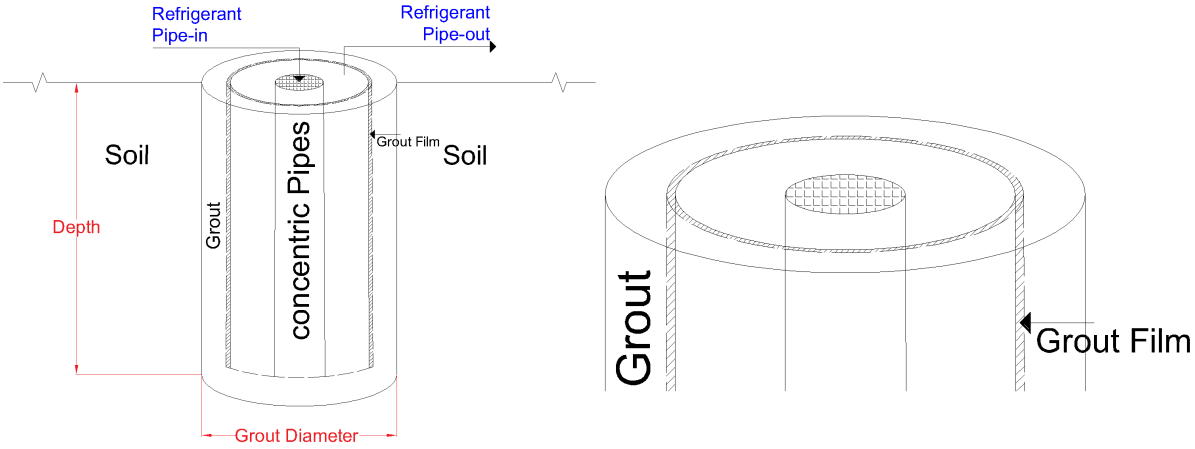

(a) Coaxial shallow geothermal **(b)** Model's schematic

Figure 4.9: SEM model for coaxial shallow geothermal systems

The heat equations for coaxial shallow geothermal system are

Pipe-in

$$\rho c\frac{\partial T_i}{\partial t}dv_i-\lambda\frac{\partial^2 T_i}{\partial z^2}dv_i+\rho cu\frac{\partial T_i}{\partial z}dv_i+b_{io}(T_i-T_o)ds_{io}=0 \tag{4.3.1}$$

Pipe-out

$$\rho c\frac{\partial T_o}{\partial t}dv_o-\lambda\frac{\partial^2 T_o}{\partial z^2}dv_o-\rho cu\frac{\partial T_o}{\partial z}dv_o+b_{io}(T_o-T_i)ds_{io}+b_{og}(T_o-T_g)ds_{og}=0 \tag{4.3.2}$$

Grout film

$$\rho_g c_g\frac{\partial T_g}{\partial t}dv_g-\lambda_g\frac{\partial^2 T_g}{\partial z^2}dv_g+b_{og}(T_g-T_o)ds_{og}+b_{gg}(T_g-T_{Grout}|_{r=r_g})ds_{gg}=0 \tag{4.3.3}$$

where the subscript i, o and g represent pipe-in, pipe-out and grout film respectively. T_i, T_o and T_g are the temperatures of pipe-in, pipe-out and grout film which are a function of z; λ and λ_g $(W/m.K)$ are the thermal conductivity of fluid and grout film; u (m/s) is the velocity of the refrigerant in the pipes; b_{io}, b_{og}, and b_{gg} $W/m^2.K$ are the reciprocal of the thermal resistance between pipe-in-pipe-out, pipe-out-gout film and grout film-grout domain; c $(J/kg.K)$ stands for the specific heat of the domain and $\rho(kg/m^3)$ is the mass density; dv_i, dv_o and dv_g (m^3) are partial volume of pipe-in, pipe-out and grout film; ds_{io}, ds_{og} and ds_{gg} (m^2) are partial surface area between pipe-in-pipe-out, pipe-out-grout and grout-film-grout respectively. The initial and boundary conditions for these domains are:

$$T_i(z,0)=T_o(z,0)=T_g(z,0)=T_{grout}(r,z,0)=T_{soil}(r,z,0) \quad \text{Initial temperature of all domains} \tag{4.3.4}$$

$$T_i(0,t)=T_{in}(t) \quad \text{Input temperature} \tag{4.3.5}$$

$$T_i(L,t)=T_o(L,t) \quad \text{Connecting the pipes} \tag{4.3.6}$$

In an axial-symmetric system, the transient heat conduction equation for the grout and the soil mass can be described as:

$$\frac{1}{\alpha_{grout}}\frac{\partial T_{grout}}{\partial t}-\frac{\partial^2 T_{grout}}{\partial r^2}-\frac{1}{r}\frac{\partial T_{grout}}{\partial r}=0 \qquad \text{Grout Domain} \qquad \alpha_{grout}=\frac{\lambda_g}{\rho_g c_g} \tag{4.3.7}$$

$$\frac{1}{\alpha_{soil}}\frac{\partial T_{soil}}{\partial t}-\frac{\partial^2 T_{soil}}{\partial r^2}-\frac{1}{r}\frac{\partial T_{soil}}{\partial r}=0 \qquad \text{Soil Domain} \qquad \alpha_{soil}=\frac{\lambda_{soil}}{\rho_{soil} c_{soil}} \tag{4.3.8}$$

The corresponding boundary conditions are:

$$\lambda_{grout}\frac{\partial T_{grout}(r,t)}{\partial r}|_{r=r_g} ds_{gg} = b_{gg}(T_{grout}(r_g,t)-T_g(z,t))ds_{gg} \tag{4.3.9}$$

$$\lambda_{grout}\frac{\partial T_{grout}(r,t)}{\partial r}|_{r=r_s} ds_{gs} = \lambda_{soil}\frac{\partial T_{soil}(r,t)}{\partial r}|_{r=r_s} ds_{gs} \tag{4.3.10}$$

$$T_{grout}|_{r=r_s} = T_{soil}|_{r=r_s} \tag{4.3.11}$$

$$\Delta T|_{r=\infty} = T|_{r=\infty} - T_{st} = 0 \tag{4.3.12}$$

in which r_g is where the grout and the grout film are in contact. Similarly r_s is where the grout and the soil domain are in contact. T_{st} is the initial steady state temperature. (4.3.9) is a Neumann boundary condition equalizing the flux between the grout film and the grout domain. (4.3.12) is a Dirichlet boundary condition which states that at infinity the effect of the system disappears.

Moreover, the differential terms ds_{gg} and ds_{gs} on the right and left hand side of (4.3.9) and (4.3.10) will cancel out each other.

SOLUTION OF EQUATIONS

Using Fourier transform, the transformed equations in the frequency domain would be:

Pipe-in

$$-\lambda\frac{d^2\hat{T}_i}{dz^2}dv_i+\rho cu\frac{d\hat{T}_i}{dz}dv_i+(i\omega\rho c dv_i+b_{io}ds_{io})\hat{T}_i-b_{io}ds_{io}\hat{T}_o=0 \tag{4.3.13}$$

Pipe-out

$$-\lambda\frac{d^2\hat{T}_o}{dz^2}dv_o-\rho cu\frac{d\hat{T}_o}{dz}dv_o+(i\omega\rho c dv_o+b_{io}ds_{io}+b_{og}ds_{og})\hat{T}_o-b_{io}ds_{io}\hat{T}_i-b_{og}ds_{og}\hat{T}_g=0 \tag{4.3.14}$$

Grout film

$$-\lambda_g\frac{\partial^2\hat{T}_g}{\partial z^2}dv_g+(i\omega\rho_g c_g dv_g+b_{og}ds_{og}+b_{gg}ds_{gg})\hat{T}_g-b_{og}ds_{og}\hat{T}_o-b_{gg}ds_{gg}\hat{T}_{Grout}|_{r=r_g}=0 \tag{4.3.15}$$

Equations (4.3.13)-(4.3.15) form a system of non-homogeneous ordinary differential equations. The non-homogeneity is due to the presence of $\hat{T}_{Grout}$ in equation (4.3.15). As will be seen, after solving the radial transient heat conduction equations for the grout and the soil mass, the system will be changed to a homogeneous set of equations (see equation 4.3.32).

Using Fourier transform, the transient heat conduction equation for the grout and the soil mass can be transformed to the frequency domain as well:

$$\frac{i\omega}{\alpha_{grout}}\hat{T}_{grout}-\frac{\partial^2\hat{T}_{grout}}{\partial r^2}-\frac{1}{r}\frac{\partial\hat{T}_{grout}}{\partial r}=0 \qquad \text{Grout Domain} \tag{4.3.16}$$

$$\frac{i\omega}{\alpha_{soil}}\hat{T}_{soil}-\frac{\partial^2\hat{T}_{soil}}{\partial r^2}-\frac{1}{r}\frac{\partial\hat{T}_{soil}}{\partial r}=0 \qquad \text{Soil Domain} \tag{4.3.17}$$

The boundary conditions can also be transformed to the frequency domain as:

$$\lambda_{grout}\frac{\partial \hat{T}_{grout}(\omega,t)}{\partial r}|_{r=r_g} = b_{gg}(\hat{T}_{grout}(r_g,\omega) - \hat{T}_g(z,\omega)) \tag{4.3.18}$$

$$\lambda_{grout}\frac{\partial \hat{T}_{grout}(r,\omega)}{\partial r}|_{r=r_s} = \lambda_{soil}\frac{\partial \hat{T}_{soil}(r,\omega)}{\partial r}|_{r=r_s} \tag{4.3.19}$$

$$\hat{T}_{grout}|_{r=r_s} = \hat{T}_{soil}|_{r=r_s} \tag{4.3.20}$$

$$\Delta\hat{T}|_{r=\infty} = \hat{T}|_{r=\infty} - \hat{T}_{st} = 0 \tag{4.3.21}$$

Equation (4.3.16) and (4.3.17) are complex ordinary differential equation, describing a modified Bessel equation. The solution of these equations can be expressed as:

$$\hat{T}_{grout}(r,\omega) = A_g K_0(k_{grout}r) + B_g I_0(k_{grout}r) \tag{4.3.22}$$

$$\hat{T}_{soil}(r,\omega) = A_s K_0(k_{soil}r) + B_s I_0(k_{soil}r) \tag{4.3.23}$$

in which I_0 and K_0 are the modified Bessel functions of the first and second kind and $k_{grout} = \sqrt{\frac{i\omega}{\alpha_{grout}}}$ and $k_{soil} = \sqrt{\frac{i\omega}{\alpha_{soil}}}$.

Applying boundary condition (4.3.21) to (4.3.23), the 2nd term in (4.3.23) can be eliminated:

$$\hat{T}_{soil}(r,\omega) = A_s K_0(k_{soil}r) \tag{4.3.24}$$

By imposing the remaining boundary conditions, namely (4.3.18)-(4.3.20), on (4.3.22) and (4.3.23), $\hat{T}_{grout}(r,\omega)$ and $\hat{T}_{soil}(r,\omega)$ can be calculated using Maple [5] software as:
By imposing boundary condition (4.3.18), (4.3.19) and (4.3.20), $\hat{T}_{grout}(r,\omega)$ and $\hat{T}_{soil}(r,\omega)$ can be calculated as

$$\hat{T}_{grout}(r,\omega) = (\frac{Q_1}{\xi}K_0(k_{grout}r) + \frac{Q_2}{\xi}I_0(k_{grout}r))\hat{T}_g \tag{4.3.25}$$

$$\hat{T}_{soil}(r,\omega) = \frac{Q_3}{\xi}K_0(k_{soil}r)\hat{T}_g \tag{4.3.26}$$

where Q_1, Q_2, Q_3 and ξ are:

$$Q_1 = b_{gg}\left(I_1\left(k_{grout}r_s\right)K_0\left(k_{soil}r_s\right)k_{grout}\lambda_{grout} + K_1\left(k_{soil}r_s\right)I_0\left(k_{grout}r_s\right)k_{soil}\lambda_s\right) \tag{4.3.27}$$

$$Q_2 = b_{gg}\left(K_1\left(k_{grout}r_s\right)K_0\left(k_{soil}r_s\right)k_{grout}\lambda_{grout} - K_1\left(k_{soil}r_s\right)k_{soil}\lambda_s K_0\left(k_{grout}r_s\right)\right) \tag{4.3.28}$$

$$Q_3 = k_{grout}\lambda_{grout}\left(K_1\left(k_{grout}r_s\right)I_0\left(b_{gg}k_{grout}r_s\right) + I_1\left(k_{grout}r_s\right)K_0\left(k_{grout}r_s\right)\right) \tag{4.3.29}$$

$$\begin{aligned}\xi = {} & K_0\left(k_{grout}r_s\right)I_1\left(k_{grout}r_g\right)K_1\left(k_{soil}r_s\right)k_{grout}k_{soil}\lambda_g\lambda_s + I_0\left(k_{grout}r_s\right)K_1\left(k_{grout}r_g\right)K_1\left(k_{soil}r_s\right)k_{grout}k_{soil}\lambda_g\lambda_s + \\ & K_0\left(k_{soil}r_s\right)K_1\left(k_{grout}r_g\right)I_1\left(k_{grout}r_s\right){k_{grout}}^2\lambda_g{}^2 - K_0\left(k_{soil}r_s\right)I_1\left(k_{grout}r_g\right)K_1\left(k_{grout}r_s\right){k_{grout}}^2\lambda_g{}^2 - \\ & K_0\left(k_{grout}r_s\right)I_0\left(k_{grout}r_g\right)K_1\left(k_{soil}r_s\right)b_{gg}k_{soil}\lambda_s + I_0\left(k_{grout}r_s\right)K_0\left(k_{grout}r_g\right)K_1\left(k_{soil}r_s\right)b_{gg}k_{soil}\lambda_s + \\ & K_0\left(k_{soil}r_s\right)K_0\left(k_{grout}r_g\right)I_1\left(k_{grout}r_s\right)b_{gg}k_{grout}\lambda_g + K_0\left(k_{soil}r_s\right)I_0\left(k_{grout}r_g\right)K_1\left(k_{grout}r_s\right)b_{gg}k_{grout}\lambda_g\end{aligned} \tag{4.3.30}$$

Subsequently $\hat{T}_{grout}(r_g,\omega)$ can be calculated as:

$$\hat{T}_{grout}(r_g,\omega) = \bar{A}_m \hat{T}_g(z,\omega) \tag{4.3.31}$$

Substituting (4.3.31) into (4.3.15), the grout film equations can be re-written as:

Grout film

$$-\lambda_g \frac{\partial^2 \hat{T}_g}{\partial z^2} dv_g + (i\omega\rho_g c_g dv_g + b_{og} ds_{og} + b_{gg} ds_{gg})\hat{T}_g - b_{og} ds_{og} \hat{T}_o - b_{gg} ds_{gg} \bar{A}_m \hat{T}_g = 0$$

upon re-arrangement, above equation yields:

$$-\lambda_g \frac{\partial^2 \hat{T}_g}{\partial z^2} dv_g + (i\omega\rho_g c_g dv_g + b_{og} ds_{og} + b_{gg} ds_{gg}(1-\bar{A}_m))\hat{T}_g - b_{og} ds_{og} \hat{T}_o = 0 \tag{4.3.32}$$

Using equation 4.3.32 instead of equation 4.3.15, the system of homogeneous differential equations for the coaxial shallow geothermal system can be solved by eigenfunction expansion. As a result, the following solutions are proposed for each domain:

$$\hat{T}_i = A_i e^{-ikz} \quad \hat{T}_o = A_o e^{-ikz} \quad \hat{T}_g = A_g e^{-ikz} \tag{4.3.33}$$

Substitution of proposed solutions in 4.3.33 into each component of the system gives:

Pipe-in

$$k^2 \lambda dv_i A_i e^{-ikz} - ik\rho cud v_i A_i e^{-ikz} + (i\omega\rho cd v_i + b_{io} ds_{io}) A_i e^{-ikz} - b_{io} ds_{io} A_g e^{-ikz} = 0 \tag{4.3.34}$$

Pipe-out

$$k^2 \lambda dv_o A_o e^{-ikz} + ik\rho cud v_o A_o e^{-ikz} + (i\omega\rho cd v_o + b_{io} ds_{io} + b_{og} ds_{og}) A_o e^{-ikz}$$
$$-b_{io} ds_{io} A_i e^{-ikz} - b_{og} ds_{og} A_g e^{-ikz} = 0 \tag{4.3.35}$$

Grout film

$$k^2 \lambda_g dv_g A_g e^{-ikz} + (i\omega\rho_g c_g dv_g + b_{og} ds_{og} + b_{gg} ds_{gg}(1-\bar{A}_m)) A_g e^{-ikz} - b_{og} ds_{og} A_o e^{-ikz} = 0 \tag{4.3.36}$$

The above equation can be further simplified to:

$$\mathrm{H} = \begin{pmatrix} a_{11} & a_{12} & 0 \\ a_{21} & a_{22} & a_{23} \\ 0 & a_{32} & a_{33} \end{pmatrix} \begin{pmatrix} A_i \\ A_o \\ A_g \end{pmatrix} = 0 \tag{4.3.37}$$

where

$$\begin{aligned}
a_{11} &= k^2 \lambda dv_i - ik\rho cud v_i + i\omega\rho cd v_i + b_{io} ds_{io} \\
a_{12} &= -b_{io} ds_{io} \\
a_{21} &= -b_{io} ds_{io} \\
a_{22} &= k^2 \lambda dv_o + i\omega\rho cd v_o + b_{io} ds_{io} + b_{og} ds_{og} \\
a_{23} &= -b_{og} ds_{og} \\
a_{32} &= -b_{og} ds_{og} \\
a_{33} &= k^2 \lambda_g dv_g + i\omega\rho_g c_g dv_g + b_{og} ds_{og} + b_{gg} ds_{gg}(1-\bar{A}_m)
\end{aligned} \tag{4.3.38}$$

Non-trivial solution of (4.3.37) can only be obtained by letting the determinant equal to zero. This will lead to the following complex sixth degree polynomial:

$$a_6 k^6 + a_5 k^5 + a_4 k^4 + a_3 k^3 + a_2 k^2 + a_1 k + a_0 = 0 \tag{4.3.39}$$

By solving the above polynomial the eigenvalues of the system can be calculated. Six eigenvalues can be calculated which will be denoted by $k_i, i = 1\ldots6$. Because all the elements in the system are coupled, the constants in (4.3.39) can be related to each other:

$$\begin{aligned}
A_i &= Y^{io} A_o \ (Y^{io} = -\frac{a_{12}}{a_{11}}) \\
A_g &= Y^{go} A_o \ (Y^{go} = -\frac{a_{32}}{a_{33}})
\end{aligned} \tag{4.3.40}$$

SPECTRAL ELEMENT FORMULATION

The coaxial shallow geothermal system is described by a one-dimensional spectral element which has two nodes. Following the eigenvalues from equation (4.3.39) the temperature of each component of the system can be described as:

$$\hat{T}_i = A_{i1}e^{-ik_1 z} + B_{i1}e^{-ik_2 z} + C_{i1}e^{-ik_3 z} A_{i2}e^{-ik_4(h-z)} + B_{i2}e^{-ik_5(h-z)} + C_{i2}e^{-ik_6(h-z)} \tag{4.3.41}$$

$$\hat{T}_o = A_{o1}e^{-ik_1 z} + B_{o1}e^{-ik_2 z} + C_{o1}e^{-ik_3 z} A_{o2}e^{-ik_4(h-z)} + B_{o2}e^{-ik_5(h-z)} + C_{o2}e^{-ik_6(h-z)} \tag{4.3.42}$$

$$\hat{T}_g = A_{g1}e^{-ik_1 z} + B_{g1}e^{-ik_2 z} + C_{g1}e^{-ik_3 z} A_{g2}e^{-ik_4(h-z)} + B_{g2}e^{-ik_5(h-z)} + C_{g2}e^{-ik_6(h-z)} \tag{4.3.43}$$

At z=0:

$$\hat{T}_{i1} = A_{o1}Y_1^{io} + B_{o1}Y_2^{io} + C_{o1}Y_3^{io} + A_{o2}Y_4^{io}e^{-ik_4 h} + B_{o2}Y_5^{io}e^{-ik_5 h} + C_{o2}Y_6^{io}e^{-ik_6 h} \tag{4.3.44}$$

$$\hat{T}_{o1} = A_{o1} + B_{o1} + C_{o1} + A_{o2}e^{-ik_4 h} + B_{o2}e^{-ik_5 h} + C_{o2}e^{-ik_6 h} \tag{4.3.45}$$

$$\hat{T}_{g1} = A_{o1}Y_1^{go} + B_{o1}Y_2^{go} + C_{o1}Y_3^{go} + A_{o2}Y_4^{go}e^{-ik_4 h} + B_{o2}Y_5^{go}e^{-ik_5 h} + C_{o2}Y_6^{go}e^{-ik_6 h} \tag{4.3.46}$$

At z=h:

$$\hat{T}_{i2} = A_{o1}Y_1^{io}e^{-ik_1 h} + B_{o1}Y_2^{io}e^{-ik_2 h} + C_{o1}Y_3^{io}e^{-ik_3 h} + A_{o2}Y_4^{io} + B_{o2}Y_5^{io} + C_{o2}Y_6^{io} \tag{4.3.47}$$

$$\hat{T}_{o2} = A_{o1}e^{-ik_1 h} + B_{o1}e^{-ik_2 h} + C_{o1}e^{-ik_3 h} + A_{o2} + B_{o2} + C_{o2} \tag{4.3.48}$$

$$\hat{T}_{g2} = A_{o1}Y_1^{go}e^{-ik_1 h} + B_{o1}Y_2^{go}e^{-ik_2 h} + C_{o1}Y_3^{go}e^{-ik_3 h} + A_{o2}Y_4^{go} + B_{o2}Y_5^{go} + C_{g2}Y_6^{go} \tag{4.3.49}$$

In a matrix form:

$$\hat{\mathbf{T}}_{node} = \mathbf{H}(k,\omega_n)\mathbf{A} \rightarrow \mathbf{A} = \mathbf{H}^{-1}(k,\omega_n)\hat{\mathbf{T}}_{node} \tag{4.3.50}$$

$$\mathrm{H} = \begin{pmatrix} Y_1^{io} & Y_2^{io} & Y_3^{io} & Y_4^{io}e^{-ik_4 h} & Y_5^{io}e^{-ik_5 h} & Y_6^{io}e^{-ik_6 h} \\ 1 & 1 & 1 & e^{-ik_4 h} & e^{-ik_5 h} & e^{-ik_6 h} \\ Y_1^{go} & Y_2^{go} & Y_3^{go} & Y_4^{go}e^{-ik_4 h} & Y_5^{go}e^{-ik_5 h} & Y_6^{go}e^{-ik_6 h} \\ Y_1^{io}e^{-ik_1 h} & Y_2^{io}e^{-ik_2 h} & Y_3^{io}e^{-ik_3 h} & Y_4^{io} & Y_5^{io} & Y_6^{io} \\ e^{-ik_1 h} & e^{-ik_2 h} & e^{-ik_3 h} & 1 & 1 & 1 \\ Y_1^{go}e^{-ik_1 h} & Y_2^{go}e^{-ik_2 h} & Y_3^{go}e^{-ik_3 h} & Y_4^{go} & Y_5^{go} & Y_6^{go} \end{pmatrix}, \quad \mathrm{A} = \begin{pmatrix} A_{o1} \\ B_{o1} \\ C_{o1} \\ A_{o2} \\ B_{o2} \\ C_{o2} \end{pmatrix} \tag{4.3.51}$$

Relating the heat flux of each domain to its temperature gives:

$$\hat{q}_i = \mp\lambda\frac{\partial\hat{T}_i}{\partial z}dA_i \tag{4.3.52}$$

$$\hat{q}_o = \mp\lambda\frac{\partial\hat{T}_o}{\partial z}dA_o \tag{4.3.53}$$

$$\hat{q}_g = \mp\lambda_g\frac{\partial\hat{T}_g}{\partial z}dA_g \tag{4.3.54}$$

Substituting (4.3.41)-(4.3.43) into (4.3.52)-(4.3.54) gives:

$$\begin{aligned}\hat{q}_i = \mp\lambda dA_i(&-ik_1A_{o1}Y_1^{io}e^{-ik_1 z} - ik_2B_{o1}Y_2^{io}e^{-ik_2 z} - ik_3C_{o1}Y_3^{io}e^{-ik_3 z} \\ &+ ik_4A_{o2}Y_4^{io}e^{-ik_4(h-z)} + ik_5B_{o2}Y_5^{io}e^{-ik_5(h-z)} + ik_6C_{o2}Y_6^{io}e^{-ik_6(h-z)})\end{aligned} \tag{4.3.55}$$

$$\begin{aligned}\hat{q}_o = \mp\lambda_g dA_g(&-ik_1A_{o1}e^{-ik_1 z} - ik_2B_{o1}e^{-ik_2 z} - ik_3C_{o1}e^{-ik_3 z} \\ &+ ik_4A_{o2}e^{-ik_4(h-z)} + ik_5B_{o2}e^{-ik_5(h-z)} + ik_6C_{o2}e^{-ik_6(h-z)})\end{aligned} \tag{4.3.56}$$

$$\begin{aligned}\hat{q}_g = \mp\lambda dA_o(&-ik_1A_{o1}Y_1^{go}e^{-ik_1 z} - ik_2B_{o1}Y_2^{go}e^{-ik_2 z} - ik_3C_{o1}Y_3^{go}e^{-ik_3 z} \\ &+ ik_4A_{o2}Y_4^{io}e^{-ik_4(h-z)} + ik_5B_{o2}Y_5^{io}e^{-ik_5(h-z)} + ik_6C_{o2}Y_6^{io}e^{-ik_6(h-z)})\end{aligned} \tag{4.3.57}$$

At z=zero:

$$\hat{q}_{i1} = -\lambda d A_i(-ik_1 A_{o1} Y_1^{io} - ik_2 B_{o1} Y_2^{io} - ik_3 C_{o1} Y_3^{io} + ik_4 A_{o2} Y_4^{io} e^{-ik_4 h} + ik_5 A_{o2} Y_5^{io} e^{-ik_5 h} + ik_6 B_{o2} Y_6^{io} e^{-ik_6 h}) \tag{4.3.58}$$

$$\hat{q}_{o1} = -\lambda_g d A_g(-ik_1 A_{o1} - ik_2 B_{o1} - ik_3 C_{o1} + ik_4 A_{o2} e^{-ik_4 h} + ik_5 B_{o2} e^{-ik_5 h} + ik_6 C_{o2} e^{-ik_6 h}) \tag{4.3.59}$$

$$\hat{q}_{g1} = -\lambda_o d A_o(-ik_1 A_{o1} Y_1^{go} - ik_2 B_{o1} Y_2^{go} - ik_3 C_{o1} Y_3^{go} + ik_4 A_{o2} Y_4^{go} e^{-ik_4 h} + ik_5 A_{o2} Y_5^{go} e^{-ik_5 h} + ik_6 B_{o2} Y_6^{go} e^{-ik_6 h}) \tag{4.3.60}$$

At z=h:

$$\hat{q}_{i2} = \lambda d A_i(-ik_1 A_{o1} Y_1^{io} e^{-ik_1 h} - ik_2 B_{o1} Y_2^{io} e^{-ik_2 h} - ik_3 C_{o1} Y_3^{io} e^{-ik_3 h} + ik_4 A_{o2} Y_4^{io} + ik_5 B_{o2} Y_5^{io} + ik_6 C_{o2} Y_6^{io}) \tag{4.3.61}$$

$$\hat{q}_{o2} = \lambda_g d A_g(-ik_1 A_{o1} e^{-ik_1 h} - ik_2 B_{o1} e^{-ik_2 h} - ik_3 C_{o1} e^{-ik_3 h} + ik_4 A_{o2} + ik_5 B_{o2} + ik_6 C_{o2}) \tag{4.3.62}$$

$$\hat{q}_{g2} = \lambda_o d A_o(-ik_1 A_{o1} Y_1^{go} e^{-ik_1 h} - ik_2 B_{o1} Y_2^{go} e^{-ik_2 h} - ik_3 C_{o1} Y_3^{go} e^{-ik_3 h} + ik_4 A_{o2} Y_4^{go} + ik_5 B_{o2} Y_5^{go} + ik_6 C_{g2} Y_6^{go}) \tag{4.3.63}$$

In a matrix form the above relations can be written as:

$$\hat{\mathbf{q}}_{node} = \mathbf{M}(k, \omega_n)\mathbf{A} \tag{4.3.64}$$

$$\mathrm{M} = \begin{pmatrix} b_{11} & b_{12} & b_{13} & b_{14} & b_{15} & b_{16} \\ b_{21} & b_{22} & b_{23} & b_{24} & b_{26} & b_{26} \\ b_{31} & b_{32} & b_{33} & b_{34} & b_{36} & b_{36} \\ b_{41} & b_{42} & b_{43} & b_{44} & b_{46} & b_{46} \\ b_{51} & b_{52} & b_{53} & b_{54} & b_{56} & b_{56} \\ b_{61} & b_{62} & b_{63} & b_{64} & b_{66} & b_{66} \end{pmatrix}, \quad \mathrm{A} = \begin{pmatrix} A_{o1} \\ B_{o1} \\ C_{o1} \\ A_{o2} \\ B_{o2} \\ C_{o2} \end{pmatrix} \tag{4.3.65}$$

where:

$$
\begin{aligned}
b_{11} &= ik_1 Y_1^{io} \lambda dA_i & b_{12} &= ik_2 Y_2^{io} \lambda dA_i \\
b_{13} &= ik_3 Y_3^{io} \lambda dA_i & b_{14} &= -ik_4 Y_4^{io} \lambda dA_i e^{-ik_4 h} \\
b_{15} &= -ik_5 Y_5^{io} \lambda dA_i e^{-ik_5 h} & b_{16} &= -ik_6 Y_6^{io} \lambda dA_i e^{-ik_6 h} \\
b_{21} &= ik_1 \lambda_g dA_g & b_{22} &= ik_2 \lambda_g dA_g \\
b_{23} &= ik_3 \lambda_g dA_g & b_{24} &= -ik_4 \lambda_g dA_g e^{-ik_4 h} \\
b_{25} &= -ik_5 \lambda_g dA_g e^{-ik_5 h} & b_{26} &= -ik_6 \lambda_g dA_g e^{-ik_6 h} \\
b_{31} &= ik_1 Y_1^{go} \lambda dA_o & b_{32} &= ik_2 Y_2^{go} \lambda dA_o \\
b_{33} &= ik_3 Y_3^{go} \lambda dA_o & b_{34} &= -ik_4 Y_4^{go} \lambda dA_o e^{-ik_4 h} \\
b_{35} &= -ik_5 Y_5^{go} \lambda dA_o e^{-ik_5 h} & b_{36} &= -ik_6 Y_6^{go} \lambda dA_o e^{-ik_6 h} \\
b_{41} &= -ik_1 Y_1^{io} \lambda dA_i e^{-ik_1 h} & b_{42} &= -ik_2 Y_2^{io} \lambda dA_i e^{-ik_2 h} \\
b_{43} &= -ik_3 Y_3^{io} \lambda dA_i e^{-ik_3 h} & b_{44} &= ik_4 Y_4^{io} \lambda dA_i \\
b_{45} &= ik_5 Y_5^{io} \lambda dA_i & b_{46} &= ik_6 Y_6^{io} \lambda dA_i \\
b_{51} &= -ik_1 \lambda_g dA_g e^{-ik_1 h} & b_{52} &= -ik_2 \lambda_g dA_g e^{-ik_2 h} \\
b_{53} &= -ik_3 \lambda_g dA_g e^{-ik_3 h} & b_{54} &= ik_4 \lambda_g dA_g \\
b_{55} &= ik_5 \lambda_g dA_g & b_{56} &= ik_6 \lambda_g dA_g \\
b_{61} &= -ik_1 Y_1^{go} \lambda dA_o e^{-ik_1 h} & b_{62} &= -ik_2 Y_2^{go} \lambda dA_o e^{-ik_2 h} \\
b_{63} &= -ik_3 Y_3^{go} \lambda dA_o e^{-ik_3 h} & b_{64} &= ik_4 Y_4^{go} \lambda dA_o \\
b_{65} &= ik_5 Y_5^{go} \lambda dA_o & b_{66} &= ik_6 Y_6^{go} \lambda dA_o
\end{aligned}
\tag{4.3.66}
$$

Based on (4.3.50), (4.3.64) can be re-written as:

$$
\begin{aligned}
&\hat{\mathbf{q}}_{node} = \mathbf{K}(k,\omega_n)\hat{\mathbf{T}}_{node} \\
&\mathbf{K}(k,\omega_n) = \mathbf{M}(k,\omega_n)\mathbf{H}^{-1}(k,\omega_n)
\end{aligned}
\tag{4.3.67}
$$

In the same manner as the previous section, a two-node spectral element for the domain can be formulated. The temperature of the BHE components can be calculated in the z direction while the temperature of the grout and the soil mass is calculated radially.

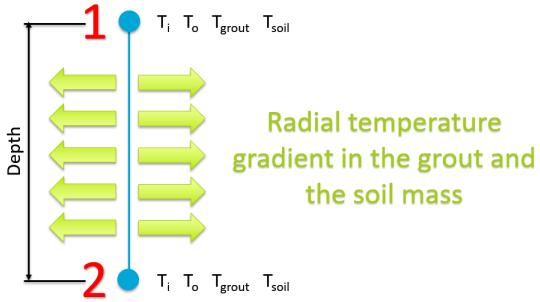

Figure 4.10: 2-node spectral element

THERMAL INTERACTION COEFFICIENTS

The thermal interaction coefficients of the above model are as following:

$$b_{io} = \frac{1}{R_{pipei} + R_{convi}} \quad \left(R_{convi} = \frac{1}{r_{ii}/r_{io}\bar{h}} \; (\bar{h} = \frac{Nu \cdot \lambda}{2r_{ii}}), \quad R_{pipei} = r_{io}\frac{\mathrm{Ln}(r_{io}/r_{ii})}{\lambda_{pipe}}\right) \tag{4.3.68}$$

$$b_{of} = \frac{1}{R_{pipeo} + R_{convo}} \quad \left(R_{convo} = \frac{1}{r_{oi}/r_{oo}\bar{h}} \; (\bar{h} = \frac{Nu \cdot \lambda}{2r_{oi}}), \quad R_{pipeo} = r_{oo}\frac{\mathrm{Ln}(r_{oo}/r_{oi})}{\lambda_{pipe}}\right) \tag{4.3.69}$$

$$b_{gg} = \frac{1}{R_g} \quad \left(R_{gg} = r_g\frac{\mathrm{Ln}(r_g/r_{oo})}{\lambda_g}\right) \tag{4.3.70}$$

In which r_{ii} and r_{io} are the inner and the outer radius of pipe-in and r_{oi} and r_{oo} are the inner and the outer radius of pipe-out ; r_g is the grout film radius from the origin of the system. $\bar{h}$ is the convective heat transfer coefficient where Nu is the Nusselt number.

4.4. NUMERICAL EXAMPLE

A 100-meter coaxial shallow geothermal system is modeled. The velocity of the refrigerant is assumed to be 0.1m/s. More details of the model are given in table 4.4 and 4.5. Some of the geometrical properties are based on the paper on Borehole resistance and vertical temperature profiles in coaxial borehole heat exchangers [6].

SEM Model	
Number of Elements	1
Computational Time	Around 5 minutes

Table 4.4: Computational information

Borehole's Properties	
Borehole Length (L) [m]	100
Borehole Radius (r_g) [m]	0.05
Pipe Inner Radius (r_i) [m]	0.015
Pipe wall thickness (ds) [m]	0.002
Fluid Flow Situation	Laminar
Pipe wall Thermal Conductivity) (λ_{pipe}) [W/(m.K)]	0.42
Fluid's Properties	
Density (ρ) [$kg/(m^3)$]	1000
Specific Thermal Capacity (c) [J/(kg.K)]	4186
Thermal Conductivity (λ) [W/(m.K)]	0.56
Dynamic Viscosity (μ) [Pa.s]	0.001
Velocity (u) [m/s]	0.1
Input temperature (T_{in}) [°C]	3
Grout's Properties	
Density (ρ_g) [$kg/(m^3)$]	1420
Specific Thermal Capacity (c_g) [J/(kg.K)]	1197
Thermal Conductivity (λ) [W/(m.K)]	0.65
Grout Film Thickness (dg) [m]	Varying
Soil's Properties	
Density (ρ_g) [$kg/(m^3)$]	1680
Specific Thermal Capacity (c_g) [J/(kg.K)]	400
Thermal Conductivity (λ) [W/(m.K)]	2.5

Table 4.5: Properties of the model

4.4.1. PIPES TEMPERATURE

The temperature profiles of Pipe-in and Pipe-out versus depth are shown after 500 seconds, 1 hour, 5 hours, 24 hours and 48 hours in figure 4.11. In order to investigate the dependency of the model on grout film thickness, 3 different grout film thicknesses are considered (1mm, 2mm and 5mm). The figures show that the results are indeed independent of the grout film thickness.

After 500 seconds, the refrigerant reaches the middle of the pipe-in. Even though the refrigerant has not reached pipe-out, it can be clearly observed that the pipe-out temperature is influenced by the pipe-in within the affected length (from 0-50 meters). The results also show that the system reaches the steady state after 5 hours.

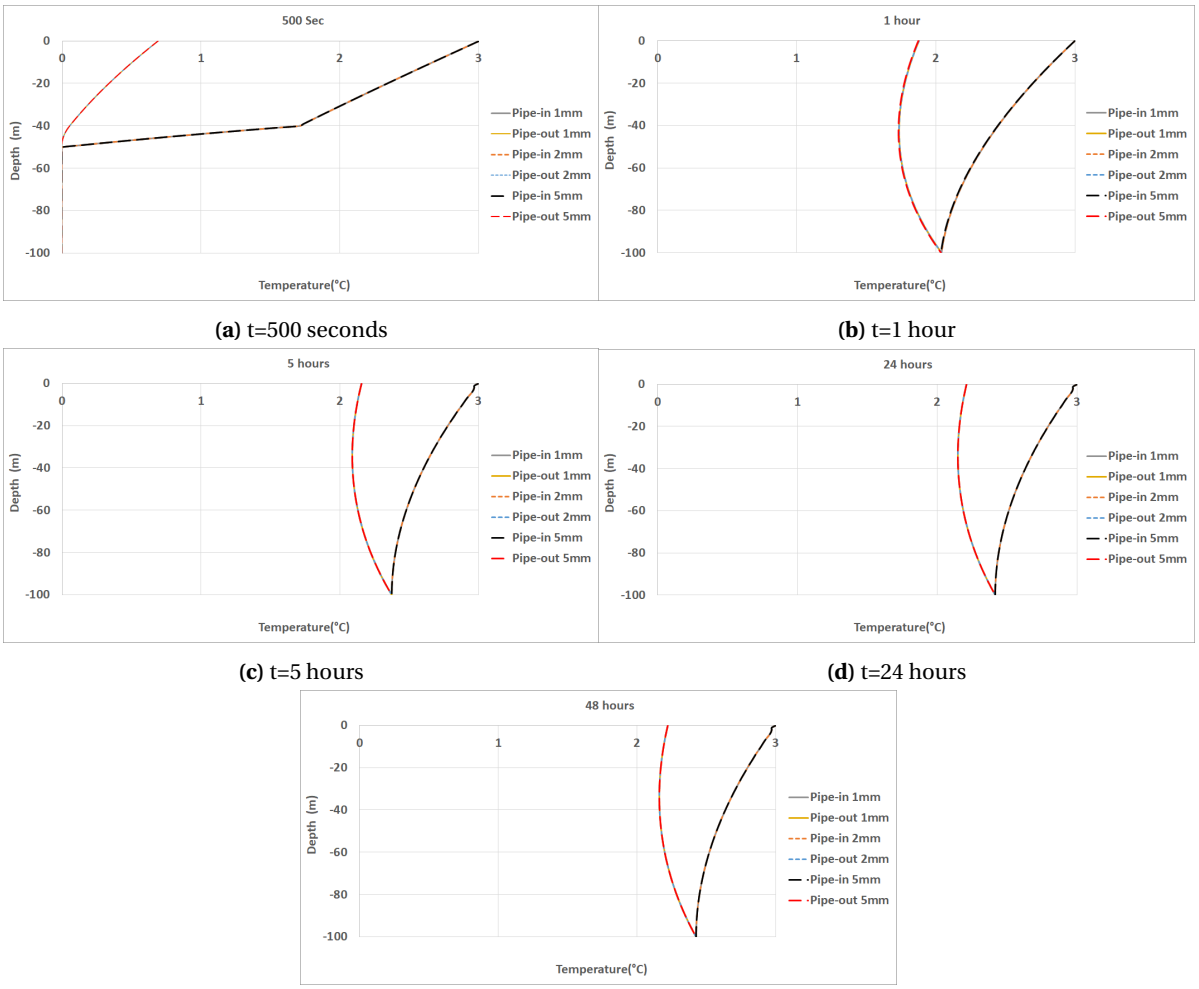

(a) t=500 seconds

(b) t=1 hour

(c) t=5 hours

(d) t=24 hours

(e) t=48 hours

Figure 4.11: Temperature of pipe-in and pipe-out at different times

4.4.2. GROUT AND SOIL DOMAIN TEMPERATURE

The temperature of the grout and the soil mass are shown here versus radial distance from the grout film and the grout domain contact location. The temperature profiles are shown after 1 hour, 5 hours, 24 hours and 48 hours. As can be seen from the figures, by assuming a thicker grout film, a smaller domain of the grout can be outputted radially (This can be clearly observed in figure 4.12a). The temperature profile of the grout and the soil mass in the radial direction proves to have little dependency on the grout film thickness.

After 1 hour, only the grout domain is affected, it is worth mentioning that compared to subsection 4.2.2 the grout absorbs the temperature slower. This can be explained by the fact that the pipe-in is inside the pip-out and the pipe-out exchanges heat with grout. In other words, the presence of the pipe out adds to the thermal resistance between the pipe-in and the grout. In contrast, in subsection 4.2.2, the pipe has a direct contact with the grout which results in more heat absorption of the grout.

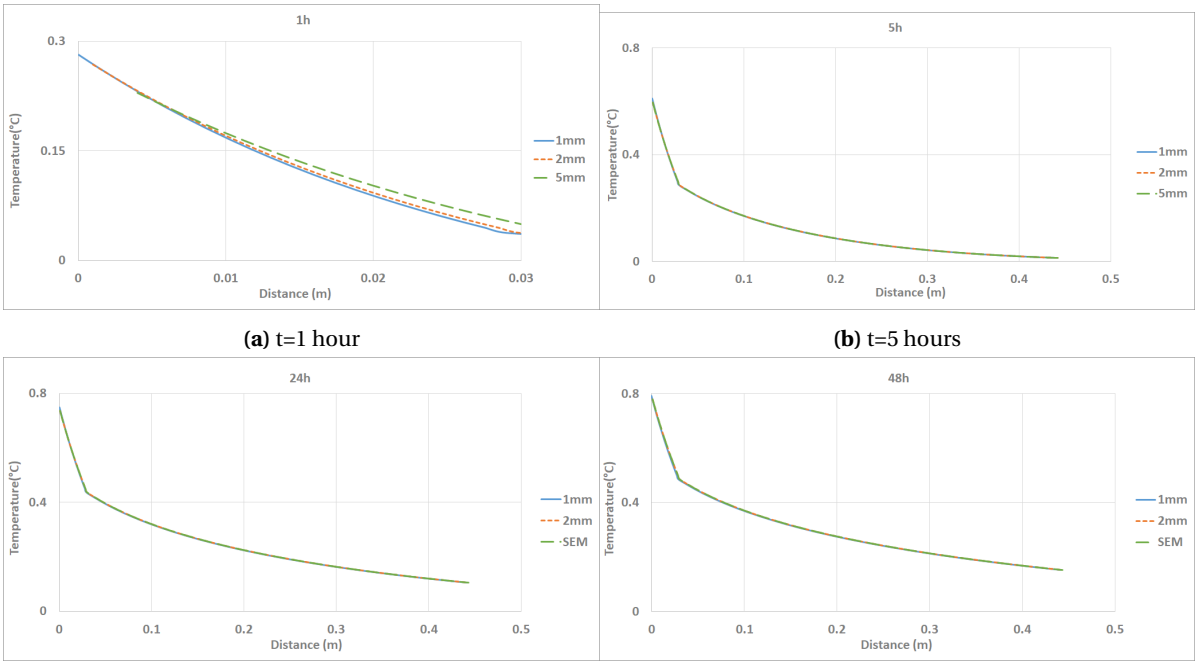

(a) t=1 hour

(b) t=5 hours

(c) t=24 hours

(d) t=48 hours

Figure 4.12: Radial temperature profile of grout and soil mass at different times

4.5. CONCLUSION

A new SEM model for coaxial shallow geothermal systems has been developed. One of the main goals of developing this model was to study the temperature distribution in the radial direction in the grout. The main difference compared to the SEM model for U-tube shallow geothermal systems is that the grout domain is modeled both in the radial and the z direction. The computational results for the temperature profile in the grout show that the radial temperature gradient is indeed present in this domain. This explains the difference between SEM and FEM results for the grout domain in U-tube shallow geothermal systems which was presented both in section 2.4 and 3.1. The results of this chapter motivate further research in modeling the grout domain using a cylindrical coordinates system in the SEM model for U-tube shallow geothermal systems.

5

CONCLUSIONS

In this thesis a spectral element model for heat flow in U-tube shallow geothermal systems, developed at TU Delft, has been examined, modified and verified. Moreover, a new model based on spectral element method (SEM) for coaxial shallow geothermal systems has been developed. Three main objectives have been achieved which can be summarized below:

- **The effect of the soil film thickness on heat flow in the SEM model for U-tube shallow geothermal systems has been diminished.** One of the components of the borehole heat exchnager (BHE) in the spectral element model for U-tube shallow geothermal systems is the soil film which couples the grout to the soil mass. The soil film does not have any physical purpose and it was introduced in order to connect the grout which is modeled in the z direction to the soil mass which is modeled radially. With this approach, the temperature of the soil film acts as an amplitude for the temperature of the soil mass and hence alleviate the need for modeling the soil mass in a cylindrical coordinates system (r,z). In order to diminish the effect of the soil film thickness on the temperature profile of the system, two main modifications have been implemented: 1)modifying the prescription of the boundary condition between the soil film and the soil mass and 2)modifying the coupling thermal coefficients. Initially the boundary condition between the soil film and the soil mass was prescribed as Dirichlet but in here it was modified to the Nuemann boundary condition. The computational results show that the soil film thickness became less pronounce, though the improvement was not significant. On the other hand, the modification of the thermal coefficients has proven to be very effective and the results show little to no dependency on the soil film thickness.

- **The SEM model has been verified by a detailed finite element model using COMSOL Multiphysics [4].** Upon implementing the modifications to the SEM model, it was verified against detail 3D finite element models using COMSOL Multiphysics. Two finite element models with realistic geometrical dimensions have been simulated and the results have been compared to the SEM model. The geometry of the shallow geothermal system consists of a single U-tube borehole heat exchanger embedded in a single-layer and a multi-layer soil mass. The number of elements for the FEM model was in order of half million elements for the multi-layer system whereas in the SEM model only 5 elements were used. In both cases the temperature distribution of pipe-in, pipe-out, grout and soil mass are in a good match. However, the differences between the two models are more apparent in the grout and in the outlet of pipe-out. These differences however, do not exceed 1°C.

- **A new spectral element model for coaxial shallow geothermal systems has been developed.** The same approach as the SEM model for the U-tube shallow geothermal systems has been utilized in formulating a new SEM model for coaxial shallow geothermal systems. The main difference in the modeling of the two systems lies in the grout domain. The heat flow in the grout domain in the U-tube sallow geothermal system is modeled in one direction, while for the coaxial shallow geothermal system, the heat flow of the grout is modeled both in the radial and the z direction. The computational results of the SEM model for the coaxial shallow geothermal system show a noticeable temperature gradient in the grout domain. This is an important observation and it can motivate further research on modeling the non-uniform radial heat flow in the grout for the U-tube shallow geothermal systems as well.

The current models available for shallow geothermal systems are either extremely computationally expensive or they have numerous simplifications in modeling the phenomena. The SEM model provides an accurate and reliable tool for these types of problems. In addition, the computational cost of the SEM model is extremely less than typical numerical models. In realistic projects, the numerical models have to deal with millions of elements and days of computations. All the meshing techniques and trial and error processes add to the involvements of numerical models. The SEM model on the other hand, can deliver results within seconds and can be used very easily.

In terms of versatility, the numerical techniques are superior to the SEM model. The numerical models can handle various types of geometrical and physical complexities along with complicated boundary conditions. In case of shallow geothermal systems, if the soil layers are not horizontal and parallel to each other or if the boundary conditions are nonuniform, they can introduce additional issues which cannot be handled by the SEM model. The physical complexities such as material nonlinearities cannot be tackled by the SEM model as well.

For typical engineering projects dealing with shallow geothermal systems and without any complexity related to physics, geometry and boundary conditions of the system, the SEM model can highly reduce the computational costs which makes it highly suitable for engineering practices

6

RECOMMENDATION

Although the current formulation of the SEM model is proven to be suitable, it is attempted to address some beneficial recommendations in order to enhance the SEM model's capabilities. The following recommendations can be a subject of more research in the future.

- As it was mentioned several times during this research, the grout domain of the SEM model for U-tube shallow geothermal systems has a heat flow only in one direction (z direction). Moreover, all the components in the BHE have the same coinciding axis in the z direction (Figure(2.3c)). The model which has been developed for coaxial shallow geothermal systesms proves the presence of a temperature gradient in the radial direction of the grout. All these issues can motivate a research to model the grout using a cylindrical coordinates system and add the pipes insidde the grout as cylindrical sources by considering the real geometry of the system without any simplifications. Some initial steps towards this goal can be taken by means of direct analytical approaches for simulating heat flow in an eccentric annulus or using approximations such as perturbation method ([7] and [8]). Furthermore, in section 4.2 a model is developed which consists of a single pipe surrounded by a grout domain and a soil mass. In theory, this can also be used in order to develop a simplified model for U-tube shallow geothermal systems by means of superposition (Figure 6.1). This can be done by superposition of the temperatures or the fluxes of both pipe-in and pipe-out in the grout. A model already exists for an infinite medium subjected to multiple cylindrical heat sources which uses the similar concept [9]. The difference in case of the U-tube shallow geothermal system would be the replacement of multiple cylindrical heat sources with pipes.

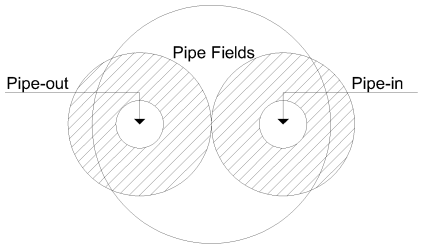

Figure 6.1: Pipe-in and Pipe-out Temperature Field

- One of the fundamental parts of the SEM model is the fast Fourier algorithm used in its calculations. The adequate number of samples, the accurate sampling time and time windowing are some of the crucial properties of this algorithm which can affect the results. Physically speaking, different domains in the model experience more temperature gradient at the earlier stages of the analysis compared to the later stages. Therefore, it would be extremely beneficial to define an optimized FFT algorithm in order to have more samples at the initial stages of the analysis (with less time between each sample) while the number of samples reduces in the later stages of analysis. In theory this should improve the model's performance and remove any potential error due to the FFT and IFFT algorithms.
- The developed coaxial model requires further verification with a FEM model or experimental data.

7

APPENDIX A

SPECTRAL ELEMENT FORMULATION

The BHE is described by a one-dimensional spectral element which has two nodes. Following the eigenvalues from equation (2.2.34) the temperature in each component of the BHE can be described as:

$$\hat{T}_i = A_{i1}e^{-ik_1 z} + B_{i1}e^{-ik_2 z} + C_{i1}e^{-ik_3 z} + D_{i1}e^{-ik_4 z} + A_{i2}e^{-ik_5(h-z)} + B_{i2}e^{-ik_6(h-z)} + C_{i2}e^{-ik_7(h-z)} + D_{i2}e^{-ik_8(h-z)} \tag{7.0.1}$$

$$\hat{T}_o = A_{o1}e^{-ik_1 z} + B_{o1}e^{-ik_2 z} + C_{o1}e^{-ik_3 z} + D_{o1}e^{-ik_4 z} + A_{o2}e^{-ik_5(h-z)} + B_{o2}e^{-ik_6(h-z)} + C_{o2}e^{-ik_7(h-z)} + D_{o2}e^{-ik_8(h-z)} \tag{7.0.2}$$

$$\hat{T}_g = A_{g1}e^{-ik_1 z} + B_{g1}e^{-ik_2 z} + C_{g1}e^{-ik_3 z} + D_{g1}e^{-ik_4 z} + A_{g2}e^{-ik_5(h-z)} + B_{g2}e^{-ik_6(h-z)} + C_{g2}e^{-ik_7(h-z)} + D_{g2}e^{-ik_8(h-z)} \tag{7.0.3}$$

$$\hat{T}_s = A_{s1}e^{-ik_1 z} + B_{s1}e^{-ik_2 z} + C_{s1}e^{-ik_3 z} + D_{s1}e^{-ik_4 z} + A_{s2}e^{-ik_5(h-z)} + B_{s2}e^{-ik_6(h-z)} + C_{s2}e^{-ik_7(h-z)} + D_{s2}e^{-ik_8(h-z)} \tag{7.0.4}$$

Using (2.2.35) combined with (7.0.1)-(7.0.4) the temperature of each component at each node, namely node 1 (z=0) and node 2 (z=h), can be calculated.
At z=0:

$$\hat{T}_{i1} = A_{g1}Y_1^{ig} + B_{g1}Y_2^{ig} + C_{g1}Y_3^{ig} + D_{g1}Y_4^{ig} + A_{g2}Y_5^{ig}e^{-ik_5 h} + B_{g2}Y_6^{ig}e^{-ik_6 h} + C_{g3}Y_7^{ig}e^{-ik_7 h} + D_{g2}Y_8^{ig}e^{-ik_8 h} \tag{7.0.5}$$

$$\hat{T}_{o1} = A_{g1}Y_1^{og} + B_{g1}Y_2^{og} + C_{g1}Y_3^{og} + D_{g1}Y_4^{og} + A_{g2}Y_5^{og}e^{-ik_5 h} + B_{g2}Y_6^{og}e^{-ik_6 h} + C_{g3}Y_7^{og}e^{-ik_7 h} + D_{g2}Y_8^{og}e^{-ik_8 h} \tag{7.0.6}$$

$$\hat{T}_{g1} = A_{g1} + B_{g1} + C_{g1} + D_{g1} + A_{g2}e^{-ik_5 h} + B_{g2}e^{-ik_6 h} + C_{g2}e^{-ik_7 h} + D_{g2}e^{-ik_8 h} \tag{7.0.7}$$

$$\hat{T}_{s1} = A_{g1}Y_1^{sg} + B_{g1}Y_2^{sg} + C_{g1}Y_3^{sg} + D_{g1}Y_4^{sg} + A_{g2}Y_5^{sg}e^{-ik_5 h} + B_{g2}Y_6^{sg}e^{-ik_6 h} + C_{g3}Y_7^{sg}e^{-ik_7 h} + D_{g2}Y_8^{sg}e^{-ik_8 h} \tag{7.0.8}$$

At z=h:

$$\hat{T}_{i2} = A_{g1}Y_1^{ig}e^{-ik_1h} + B_{g1}Y_2^{ig}e^{-ik_2h} + C_{g1}Y_3^{ig}e^{-ik_3h} + D_{g1}Y_4^{ig}e^{-ik_4h} + A_{g2}Y_5^{ig} + B_{g2}Y_6^{ig} + C_{g3}Y_7^{ig} + D_{g2}Y_8^{ig} \tag{7.0.9}$$

$$\hat{T}_{o2} = A_{g1}Y_1^{og}e^{-ik_1h} + B_{g1}Y_2^{og}e^{-ik_2h} + C_{g1}Y_3^{og}e^{-ik_3h} + D_{g1}Y_4^{og}e^{-ik_4h} + A_{g2}Y_5^{og} + B_{g2}Y_6^{og} + C_{g3}Y_7^{og} + D_{g2}Y_8^{og} \tag{7.0.10}$$

$$\hat{T}_{g2} = A_{g1}e^{-ik_1h} + B_{g1}e^{-ik_2h} + Ce_{g1}^{-ik_3h} + D_{g1}e^{-ik_4h} + A_{g2} + B_{g2} + C_{g2} + D_{g2} \tag{7.0.11}$$

$$\hat{T}_{s2} = A_{g1}Y_1^{sg}e^{-ik_1h} + B_{g1}Y_2^{sg}e^{-ik_2h} + C_{g1}Y_3^{sg}e^{-ik_3h} + D_{g1}Y_4^{sg}e^{-ik_4h} + A_{g2}Y_5^{sg} + B_{g2}Y_6^{sg} + C_{g2}Y_7^{sg} + D_{g2}Y_8^{sg} \tag{7.0.12}$$

In a matrix form we can write:

$$\hat{\mathbf{T}}_{node} = \mathbf{H}(k,\omega_n)\mathbf{A} \rightarrow \mathbf{A} = \mathbf{H}^{-1}(k,\omega_n)\hat{\mathbf{T}}_{node} \tag{7.0.13}$$

$$\mathbf{H} = \begin{pmatrix} Y_1^{ig} & Y_2^{ig} & Y_3^{ig} & Y_4^{ig} & Y_5^{ig}e^{-ik_5h} & Y_6^{ig}e^{-ik_6h} & Y_7^{ig}e^{-ik_7h} & Y_8^{ig}e^{-ik_8h} \\ Y_1^{og} & Y_2^{og} & Y_3^{og} & Y_4^{og} & Y_5^{og}e^{-ik_5h} & Y_6^{og}e^{-ik_6h} & Y_7^{og}e^{-ik_7h} & Y_8^{og}e^{-ik_8h} \\ 1 & 1 & 1 & 1 & e^{-ik_5h} & e^{-ik_6h} & e^{-ik_7h} & e^{-ik_8h} \\ Y_1^{sg} & Y_2^{sg} & Y_3^{sg} & Y_4^{sg} & Y_5^{sg}e^{-ik_5h} & Y_6^{sg}e^{-ik_6h} & Y_7^{sg}e^{-ik_7h} & Y_8^{sg}e^{-ik_8h} \\ Y_1^{ig}e^{-ik_1h} & Y_2^{ig}e^{-ik_2h} & Y_3^{ig}e^{-ik_3h} & Y_4^{ig}e^{-ik_4h} & Y_5^{ig} & Y_6^{ig} & Y_7^{ig} & Y_8^{ig} \\ Y_1^{og}e^{-ik_1h} & Y_2^{og}e^{-ik_2h} & Y_3^{og}e^{-ik_3h} & Y_4^{og}e^{-ik_4h} & Y_5^{og} & Y_6^{og} & Y_7^{og} & Y_8^{og} \\ e^{-ik_1h} & e^{-ik_2h} & e^{-ik_3h} & e^{-ik_4h} & 1 & 1 & 1 & 1 \\ Y_1^{sg}e^{-ik_1h} & Y_2^{sg}e^{-ik_2h} & Y_3^{sg}e^{-ik_3h} & Y_4^{sg}e^{-ik_4h} & Y_5^{sg} & Y_6^{sg} & Y_7^{sg} & Y_8^{sg} \end{pmatrix},$$

$$\mathbf{A} = \begin{pmatrix} A_{g1} \\ B_{g1} \\ C_{g1} \\ D_{g1} \\ A_{g2} \\ B_{g2} \\ C_{g2} \\ D_{g2} \end{pmatrix}, \hat{\mathbf{T}}_{node} = \begin{pmatrix} T_{i1} \\ T_{o1} \\ T_{g1} \\ T_{s1} \\ T_{i2} \\ T_{o2} \\ T_{g2} \\ T_{s2} \end{pmatrix} \tag{7.0.14}$$

The heat flux in the BHE components are:

$$\begin{aligned} \hat{q}_i &= \mp\lambda\frac{\partial\hat{T}_i}{\partial z}dA_i \\ \hat{q}_o &= \mp\lambda\frac{\partial\hat{T}_o}{\partial z}dA_o \\ \hat{q}_g &= \mp\lambda_g\frac{\partial\hat{T}_g}{\partial z}dA_g \\ \hat{q}_s &= \mp\lambda\frac{\partial\hat{T}_s}{\partial z}dA_s \end{aligned} \tag{7.0.15}$$

where the $\mp$ sign has to do with the flux direction at each node, at top node the flux direction is negative, while at bottom it is positive.
Substituting (7.0.1)-(7.0.4) into (7.0.15) gives:

$$\hat{q}_i = \mp\lambda d A_i(-ik_1 A_{g1} Y_1^{ig} e^{-ik_1 z} - ik_2 B_{g1} Y_2^{ig} e^{-ik_2 z} - ik_3 C_{g1} Y_3^{ig} e^{-ik_4 z} - ik_4 D_{g1} Y_4^{ig} e^{-ik_4 z} + ik_5 A_{g2} Y_5^{ig} e^{-ik_5(h-z)} + ik_6 B_{g2} Y_6^{ig} e^{-ik_6(h-z)} + ik_7 C_{g2} Y_7^{ig} e^{-ik_7(h-z)} + ik_8 D_{g2} Y_8^{ig} e^{-ik_8(h-z)}) \tag{7.0.16}$$

$$\hat{q}_o = \mp\lambda d A_o(-ik_1 A_{g1} Y_1^{og} e^{-ik_1 z} - ik_2 B_{g1} Y_2^{og} e^{-ik_2 z} - ik_3 C_{g1} Y_3^{og} e^{-ik_4 z} - ik_4 D_{g1} Y_4^{og} e^{-ik_4 z} + ik_5 A_{g2} Y_5^{og} e^{-ik_5(h-z)} + ik_6 B_{g2} Y_6^{og} e^{-ik_6(h-z)} + ik_7 C_{g2} Y_7^{og} e^{-ik_7(h-z)} + ik_8 D_{g2} Y_8^{og} e^{-ik_8(h-z)}) \tag{7.0.17}$$

$$\hat{q}_g = \mp\lambda_g d A_g(-ik_1 A_{g1} e^{-ik_1 z} - ik_2 B_{g1} e^{-ik_2 z} - ik_3 C_{g1} e^{-ik_4 z} - ik_4 D_{g1} e^{-ik_4 z} + ik_5 A_{g2} e^{-ik_5(h-z)} + ik_6 B_{g2} e^{-ik_6(h-z)} + ik_7 C_{g2} e^{-ik_7(h-z)} + ik_8 D_{g2} e^{-ik_8(h-z)}) \tag{7.0.18}$$

$$\hat{q}_s = \mp\lambda_s d A_s(-ik_1 A_{g1} Y_1^{sg} e^{-ik_1 z} - ik_2 B_{g1} Y_2^{sg} e^{-ik_2 z} - ik_3 C_{g1} Y_3^{sg} e^{-ik_4 z} - ik_4 D_{g1} Y_4^{sg} e^{-ik_4 z} + ik_5 A_{g2} Y_5^{sg} e^{-ik_5(h-z)} + ik_6 B_{g2} Y_6^{sg} e^{-ik_6(h-z)} + ik_7 C_{g2} Y_7^{sg} e^{-ik_7(h-z)} + ik_8 D_{g2} Y_8^{sg} e^{-ik_8(h-z)}) \tag{7.0.19}$$

At z=0:

$$\hat{q}_{i1} = -\lambda d A_i(-ik_1 A_{g1} Y_1^{ig} - ik_2 B_{g1} Y_2^{ig} - ik_3 C_{g1} Y_3^{ig} - ik_4 D_{g1} Y_4^{ig} + ik_5 A_{g2} Y_5^{ig} e^{-ik_5 h} + ik_6 B_{g2} Y_6^{ig} e^{-ik_6 h} + ik_7 C_{g2} Y_7^{ig} e^{-ik_7 h} + ik_8 D_{g2} Y_8^{ig} e^{-ik_8 h}) \tag{7.0.20}$$

$$\hat{q}_{o1} = -\lambda d A_o(-ik_1 A_{g1} Y_1^{og} - ik_2 B_{g1} Y_2^{og} - ik_3 C_{g1} Y_3^{og} - ik_4 D_{g1} Y_4^{og} + ik_5 A_{g2} Y_5^{og} e^{-ik_5 h} + ik_6 B_{g2} Y_6^{og} e^{-ik_6 h} + ik_7 C_{g2} Y_7^{og} e^{-ik_7 h} + ik_8 D_{g2} Y_8^{og} e^{-ik_8 h}) \tag{7.0.21}$$

$$\hat{q}_{g1} = -\lambda_g d A_g(-ik_1 A_{g1} - ik_2 B_{g1} - ik_3 C_{g1} - ik_4 D_{g1} + ik_5 A_{g2} e^{-ik_5 h} + ik_6 B_{g2} e^{-ik_6 h} + ik_7 C_{g2} e^{-ik_7 h} + ik_8 D_{g2} e^{-ik_8 h}) \tag{7.0.22}$$

$$\hat{q}_{s1} = -\lambda d A_o(-ik_1 A_{g1} Y_1^{sg} - ik_2 B_{g1} Y_2^{sg} - ik_3 C_{g1} Y_3^{sg} - ik_4 D_{g1} Y_4^{sg} + ik_5 A_{g2} Y_5^{sg} e^{-ik_5 h} + ik_6 B_{g2} Y_6^{sg} e^{-ik_6 h} + ik_7 C_{g2} Y_7^{sg} e^{-ik_7 h} + ik_8 D_{g2} Y_8^{sg} e^{-ik_8 h}) \tag{7.0.23}$$

At z=h:

$$\hat{q}_{i2} = \lambda d A_i(-ik_1 A_{g1} Y_1^{ig} e^{-ik_1 h} - ik_2 B_{g1} Y_2^{ig} e^{-ik_2 h} - ik_3 C_{g1} Y_3^{ig} e^{-ik_3 h} - ik_4 D_{g1} Y_4^{ig} e^{-ik_4 h} + ik_5 A_{g2} Y_5^{ig} + ik_6 B_{g2} Y_6^{ig} + ik_7 C_{g2} Y_7^{ig} + ik_8 D_{g2} Y_8^{ig}) \tag{7.0.24}$$

$$\hat{q}_{o2} = \lambda d A_o(-ik_1 A_{g1} Y_1^{og} e^{-ik_1 h} - ik_2 B_{g1} Y_2^{og} e^{-ik_2 h} - ik_3 C_{g1} Y_3^{og} e^{-ik_3 h} - ik_4 D_{g1} Y_4^{og} e^{-ik_4 h} + ik_5 A_{g2} Y_5^{og} + ik_6 B_{g2} Y_6^{og} + ik_7 C_{g2} Y_7^{og} + ik_8 D_{g2} Y_8^{og}) \tag{7.0.25}$$

$$\hat{q}_{g2} = \lambda_g d A_g(-ik_1 A_{g1} e^{-ik_1 h} - ik_2 B_{g1} e^{-ik_2 h} - ik_3 C_{g1} e^{-ik_3 h} - ik_4 D_{g1} e^{-ik_4 h} + ik_5 A_{g2} + ik_6 B_{g2} + ik_7 C_{g2} + ik_8 D_{g2}) \tag{7.0.26}$$

$$\hat{q}_{s2} = \lambda_s d A_s(-ik_1 A_{g1} Y_1^{sg} e^{-ik_1 h} - ik_2 B_{g1} Y_2^{sg} e^{-ik_2 h} - ik_3 C_{g1} Y_3^{sg} e^{-ik_3 h} - ik_4 D_{g1} Y_4^{sg} e^{-ik_4 h} + ik_5 A_{g2} Y_5^{sg} + ik_6 B_{g2} Y_6^{sg} + ik_7 C_{g2} Y_7^{sg} + ik_8 D_{g2} Y_8^{sg}) \tag{7.0.27}$$

In a matrix form we can write:

$$\hat{\mathbf{q}}_{node} = \mathbf{M}(k,\omega_n)\mathbf{A} \rightarrow \hat{\mathbf{q}}_{node} = \mathbf{K}(k,\omega_n)\hat{\mathbf{T}}_{node} \tag{7.0.28}$$

$$\mathbf{K}(k,\omega_n) = \mathbf{M}(k,\omega_n)\mathbf{H}^{-1}(k,\omega_n) \tag{7.0.29}$$

$$\mathrm{M} = \begin{pmatrix} b_{11} & b_{12} & b_{13} & b_{14} & b_{15} & b_{16} & b_{17} & b_{18} \\ b_{21} & b_{22} & b_{23} & b_{24} & b_{25} & b_{26} & b_{27} & b_{28} \\ b_{31} & b_{32} & b_{33} & b_{34} & b_{35} & b_{36} & b_{37} & b_{38} \\ b_{41} & b_{42} & b_{43} & b_{44} & b_{45} & b_{46} & b_{47} & b_{48} \\ b_{51} & b_{52} & b_{53} & b_{54} & b_{55} & b_{56} & b_{57} & b_{58} \\ b_{61} & b_{62} & b_{63} & b_{64} & b_{65} & b_{66} & b_{67} & b_{68} \\ b_{71} & b_{72} & b_{73} & b_{74} & b_{75} & b_{76} & b_{77} & b_{78} \\ b_{81} & b_{82} & b_{83} & b_{64} & b_{85} & b_{86} & b_{87} & b_{88} \end{pmatrix}, \ \mathrm{A} = \begin{pmatrix} A_{g1} \\ B_{g1} \\ C_{g1} \\ D_{g1} \\ A_{g2} \\ B_{g2} \\ C_{g2} \\ D_{g2} \end{pmatrix} \tag{7.0.30}$$

$$\begin{aligned}
b_{11} &= ik_1 Y_1^{ig} \lambda dA_i & b_{12} &= ik_2 Y_2^{ig} \lambda dA_i \\
b_{13} &= ik_3 Y_3^{ig} \lambda dA_i & b_{14} &= ik_4 Y_4^{ig} \lambda dA_i \\
b_{15} &= -ik_5 Y_5^{ig} \lambda dA_i e^{-ik_5 h} & b_{16} &= -ik_6 Y_6^{ig} \lambda dA_i e^{-ik_6 h} \\
b_{17} &= -ik_7 Y_7^{ig} \lambda dA_i e^{-ik_7 h} & b_{18} &= -ik_8 Y_8^{ig} \lambda dA_i e^{-ik_8 h} \\
\\
b_{21} &= ik_1 Y_1^{og} \lambda dA_o & b_{22} &= ik_2 Y_2^{og} \lambda dA_o \\
b_{23} &= ik_3 Y_3^{og} \lambda dA_o & b_{24} &= ik_4 Y_4^{og} \lambda dA_o \\
b_{25} &= -ik_5 Y_5^{og} \lambda dA_o e^{-ik_5 h} & b_{26} &= -ik_6 Y_6^{og} \lambda dA_o e^{-ik_6 h} \\
b_{27} &= -ik_7 Y_7^{og} \lambda dA_o e^{-ik_7 h} & b_{28} &= -ik_8 Y_8^{og} \lambda dA_o e^{-ik_8 h} \\
\\
b_{31} &= ik_1 \lambda_g dA_g & b_{32} &= ik_2 \lambda_g dA_g \\
b_{33} &= ik_3 \lambda_g dA_g & b_{34} &= ik_4 \lambda_g dA_g \\
b_{35} &= -ik_5 \lambda_g dA_g e^{-ik_5 h} & b_{36} &= -ik_6 \lambda_g dA_g e^{-ik_6 h} \\
b_{37} &= -ik_7 \lambda_g dA_g e^{-ik_7 h} & b_{38} &= -ik_8 \lambda_g dA_g e^{-ik_8 h} \\
\\
b_{41} &= ik_1 Y_1^{sg} \lambda dA_s & b_{42} &= ik_2 Y_2^{sg} \lambda dA_s \\
b_{43} &= ik_3 Y_3^{sg} \lambda dA_s & b_{44} &= ik_4 Y_4^{sg} \lambda dA_s \\
b_{45} &= -ik_5 Y_5^{sg} \lambda dA_s e^{-ik_5 h} & b_{46} &= -ik_6 Y_6^{sg} \lambda dA_s e^{-ik_6 h} \\
b_{47} &= -ik_7 Y_7^{sg} \lambda dA_s e^{-ik_7 h} & b_{48} &= -ik_8 Y_8^{sg} \lambda dA_s e^{-ik_8 h}
\end{aligned} \tag{7.0.31}$$

$$
\begin{aligned}
b_{51} &= -ik_1 Y_1^{ig} \lambda dA_i e^{-ik_1 h} & b_{52} &= -ik_2 Y_2^{ig} \lambda dA_i e^{-ik_2 h} \\
b_{53} &= -ik_3 Y_3^{ig} \lambda dA_i e^{-ik_3 h} & b_{54} &= -ik_4 Y_4^{ig} \lambda dA_i e^{-ik_4 h} \\
b_{55} &= ik_5 Y_5^{ig} \lambda dA_i & b_{56} &= ik_6 Y_6^{ig} \lambda dA_i \\
b_{57} &= ik_7 Y_7^{ig} \lambda dA_i & b_{58} &= ik_8 Y_8^{ig} \lambda dA_i \\
\\
b_{61} &= -ik_1 Y_1^{og} \lambda dA_o e^{-ik_1 h} & b_{62} &= -ik_2 Y_2^{og} \lambda dA_o e^{-ik_2 h} \\
b_{63} &= -ik_3 Y_3^{og} \lambda dA_o e^{-ik_3 h} & b_{64} &= -ik_4 Y_4^{og} \lambda dA_o e^{-ik_4 h} \\
b_{65} &= ik_5 Y_5^{og} \lambda dA_o & b_{66} &= ik_6 Y_6^{og} \lambda dA_o \\
b_{67} &= ik_7 Y_7^{og} \lambda dA_o & b_{68} &= ik_8 Y_8^{og} \lambda dA_o \\
\\
b_{71} &= -ik_1 \lambda dA_g e^{-ik_1 h} & b_{72} &= -ik_2 \lambda dA_g e^{-ik_2 h} \\
b_{73} &= -ik_3 \lambda dA_g e^{-ik_3 h} & b_{74} &= -ik_4 \lambda dA_g e^{-ik_4 h} \\
b_{75} &= ik_5 \lambda dA_g & b_{76} &= ik_6 \lambda dA_g \\
b_{77} &= ik_7 \lambda dA_g & b_{78} &= ik_8 \lambda dA_g \\
\\
b_{81} &= -ik_1 Y_1^{sg} \lambda dA_s e^{-ik_1 h} & b_{82} &= -ik_2 Y_2^{sg} \lambda dA_s e^{-ik_2 h} \\
b_{83} &= -ik_3 Y_3^{sg} \lambda dA_s e^{-ik_3 h} & b_{84} &= -ik_4 Y_4^{sg} \lambda dA_s e^{-ik_4 h} \\
b_{85} &= ik_5 Y_5^{sg} \lambda dA_s & b_{86} &= ik_6 Y_6^{sg} \lambda dA_s \\
b_{87} &= ik_7 Y_7^{sg} \lambda dA_s & b_{88} &= ik_8 Y_8^{sg} \lambda dA_s
\end{aligned}
\tag{7.0.32}
$$

BIBLIOGRAPHY

[1] R. Al-Khoury, *Computational modeling of shallow geothermal systems* (CRC Press, 2011).

[2] N. BniLam and R. Al-Khoury, *A spectral element model for nonhomogeneous heat flow in shallow geothermal systems,* International Journal of Heat and Mass Transfer **104**, 703 (2017).

[3] R. Al-Khoury, *A spectral model for shallow geothermal systems,* International Journal of Numerical Methods for Heat & Fluid Flow **22**, 49 (2012).

[4] C. Multiphysics®, *Comsol multiphysics® (v. 5.2),* (1986-2017).

[5] Maplesoft, a division of Waterloo Maple Inc., Waterloo, Ontario., *Maple (2015.2),* (1981-2015).

[6] R. A. Beier, J. Acuña, P. Mogensen, and B. Palm, *Borehole resistance and vertical temperature profiles in coaxial borehole heat exchangers,* Applied energy **102**, 665 (2013).

[7] Wikipedia, *Perturbation theory — wikipedia, the free encyclopedia,* (2017).

[8] S. Mihir, *Analutical Heat Transfer* (Department of Aerospace and Mechanical Engineering-University of Notre Dame, 2015).

[9] N. BniLam and R. Al-Khoury, *Transient heat conduction in an infinite medium subjected to multiple cylindrical heat sources: An application to shallow geothermal systems,* Renewable Energy **97**, 145 (2016).